NAIST-IS-DD0561038

Doctoral Dissertation

Peak Power Reduction for Multicarrier Systems in Satellite and Radio Communications

Khoirul Anwar

February 19, 2008

Department of Information Systems
Graduate School of Information Science
Nara Institute of Science and Technology

A Doctoral Dissertation
submitted to Graduate School of Information Science,
Nara Institute of Science and Technology
in partial fulfillment of the requirements for the degree of
DOCTOR of ENGINEERING

Khoirul Anwar

Thesis Committee:

Professor Minoru Okada	(Supervisor)
Professor Hiroyuki Seki	(Co-supervisor)
Associate Prof. Takao Hara	(Co-supervisor)

Peak Power Reduction for Multicarrier Systems in Satellite and Radio Communications*

Khoirul Anwar

Abstract

This dissertation contributes four new methods for improving the performances of multicarrier systems in terms of peak-to-average power ratio (PAPR), bit-error-rate (BER), out-of-band (OOB) spectrum, and computational complexities. Although multicarrier modulation systems have become popular in most of wireless communications systems due to their high spectral efficiency and robustness against multipath fading effects, the systems suffer from nonlinear channels such as high power amplifier (HPA). This drawback is caused by high peak power level (compared with its average power) when the modulated data of each subcarrier are added coherently. The ratio between the maximum peak power and the average power is then called as PAPR. Signal with high PAPR requires HPA with large back-off to avoid performance degradation and out-of-band (OOB) spectrum radiation.

Four new methods are proposed in this dissertation for the multicarrier systems in satellite and radio (terrestrial) communications. The considered multicarrier systems are orthogonal frequency division multiplexing (OFDM) and multicarrier code division multiple access (MC-CDMA). One of the four proposed methods is applied for multicarrier system in satellite communications while the other three methods are for multicarrier systems in radio (terrestrial) communications which based on carrier interferometry (CI) spreading code.

The first method considers a technique to transmit digital television signal to the far island which is uncovered by plain digital broadcasting system. To

*Doctoral Dissertation, Department of Information Systems, Graduate School of Information Science, Nara Institute of Science and Technology, NAIST-IS-DD0561038, February 19, 2008.

solve the problem, a combination of clipped OFDM and constant envelope of frequency modulation (FM) is proposed to transmit the digital television signals. The problem of nonlinear satellite channel due to high PAPR can be avoided by constant envelope of FM while the FM gain can be increased by using an appropriate clipping level. The Japanese digital television system, integrated services of digital broadcasting for terrestrial (ISDB-T), is considered. The results with ISDB-T mode 3 demonstrate that the proposed method has margin (gain) about 6.3dB in a comparison with the result of OFDM transmission directly to the satellite without FM modulation.

The second method introduces new design of carrier interferometry (CI) and pseudo-orthogonal carrier interferometry (POCI) OFDM based on fast Fourier transform (FFT), called CI-FFT/OFDM and POCI-FFT/OFDM systems. The use of FFT can reduce significantly the computational complexity of spreading process. With FFT radix-2, the computational cost can be reduced more than 90%. New spreading concept and corrections of oversampling technique are introduced in this method. At last, the new design becomes an advanced design with significant computational complexity reduction while no degradation both on the PAPR and BER performances compared with the conventional CI and POCI/OFDM systems.

The third method focuses on the solution of both PAPR reduction and bit/user capacity enhancement at the same time. To achieve this goal, a new large spreading code, called large carrier interferometry (LCI), is proposed. For the N subcarriers, the proposed LCI code can support $(2N+1)$ bits/users at the same time. LCI code was designed to have low and uniform cross correlation to guarantee fair and improved BER performances of the OFDM and MC-CDMA systems while the PAPR performance is kept to be low enough. Mathematical derivations show that the cross-correlation property of the proposed LCI is better than that of the POCI code. The results of BER performance evaluation confirm that the proposed LCI code is 5dB and 3.6dB better than PO-CI code in additive white Gaussian noise (AWGN) and multipath fading channel, respectively. In term of PAPR performance, the proposed LCI code and POCI code have a similar PAPR performance.

In the last method, a combination of spreading technique with iterative clipping (IC) is proposed for CI-FFT/OFDM system to obtain lower out-of-band (OOB) spectrum after the nonlinear channel. Here, the considered nonlinear channel is a solid-state power amplifier (SSPA) at the transmitter end. The clipping with iteration is designed to minimize the hardware requirement though iteration is performed. The results confirm that CI-FFT/OFDM with the proposed iterative clipping presents many advantages in terms of BER performance and OOB spectrum radiation. Surprisingly, it is found that for a coded system, 2 and 3 iterations is an efficient iteration number for the iterative clipping in OFDM and CI-FFT/OFDM, respectively.

Finally, it can be concluded that four proposed methods above are important contributions to improve the performance of multicarrier systems in satellite and radio communications. OFDM-FM is a promising technique to broadcast digital television at far island; new CI/OFDM system provide reliable performance; proposed LCI code doubles the bit/user capacity of OFDM and MC-CDMA systems; and the effective iterative clipping gives advantages in reducing OOB spectrum radiation and BER degradation simultaneously.

Keywords:

Multicarrier systems, high power amplifier (HPA), nonlinearity, spreading code, carrier interferometry code, clipping

衛星および無線通信におけるマルチキャリアシステムのピーク電力抑圧に関する研究*

Khoirul Anwar

内容梗概

本論文はマルチキャリアシステムのピーク対平均電力比 (PAPR: Peak-to-Average Power Ratio)，ビット誤り率 (BER: Bit Error Rate) および演算量といった性能を向上させる手法について検討を行っている．多くの無線通信システムにおいて，周波数利用効率とマルチパスフェージングに対する耐性の点でマルチキャリアシステムが一般的に用いられるようになってきている．しかし，マルチキャリアシステムのもっとも大きな問題点は，各サブキャリアの変調シンボルが同相加算されることに起因する高ピーク電力である．ピーク電力を評価するために用いられる指標が，PAPR である．PAPR の大きい信号を送信する場合，伝送品質の劣化と帯域外輻射を避けるために HPA(High Power Amplifier) のバックオフを大きくとる必要がある．本論文は，衛星および無線通信におけるマルチキャリアシステムに焦点を絞り，OFDM (Orthogonal Frequency Division Multiplexing) および MC-CDMA(Multicarrier Code Division Multiple Access) 方式の二つのマルチキャリアシステム についてピーク電力の抑圧法の検討を行う．

まず，OFDM については，日本および欧州の地上デジタルテレビ放送を衛星通信回線を介して離島への中継を行う場合のピーク電力抑圧手法について検討を行う．ここでは，ピーク電力抑圧手法として，OFDM 信号をクリッピングした後，さらに周波数変調（FM）して伝送を行う手法を提案する。FM 信号はその包絡線が一定であるため，衛星通信における衛星中継器の非線形性の問題を避けることができる．一方，OFDM 信号を適当なレベルでクリッピングすることで，平均変調指数を大きくすることができ，その結果，FM 利得を向上させることが

*奈良先端科学技術大学院大学 情報科学研究科 情報システム学専攻 博士論文, NAIST-IS-DD0561038, 2008 年 2 月 19 日.

可能となる．日本の地上デジタルテレビ放送規格であるISDB-Tを仮定して解析を行った．その結果，ISDB-Tモード3において，提案された方法は，FM変調なしの直交周波数分割多重 (OFDM) の結果と比較して6.3dB利得を改善できることを明らかにした．

次に，拡散符号としてCI (Carrier Interferometry) 符号を用いたMC-CDMAであるCI/OFDM方式について検討を行う．ここでは，まず，CI符号の演算量を削減するため，高速フーリエ変換（FFT）を用いてCI符号化を行うCIFFT/OFDM方式およびCIFFT/OFDMを拡張し，周波数利用効率をさらに高めたPOCI(Pseudo-Orthogonal Carrier Interferometry)-FFT/OFDM方式を提案する．提案方式を基数2のFFTを用いて実装することで，従来のCI/OFDMに比べて演算量を90%以上減らすことを示す．また，ここでは，オーバーサンプリング法による新しい拡散手法について提案する．

提案手法は、従来のCI/OFDMおよびPOCI/OFDM方式と比較してPAPRおよびBER特性を劣化させることなく大幅に演算量を削減することができる有効な方式である．さらに，CI-OFDMにおけるPAPRの削減に加えて伝送容量あるいはユーザー容量を向上させるため，LCI (Large Carrier Interferometry) 符号と呼ぶ新しい拡散符号を提案する．提案LCI符号を用いることにより，N キャリアにより $(2N+1)$ ユーザ（またはビット）の伝送が可能である．LCI符号は，PAPR特性を低く保ちつつ，OFDMやMC-CDMAにおけるBER特性の改善効果を補償するため，相互相関が小さくかつ一様に分布するように設計されていいる．本論文では，提案LCI符号の相互相関特性が従来のPOCI符号よりも改善されることを数学的に導出している．BER特性を評価した結果，提案LCI符号は、POCI符号に対してAWGN (Additive White Gaussian Noise) 環境において5dB，とマルチパスフェージング環境において3.6dB改善することを明らかにした．また，PAPR特性については，提案LCI符号はPOCI符号とほぼ同じであることを示した．

一方，CI-FFT/OFDM信号を非線形増幅器で増幅したときの帯域外輻射の増加を抑える手法として，繰り返しクリッピング (IC: Iterative Clipping) 法を組み合わせた方法を提案する．ここでは，非線形増幅器として，SSPA (Solid State Power Amplifer) を仮定する．提案する繰り返しクリッピングは、繰り返しによるハードウェア規模の増加を最小限に抑えるように設計されている．数値計算の結果，提案繰り返しクリッピングを適用したCI-FFT/OFDMがBER特性および

帯域外輻射特性の改善が可能であることがわかる．さらに，誤り訂正を行っている場合，OFDM では 2 回，CI-FFT/OFDM では，3 回の繰り返しが最適であることを明らかにしている

キーワード

Multicarrier systems, high power amplifier (HPA), nonlinearity, spreading code, carrier interferometry code, clipping

Bismillah ar-Rahmaan ar-Rahiim

In the Name of God, the most Gracious, the most Merciful

Contents

List of Figures

List of Tables

Chapter 1

Introduction

THE demand for high data rate and high mobility services has been rapidly increasing for many decades and predicted there will be no slowdown in the future. Almost every existing physical medium is capable of supporting broadband data including digital subscriber lines (DSL), power lines, cable modem, fiber optic and wireless media such as digital broadcast television. Most of these services suffers many degradations such as large attenuation, noise, multipath fading, nonlinearity and most of them must meet many constraints such as finite transmit power and low out-of-band (OOB) noise. One of physical-layer technologies that has gained much attention and popularity due to robustness to multipath fading environment is multicarrier modulation.

One particular problem with multicarrier technique is the large power envelope fluctuation, which is usually measured by the parameter called peak-to-average power ratio (PAPR) level. This problem arises almost in all multicarrier technologies such as orthogonal frequency division multiplexing (OFDM) [1] and orthogonal wavelet division multiplexing (OWDM) [2]. High peak appears because of the coherent summation of sinusoidal signals in all subcarriers. Since most practical transmission systems are peak-power limited and should operate perfectly in linear area, it requires large dynamic range. In practise, to avoid operating amplifier with large back-offs, occasional saturation of the power amplifiers (or clipping) must be allowed. Because saturation or clipping is a nonlinear process, it creates distortion that degrades bit-error-rate (BER) performances and

also causes spectrum broadening that acts as OOB spectrum radiation that increases adjacent channel interference. Therefore, PAPR reduction technique is inarguably important.

For multilevel modulations such as 16QAM and 64QAM, much information is included in the amplitude components as well as in the phases. Therefore, the clipping stimulates larger BER performance degradation especially for 16QAM, 64QAM and higher multilevel modulations. The solution of this problem is increasing the back-off of the amplifier or inventing a new low complexity method to reduce the PAPR without distortion (distortionless method). This fact leads to the conclusion that distortionless method is more attractive as far the technique is simple/practical. Employing spreading code in OFDM transceiver is one kind of distortionless method for PAPR reduction.

This dissertation derives some relevant results regarding PAPR and designs efficient low computational complexity methods for PAPR reduction in multicarrier satellite and radio communication systems. Though most results in this dissertation are evaluated for OFDM system that based on Fourier transform, some methods can be extended to other multicarrier system such as orthogonal wavelet division multiplexing (OWDM) or filtered multi tone (FMT) with a slight modifications.

Digital Television Broadcasting

Since the end of 2003, digital terrestrial television broadcasting has started in major cities of Japan. It is planned to expand the system to the entire country by 2006. Further, all analog broadcasting is scheduled to cease in 2011. Due to the public nature of broadcasting, the service area is required to cover the entire Japan's territory, including remote locations such as islands and mountain regions. Accomplishing such a goal is difficult if only terrestrial broadcasting is used. To resolve the problem, various methods have been discussed in which remote relaying is performed by optical fibers and satellite communications, followed by re-broadcasting [3]. In this dissertation, a relay system based on satellite communications is proposed and its effectiveness is presented. In this case, the system must not affect the configurations of the existing broadcasting transmit-

ters and widely used television receiver sets. Transparency of the satellite relay sections must be maintained.

The modulation scheme at the wireless frequency for digital terrestrial television broadcasting is OFDM [4]. In this scheme, high-speed data signals are divided into many carriers for transmission. Therefore, the transmission speed per wave becomes lower and the scheme has a frequency diversity effect. Another advantage is that it is tolerant to multipath fading. In contrast, since the signal is formed by superposition of many synchronized carriers, large peaks appear in the waveform, so that the so-called PAPR becomes very large. This is not a significant problem for the transmitters used in terrestrial broadcasting, because a high-power amplifier can be used. But when this signal is transmitted by a satellite repeater with limited power, degradation of the transmission characteristics and OOB spectrum radiation occur due to waveform distortion. To suppress these effects, sufficient back-off is needed, so that the power efficiency of the satellite is significantly degraded.

Much research has recently been conducted on reduction of the PAPR of OFDM signals such as carrier interferometry (CI)/OFDM [5, 6], and FFT-based CI Spreading [7–9]. But these methods cannot be used because they cannot align to the systems in operation. The reason is as follows. In CI/OFDM, the information on each symbol of the input data is distributed to all subcarriers. Therefore, the transmitter configuration is different from that in the conventional OFDM scheme, in which each symbol of the data is distributed to each subcarrier. As a result, the configuration of a receiver with the inverse functionality is substantially different from that used in commercially available digital terrestrial television receivers.

To transmit digital television signals via satellite, it is conceivable to use transmission with phase shift keying (PSK) modulation in the satellite section to allow the use of many channels, then to retransmit (broadcast) on the receiving side in a remote area after conversion to OFDM. In that case, however, the remotely located station must be equipped with a broadcasting setup for retransmission, such as a PSK demodulator and OFDM modulator, so that the size and configuration of the station become larger and more complicated. In this dissertation,

to simplify and miniaturize ground station and the configuration of re-broadcast setups in disadvantaged remote locations, a frequency modulation (FM) system that has a constant signal envelope is used in secondary modulation for the modulation scheme in the satellite section, and the signal is re-converted into OFDM on the receiver side. There have been previous investigations of the OFDM-FM system [10–13], but there is no research on the transmission characteristics in a system with nonlinearity in the transmission section.

The system proposed in this dissertation, which has no amplitude components, can be used up to the saturation region of the satellite repeater. However, even with this system, the bandwidth of the FM signal is increased by the peak of the OFDM signal if the OFDM signal is directly applied to the FM modulator. Therefore, the peak of the OFDM signal is limited by clipping. In this case, the BER degradation of the OFDM signal increases as the degree of clipping is deepened. Also, in the FM system, the overall transmission characteristics are determined by the bandwidth of the FM signals, which depends on that of the satellite repeater, and by the modulation index of the FM signals. Therefore, it is necessary to optimize the system by a tradeoff of these factors.

Carrier Interferometry OFDM

Carrier Interferometry (CI) codes have been introduced to reduce the PAPR, while providing frequency diversity benefit and it is called CI/OFDM [5, 14]. Radio frequency (RF) testing on CI/OFDM has also been performed in a typical indoor office environment for wireless local area networks (W-LAN) IEEE.802.11a [15]. The results show that CI/OFDM provides BER performance improvement of 5-7dB at BER=10^{-3} over the current OFDM system.

In [16], pseudo-orthogonal carrier interferometry (POCI) codes is introduced for increasing the OFDM's throughput twice (especially for binary phase shift keying: BPSK), while keeping the PAPR level is low. Double throughput means that $2N$ data streams can be assigned on N subcarriers. Other benefit of POCI codes is its possibility of implementing two kinds of interleaving architectures [17] which improves the BER performance.

The previous works in [18] confirms that CI codes can reduce PAPR level up to

8-9dB from the original PAPR 12dB at cumulative distribution function (CCDF) of 10^{-4}. In [2] and [6], iterative processing of clipping (in frequency domain) is employed and resulting further low PAPR level, up to 3dB from the original CI/OFDM's PAPR of 8-9dB with minimum BER performance degradation. More elaborated analysis of CI codes and PO-CI codes for higher level modulation was reported in [2].

However, the CI/OFDM system has very high complexity due to the complex multiplication of CI spreading codes. Consequently, as our best knowledge, up to now CI/OFDM has been far from the practical implementation in a device. Therefore, it has been an important issue to decrease the computational complexity of CI/OFDM system that suitable for the implementation.

In order to solve this issue, in this dissertation we propose the use of FFT spreading instead of the conventional CI spreading. Also by use of double FFT spreading, we can increase the throughput of OFDM system as well as achieving low level of PAPR. The proposed design can be considered as a new efficient design of CI/OFDM and POCI/OFDM that is capable of achieving lower computational complexity [7–9]. First, a correction is obtained by using a correct oversampling instead of the conventional oversampling in [14, 16, 17, 19, 20]. It results in an advanced design. Second, employing FFT spreading for CI (called CI-FFT spreading) and double FFT spreading for POCI (called POCI-FFT) achieve lower computational complexity with a computational complexity reduction more than 90% for a number subcarriers more than 64.

Large Spreading Code

A combination of OFDM and code division multiple access (CDMA), called multicarrier code division multiple access (MC-CDMA) also has been drawing much attention as an alternative to conventional direct-sequence CDMA (DS-CDMA) [21]. Each user's data are transmitted over the same set of subcarriers but with unique spreading code to guarantee their separability (because of its orthogonality) at the receiver. If the number of and spacing between subcarriers are appropriately chosen in order that all subcarriers do not undergo a deep fading, the transmitted data can be reconstructed from the subcarrier which has no deep

fading. It is the reason why full frequency diversity can be achieved by assigning a (frequency domain) spreading code prior to the inverse fast Fourier transform (IFFT) in OFDM and MC-CDMA systems. This assignment provides better BER performance due to the frequency diversity benefits.

In conventional OFDM with spreading code [22] and MC-CDMA [23], each user's data bit is transmitted simultaneously over N narrowband subcarriers where each subcarrier is encoded with orthogonal combination of +1 or -1 (Walsh-Hadamard code). However, the Walsh- Hadamard code is not an optimum spreading code in terms of diversity benefit, because of the appearance of bad pairs of vectors (due to the limited number of distinct elements) that reduce the diversity gain as shown in [24]. In [5], CI code, a complex spreading code, was introduced and its low computational complexity design have been presented in [7, 8, 25]. CI code has better peak-to-average power ratio (PAPR) performance than Hadamard code in OFDM system as shown in [26].

Recently, there is an interest in increasing the number of codes, called code-number from N to $K = N + A$, where $A \leqslant N$, while the length of the code, called code-length is kept to N. The purpose is to acquire higher user capacity, such as two orthogonal code set (TOCS) [27], quadriphase code [28], pseudo-orthogonal gold code (POGC) [29] and pseudo-orthogonal carrier interferometry (POCI) code [16, 19, 29]. Among these codes, POCI is the most attractive one in better BER performance and its capability to reduce the PAPR level of OFDM signals. In addition, POCI's Implementation is becoming uncomplicated via double FFTs (with N additional constant separator of $(e^{j\frac{\pi}{N}\cdot n})$ for the second data set) as shown in [8].

As shown in [2] and later in [30], the cross-correlation amongst codes in the POCI code set is not low enough to mitigate the BER performance degradation (especially for multilevel modulations). High cross-correlation causes intercode interferences between the codes in a code set. POCI code has problem of large cross-correlation (both real and imaginary parts) that lead to the performance degradation. In addition, the cross-correlation of POCI code are nonuniform between the code sets.

The nonuniform cross-correlation causes the signals to have unequality in

probability of error [31] amongst the assigned users. Therefore, a code set with lower and uniform cross-correlations is more interesting to guarantee fairness in multiuser systems. If the cross-correlations are uniform, the signals have equal 'a priori probability' that result in minimum error. Literatures [31] and [32] were pointed out that the desirable code set has uniform and low cross-correlation property. Although one could construct a code set having uniform cross-correlation property, the code set size will diminish. It was also pointed out though one could construct a set of code in which all cross correlation were equal (uniform), it comes to diminish in the size [31]. Consequently, finding optimum large code set with minimal cross-correlation is very difficult in general [33].

With some difficulties and limitations of constructing good code sets, this dissertation tries to improve the performance of OFDM and MC-CDMA system by proposing a new large code set called large carrier interferometry (LCI). The proposed LCI code set has length of N but is capable of supporting $(2N+1)$ data symbols or maximum $(2N+1)$ users. We derive a new code set that satisfy uniform low cross-correlation to guarantee minimal BER performance degradation and at the same time reduce the PAPR level of the OFDM system. In addition, there is no restriction in its code size. Any value of N is acceptable in the proposed LCI codes.

To present a fair performance evaluation, a comparison with POCI code is considered to show the effectiveness of the proposed LCI code set. POCI outperforms other pseudo orthogonal codes as demonstrated in [20, 29] and [16], therefore a comparison with other large code sets is enough by comparing the proposed LCI codes with the POCI code. An example is presented for a length of $N = 16$. The results confirm that the proposed LCI outperforms POCI code by improving the BER more than 6dB in additive white Gaussian noise (AWGN) channel and more than 4dB in multipath fading channel.

Iterative Clipping

A number of methods have been proposed to deal with PAPR problem in OFDM system [34]. These methods include amplitude clipping and filtering, coding, and multiple signal representation techniques such as partial transmit sequence

(PTS) and selected mapping (SLM). These methods achieve PAPR reduction at the expense of BER increase, data rate loss, computational complexity increases, and so on.

PTS and SLM are well known method in the area of PAPR reduction. In PTS technique, an input data block is partitioned into disjoint sub-blocks. The subcarrier in each sub-block is weighted by a phase factor so that the PAPR of signal combined from each sub-block is minimized. In SLM method, the transmitter generates a set of sufficiently different candidate OFDM signals. These candidates represent the same information though have different peak power level. The transmitter selects the most favorable signals with minimum PAPR for transmission. However, these techniques cause computational complexity especially at the transmitter. PTS has exponentially increasing in optimization (search) complexity, while SLM increases the number of required FFTs to generate many candidates of OFDM signal that has low PAPR. In addition, the side information in PTS and SLM cause data rate loss and may increase BER at the receiver.

The simplest method for PAPR reduction might be the clipping and filtering (CAF) method. The clipping limits the envelope of an OFDM signal to a predetermined level or otherwise passes the signals without clipping. However, clipping causes distortion that can be viewed as another source of noise. The noise by the clipping falls both in-band and out-band of the desired spectrum. In-band noise can not be reduced by filtering and results in BER performance degradation. The OOB noise, that reduces the spectral efficiency of the OFDM system, can be removed by filtering. Though filtering reduces the OOB noise, however, it causes peak re-growth that exceeds the clipping level at some points. To reduce overall peak re-growth, repeated clipping and filtering can be employed as in [35].

Similar with [35], PAPR reduction technique called iterative processing (IP) has been introduced in [36] to reduce the PAPR of OFDM signals. IP employs clipping during peak detection process to reduce the PAPR. The OOB spectrum radiation is automatically removed in each iteration process. However, the problem of large distortion arises when the PAPR threshold is set to small value to obtain lower PAPR level. This phenomenon is similar with a clipping with a

small clipping ratio (CR) [37]. Therefore, IP certainly still introduces large BER degradations. This BER degradation may be minimized by increasing the CR (small distortion), as the consequence the number of iteration should be increased more than 5 iterations [38]. It becomes a new problem of IP technique in term of computational complexity.

The CI spreading code [5] is one of the PAPR reduction techniques which does not cause signal distortion (distortion-less PAPR reduction technique). RF testing of the codes has also been performed in typical indoor office environment for IEEE.802.11a and show performance improvement over the current OFDM system [16]. However, the PAPR of CI is not low enough (i.e. by about 3dB reduction from original OFDM's PAPR of 11dB at CCDF of 10^{-4}) [7, 25] to surpass the nonlinear channel, especially with low saturation level. It impacts to the rising of OOB spectrum radiation on the OFDM spectrum after the nonlinear channel. The other problem of CI spreading code is its computational complexity of spreading. On an OFDM with N subcarriers, one data symbol must multiplied with N complex CI codes before spread overall the subcarriers. As a consequent, the computational complexity of CI increases quadratically as the increasing of the subcarriers number.

In order to solve the problems of high peak power in OFDM signals, a method with low computational complexity and minimum BER degradation than the mentioned above is required. In this dissertation, an FFT-based CI spreading combined with iterative clipping to guarantee lower peak power level with allowable computational complexity is proposed. The proposed method is then called carrier interferometry with iterative clipping (CI-IC) method. First, to solve the computational complexity of CI, we extend our works in [7, 25] i.e. employs IFFT instead of conventional CI's matrix multiplication, called CI-IFFT. Using CI-IFFT, the computational complexity of CI can be reduced beyond 90%. Therefore, CI-IFFT is preferable to the conventional CI spreading. Second, we modify repeated clipping in [35] so that iteration of clipping can be performed and appropriate with CI-IFFT spreading. Third, this dissertation presents an efficient iteration number of a coded system. A convolutional coding is considered. The preliminary results has been presented in parts in [6] for the case of uncoded

systems.

An instantaneous normalized power (INP) that measures the distribution of power levels is interesting to be studied. The INP measures the distribution of power in all samples rather than only one sample (of the maximum value) as considered in the PAPR measurement. Thus, INP can be a powerful tool to show the power distribution of OFDM system in a practical hardware implementation. The proposed method, offers new advantages to produce OFDM signal with lower INP level while minimizes the BER degradation and OOB spectrum radiation. With a similar computational complexity, the proposed CI-IC method outperforms the well known PTS, SLM and IP techniques in terms of INP performance. Interesting results of the evaluations on OFDM through nonlinear channel show that the proposed technique is efficient and potential for future OFDM applications.

1.1. Outline of Dissertation

Chapter 2 introduces OFDM system as a kind of multicarrier modulation and its PAPR problem in satellite and radio communication systems. This chaper describes the OFDM signals using discrete-time formulations and formally introduces the concept of PAPR and power spectral density (PSD). The model of nonlinear devices is also introduced for satellite and radio communications. This chapter also investigates the performance of multilevel modulations for OFDM through the considered non-linear channel which is essential for designing efficient PAPR reduction techniques.

Chapter 3 presents the proposed PAPR reduction for an application of digital television through a satellite link. This method employs the use of FM to transmit the modified OFDM signals (by a clipping and filtering).

Chapter 4 introduces a new design of CI/OFDM system. First, we derive a general principle of the new CI/OFDM system. Then a new oversampling technique is introduced. Finally, we propose to replace the conventional matrix multiplication of CI spreading with (I)FFT, called CI-FFT, that results in significant computational complexity reduction.

Chapter 5 proposes a new spreading code set for providing two advantages

at the same time i.e. PAPR reduction and double user/bit capacity enhancement. The low cross-correlation property of the proposed code leads a better performance than the conventional two code sets such as the POCI code.

Chapter 6 presents an iterative clipping on the new CI-FFT/OFDM systems as presented in Chapter 4. This technique provides lower OOB spectrum radiation due to its lower PAPR level by the clipping, provide lower BER degradation and can efficiently be implemented to the OFDM through a solid state power amplifier (SSPA).

Chapter 7 concludes the dissertation.

1.2. Research Contributions

The main contributions of this dissertation are the analysis of PAPR for multicarrier satellite and radio communication systems and the designs of several new methods and spreading code to meet efficient and low complexity designs for reducing the PAPR. The details of these contributions are listed as below by chapter.

- Chapter 2 introduces the PSD performance of multicarrier modulation for acceptable OBO of SSPA as well as SSPA model itself. These evaluations are very important to design an efficient PAPR reduction technique through the nonlinear channel.

- Chapter 3 contributes the design of digital television transmission via satellite link using FM modulation. The results show that OFDM with FM modulation, called OFDM-FM, is really advantageous than the transmission of OFDM to the satellite system without FM modulation. This result is important for the application of digital terrestrial television broadcasting via the satellite for far rural area which is unreachable by the current radio broadcasting system.

- Chapter 4 introduces a new low complexity CI spreading by using FFT spreading for OFDM system, called as CI-FFT/OFDM. This new design

reduces the computational complexity more than 90%. Generally, the computational complexity can be reduced from N^2 to $N\log_2(N)$, where N is the number of subcarriers. This design is important to realize CI/OFDM system practically.

- CHAPTER 5 introduces for the first time, a novel large spreading code set with length of N but poses $(2N+1)$ of code-numbers. The larger code-number than its code-length guarantees the additional $(N+1)$ users to be assigned together with the other N user (results in total $(2N+1)$ users) for the multicarrier system where the number of subcarriers is only N. It is another advantage of the proposed code though its main advantage is reducing the PAPR excellently.

- CHAPTER 6 introduces a novel of lower PAPR reduction for CI-FFT/OFDM by employing an iterative clipping (IC), called as CI-IC method. With a comparable computational cost, the proposed CI-IC has the lowest INP than the other methods such as PTS, SLM and IP method. The proposed CI-IC also has a better performances in OOB radiation and BER performance almost in any conditions with or without error correction coding. For the coded systems, this chapter contributes an efficient iteration numbers i.e. 2 for OFDM and 3 for CI-FFT/OFDM system.

Chapter 2

PAPR and Nonlinear Channels

TO achieve data rates which close to the capacity over noisy linear channels with memory, sophisticated transmission schemes that combine coding and shaping with modulation and equalization are required. An alternative scheme that is more suitable for variety of high-speed applications on 'difficult' channels is the multicarrier modulation (MCM). The term of multicarrier modulation includes a number of transmission schemes whose main characteristic is the decomposition of any wideband channel into a set of independent narrowband channels. Within this family the most commonly used scheme is orthogonal frequency division multiplexing (OFDM), which is based on the discrete Fourier transform (DFT), resulting in implementable and high performance structure via the fast Fourier transform (FFT).

This chapter introduces the basic knowledge of multicarrier modulation and an analysis on OFDM system in more detail. The PAPR and nonlinear channel is presented. In addition, power spectral density (PSD) is plotted to show how the nonlinearity causes an OOB radiation that may increase the adjacent channel interference (ACI).

2.1. Multicarrier Modulation

Multicarrier modulation is an interesting research topic because of its promise to be capable in transmitting high bit rate while robust to multipath fading envi-

ronment. All multicarrier modulation techniques divide a wideband, a spectrally shaped transmission channel, into a set of parallel and (ideally) independent narrowband channel (further called subcarrier). Generally, there are two basic transform methods to generate multicarrier signal i.e. Fourier transform-based and wavelet (filter banks)-based method.

The multicarrier technology based on wavelet transform has been studied in detail in [2]. The wavelet-based multicarrier system uses waveform that is well localized both in time and frequency domain instead of sinusoid waveform such as in Fourier transform-based multicarrier. Consequently, in wavelet-based technology guard interval (GI) insertion to avoid inter-symbol interference (ISI) is not needed, since GI is, generally, reduces the system efficiency. However, in [2] it is confirmed that the wavelet-based multicarrier system also has a problem of high peak power.

The common used multicarrier technologies based on Fourier transform are discrete multi-tone modulation (DMT) and OFDM system. DMT modulators optimize the amount of energy and also the amount of bits in each subcarrier to maximize the overall performance over a given channel. This optimization is generally called as loading. DMT is used for point-to-point applications, usually on a slow time-varying channels, such as telephone line. DMT has been chosen as the modulation format for asymmetric digital subscriber line (ADSL), twisted pair telephone line standard, and also as a major discussion in the ongoing very high data rate digital subscriber line (VDSL) standard.

Being different with the DMT, OFDM is generally used for broadcasting or point-to-point transmission in a fast time-varying environment where the receiver typically can not feedback to the transmitter the optimal bits and energies. OFDM has been proposed with substantial advancement in digital signal processing (DSP) technology now, becoming an important part in the telecommunication area. OFDM has been chosen as the modulation format for the European wireless data link known as HYPERLAN, as well as adopted in US by the well-known IEEE.802.11 and adopted in integrated services digital broadcasting for terrestrial (ISDB-T), a standard of Japanese digital television broadcasting system.

An OFDM transmit signal is the sum of N, independent, quadrature-amplitude-

modulation (QAM) sub-signals, each with equal bandwidth and frequency separation $1/T$, where T is the time duration of the OFDM symbol. The discrete-time baseband representation of a single multicarrier symbol is given by

$$x(n) = \frac{1}{\sqrt{N}} \sum_{k=0}^{N-1} X(k) e^{j2\pi \cdot k \cdot \frac{n}{T}} w(n), \tag{2.1}$$

where $w(n)$ is a discrete time rectangular window (nominally of height 1 over the interval $[0, T]$) and $X(k)$ is the QAM data of the k-th sub-symbol. OFDM inserts guard interval (GI) with length of T_{GI} before every OFDM symbol to simplify the equalizer design at the receiver in the presence of finite-length-channel multipath. The GI is simply a periodic extension of the symbol over the interval $[-T_{GI}, 0]$ resulting in an OFDM symbol of length $[-T_{GI}, T]$. Equation (2.1), thus, become

$$x_{GI}(n) = \frac{1}{\sqrt{N}} \sum_{k=0}^{N-1} X(k) e^{j2\pi k \cdot \frac{n}{T}} w_{GI}(n), \tag{2.2}$$

where $w_{GI}(n)$ is a rectangular window of height 1 over the interval $[-N_{GI}, N]$. For the continuous data transmission $x(m)$, the transmitter will send these symbols sequentially

$$x(m) = \sum_{q=-\infty}^{\infty} x_{GI}(m - q(T_{GI} + T)) \tag{2.3}$$

where q is the OFDM symbol index. This transmit signal is not bandlimited due to the $\text{sinc}(f(N + N_{GI}))$ behavior exhibited by rectangular windowing function $w_{GI}(n)$, and is typically followed by a filter.

In practise, complex baseband OFDM signals are typically generated by using an inverse discrete Fourier transform (IDFT) as described in the block diagram in Fig. 2.1(a) and demodulated by using discrete Fourier transform (DFT) as in Fig. 2.1(b). Generally with N power of two, the (I)DFT can be performed faster by (I)FFT.

Vector of QAM data $\mathbf{X} = [X(0)X(1)\cdots X(N-1)]^T$ is transformed via an IFFT into vector $\mathbf{x} = [x(0)x(1)\cdots x(N-1)] = IFFT(\mathbf{X})$, where the n-th com-

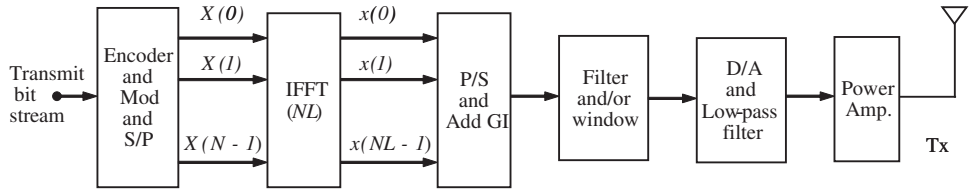

(a) Transmitter

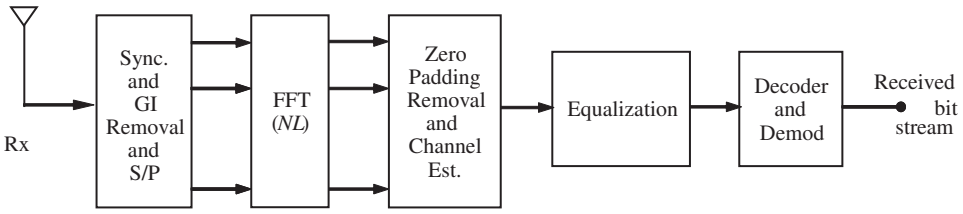

(b) Receiver

Figure 2.1. Basic OFDM transceiver block diagram

ponent of $\mathbf{x}$ is defined as.

$$x(n) = \frac{1}{\sqrt{N}} \sum_{m=0}^{N-1} X(m) e^{j\frac{2\pi}{N} m \cdot n}. \tag{2.4}$$

Since oversampling may be needed in practical designs, the notation of $X(n/L)$ is introduced to denote oversampling by factor L. The oversampled IFFT output is then expressed as

$$\begin{aligned} x(n/L) &= \frac{1}{\sqrt{N}} \sum_{k=0}^{N-1} X(k) \cdot e^{j\left(2\pi \cdot k \cdot \frac{n}{NL}\right)} w(n/L) \\ &= \frac{w(n/L)}{\sqrt{N}} \left(\sum_{k=0}^{\frac{N}{2}-1} X(k) \cdot e^{j\left(2\pi \cdot k \cdot \frac{n}{NL}\right)} + \sum_{k=NL-\frac{N}{2}}^{NL-1} X(k) \cdot e^{j\left(2\pi \cdot k \cdot \frac{n}{NL}\right)} \right) \\ &= IFFT(\sqrt{L}[\underbrace{X(0) \cdots X(\tfrac{N}{2}-1)}_{\frac{N}{2}} \underbrace{0 \cdots 0}_{N(L-1)} \underbrace{X(\tfrac{N}{2}) \cdots X(N-1)}_{\frac{N}{2}}]) \\ &= IFFT(\sqrt{L}\, \mathbf{X}_{\mathrm{L}}). \end{aligned} \tag{2.5}$$

where $w(n/L)$ is the discrete rectangular window of height 1 over the interval $n \in [0, NL]$ and $\mathbf{X}_L$ is the L times oversampled equivalent QAM vector, generated by zero-padding $\mathbf{X}_L$ with $N(L-1)$ zeros.

As mentioned earlier, to simplify inter-symbol interference (ISI) mitigation at the receiver, the transmitter must add a GI to each of oversampled vector $x(n/L)$

$$x_{GI}(n/L) = \frac{1}{\sqrt{N}} \sum_{k=0}^{N-1} X(k) e^{j(2\pi \cdot k \cdot \frac{n}{NL})} w_{GI}(n/L), \tag{2.6}$$

where $w_{GI}(n/L)$ is the rectangular window over the interval $[-\gamma L, NL]$. The length of GI is γL. These vectors are then transmitted sequentially as described by

$$x_{GI}(n/L) = \sum_{q=-\infty}^{\infty} x_{GI}\left(\frac{n - q(N+\gamma)L}{L}\right). \tag{2.7}$$

This sequence is not bandlimited because of the slow decay with increasing frequency of the Fourier transform of a rectangular window. If the transmitter must meet strict adjacent channel interference requirements such as in spectral mask with out-of-band spectrum below -40dB, some degree of filtering or windowing will be needed. Filtering can be performed on the discrete time samples before the the digital-to-analog converter (DAC) or on the continuous-time samples after the DAC.

However, the spectral properties can also be improved by smoother window [1] instead of filtering. In windowing, generally, the transmitter should increase the cyclic extension (instead of only GI) to keep the orthogonality between the data symbols and modify the rectangular window sequence as described in Fig. 2.2. For this case the transmit sequence becomes

$$x_T(n/L) = \frac{1}{\sqrt{N}} \sum_{k=0}^{N-1} X(k) e^{j2\pi \cdot k \cdot \frac{n}{NL}} w_T(n/L), \tag{2.8}$$

where tapered window sequence $w_T(n/L), n = -(\gamma+\beta)L, \cdots, (N+\beta)L$ is constant over the interval $[\gamma L, NL]$ and tapper off of the remaining βL samples with $\beta L/2$ tapered samples each at the beginning and end of the symbol. Consider-

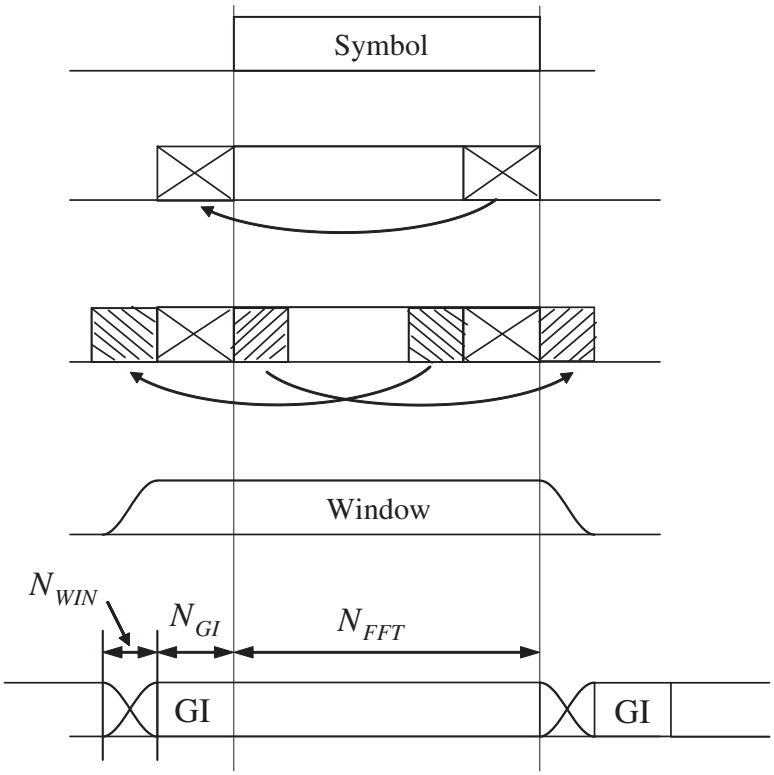

Figure 2.2. Guard interval and windowing of an OFDM symbol

ing to Fig. 2.2, $\gamma L = N_{GI}$ and $\beta L = N_{WIN}$ to represent the length of GI and windowing, respectively.

The result of windowing is shown in Fig. 2.3. The PSD in Fig. 2.3 is drawn for 50 OFDM symbols with oversampling factor $L = 3, N_{FFT} = 128, N_{GI} = 32$ and $N_{WIN} = 0, 10, 32$. The window shape is derived using a raised cosine as in [1]. Fig. 2.3 shows that windowing is required to obtain the spectrum that satisfy the spectral mask requirement. Longer window can increase the PSD performance, but the system efficiency will be reduced about $10\log_{10}(\frac{N_{WIN}}{N_{FFT}*L})$.

The sequence in (2.7) is then pass through the DAC to produce the continuous signal. At the receiver, synchronization is performed to detect the data window and remove the GI. Then the FFT is performed to extract the data and pilot for channel estimation. The result of channel estimation is used for equalization. Then, the decoder and demapping is applied to obtain the received data.

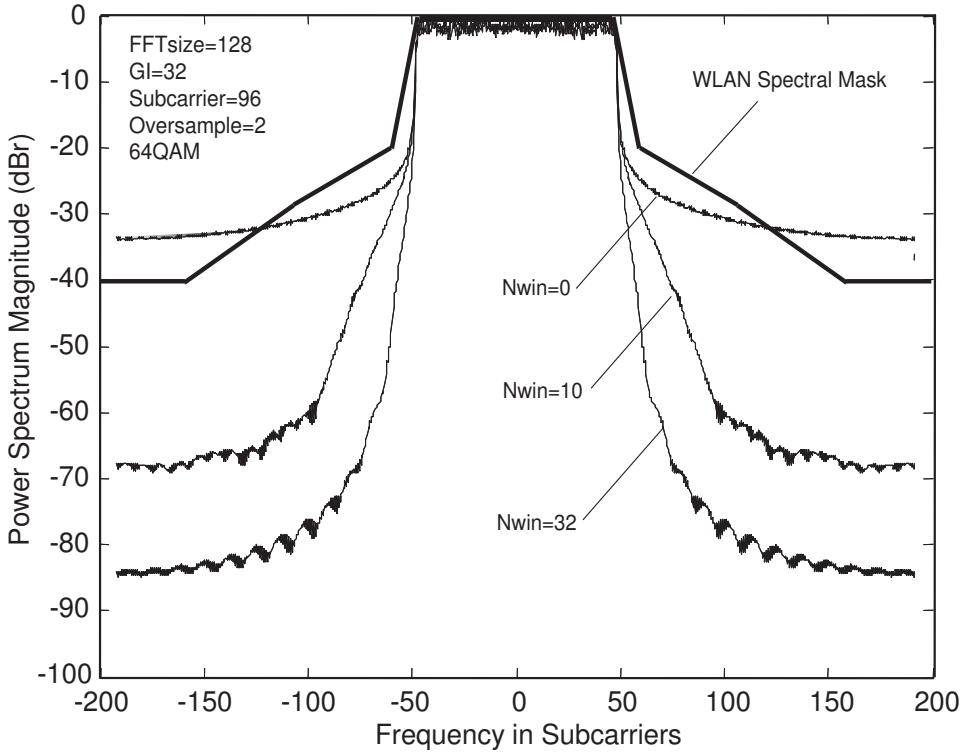

Figure 2.3. PSD of 50 OFDM symbols with FFT size of 128, subcarrier 96, GI length 32 and a spectral mask of IEEE.802.11: Wireless LAN

2.2. Peak-to-Average Power Ratio

Since all practical transmission systems are peak-power limited, designing a system to operate in a perfectly linear region often implies operating at average power levels way below the maximum power available. In practise, to avoid operating the amplifier with extremely large back-offs, occasional saturation of the amplifiers or clipping in the DAC must be allowed. This additional nonlinear distortion creates inter-modulation distortion that increases the BER in standard linear receivers and also causes spectral broadening of the transmit signal that increases adjacent channel interference to other users. Therefore, filter is required after the clipping.

PAPR is defined as the ratio of the peak instantaneous power and the average power, which is mathematically expressed as

$$\text{PAPR} = 10\log_{10}\left(\frac{\max\limits_{\tau\in T}|x(n)|^2}{E\{|x(n)|^2\}}\right)\text{dB}. \tag{2.9}$$

Here $\max\limits_{\tau}|x(n)|$ denotes the maximum instantaneous power, $E\{|x(n)|^2\}$ denotes the average power of the signal and $\tau \in T$ is the interval over the PAPR is evaluated. However, for practical design, instantaneous normalized power (INP) is sometimes useful because INP measures power level in all samples (instead of just measuring the maximum as in PAPR). The INP is mathematically expressed as

$$\text{INP} = 10\log_{10}\left(\frac{|x(n)|^2}{E\{|x(n)|^2\}}\right)\text{dB}. \tag{2.10}$$

At least a number of 100,000 randomly distributed OFDM symbols are used to measure the PAPR performance at cumulative distribution function (CCDF) of 10^-4. Increasing the number of symbols beyond it, however, shall not drastically change the curves. The CCDF of 10^{-4} means that PAPR has been measured over 99.99% of OFDM symbols.

2.3. Nonlinear Channels

Typically, most of the nonlinear behavior in the continuous time domain is caused by the high power amplifier (HPA). For most linear HPA, it is convenient to represent the input signal in bipolar coordinates as

$$x = |x|e^{j \arg x} = \rho e^{j\phi}. \tag{2.11}$$

Hence the complex envelope of the output HPA can be expressed by

$$g(x) = A(\rho)\, e^{j(\phi+\Phi(\rho))}, \tag{2.12}$$

where $A(\cdot)$ and $\Phi(\cdot)$ represent, respectively, the amplitude modulation/amplitude modulation (AM/AM) and amplitude modulation/phase modulation (AM/PM) conversion characteristics of the (memoryless) HPA nonlinearity. In particular, the most commonly used models for nonlinear amplifier [39] is solid state power amplifier (SSPA) for mobile applications and traveling wave tube amplifier (TWTA) for satellite applications.

2.3.1 Satellite Communications

The TWTA is usually located at the satellite side. The AM/AM and AM/PM characteristics for a TWTA according to Saleh Model [39] are:

$$\begin{aligned} A\{\rho\} &= \frac{\rho}{1+\frac{\rho}{2A_{sat}}} \\ \Phi\{\rho\} &= \frac{\pi}{3}\frac{\rho^2}{\rho^2+4A_{sat}^2}, \end{aligned} \tag{2.13}$$

where A_{sat} is the output amplitude saturation.

2.3.2 Radio/Terrestrial Communications

In radio/terrestrial communications (include broadcasting), SSPA is located at the transmitter end. The input-output relationship of SSPA can be modeled as

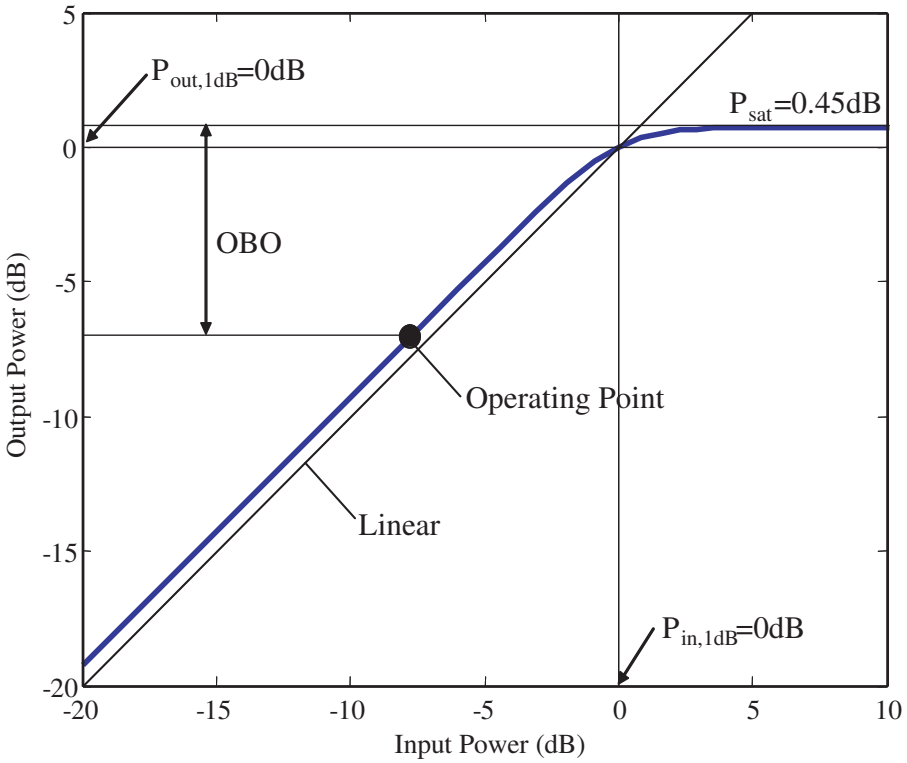

Figure 2.4. Normalized AM/AM characteristic of an SSPA model on frequency range of 1.7-3.0 GHz with $p = 4$

[39]:

$$\begin{aligned} A\{\rho\} &= \frac{\rho}{\left[1 + \left(\frac{\rho}{A_{sat}}\right)^{2p}\right]^{\frac{1}{2p}}} \\ \Phi\{\rho\} &= 0, \end{aligned} \tag{2.14}$$

where the parameter p control the smoothness of the transition from the linear region to the saturation region.

For the radio communications system, this dissertation considers Wireless local area network (LAN) application as an example [40]. The considered SSPA is assumed to be applied in frequency range of 1.7-3GHz [41] where Wireless LAN is usually operated. By investigating some practical SSPAs in this frequency range, we search suitable value of smoothness factor p.

It is found that a typical SSPA in this frequency range has output power at 1dB compression ($P_{out,1\text{dB}}$) of 50dBm with saturated output power (P_{sat}) of 50.42dBm. Here, the $P_{out,1\text{dB}}$ is about 0.42dB lower than the P_{sat}. The observation of (2.14) for various value of p to obtain $P_{1\text{dB}}$ 0.42dB lower than P_{sat} indicates that the appropriate p for Wireless LAN application is $p = 4$. The normalized relation of input and output power (dB) of SSPA with $p = 4$ is shown in Fig. 2.4.

To increase the efficiency of SSPA, we should use the SSPA at its input saturation power. Here, we define the input saturation is at its 1dB power compression ($P_{1\text{dB}}$). Therefore, it is convenient to set $P_{in,1dB} = 0\text{dB}$. As a consequence to normalization, we also set $P_{out,1\text{dB}} = 0\text{dB}$. The normalized SSPA characteristics is then shown in Fig. 2.4. This figure shows the $P_{out,1\text{dB}}$ compression point is about 0.45dB below the output saturation point P_{sat}. The output back-off (OBO) to let the signal operate in linear region of SSPA is then defined as

$$\text{OBO} \triangleq 10 \times \log_{10}\left(\frac{P_{sat}}{\tilde{P}_{out}}\right) \text{dB}, \tag{2.15}$$

where $\tilde{P}_{out}$ is the output power at the operating point.

2.4. Performances Evaluation

This section describes the evaluation of the PSD performance when the system suffers from nonlinear channel. When the transceiver signal suffers from nonlinear distortion introduced by HPA, the system experiences two main problems i.e. OOB spectrum radiation and BER performance degradation. Subsection 2.4.1 discusses the PSD while the Subsection 2.4.2 the BER performance.

2.4.1 Power Spectral Density

The previous PSD plotted in Fig. 2.3 only applies when the multicarrier signal does not suffer from nonlinearities. If any signals described in Section 2.1 suffer from nonlinear distortion, the output signal will suffer from intermodulation distortion resulting in energy being generated at frequency outside the allocated

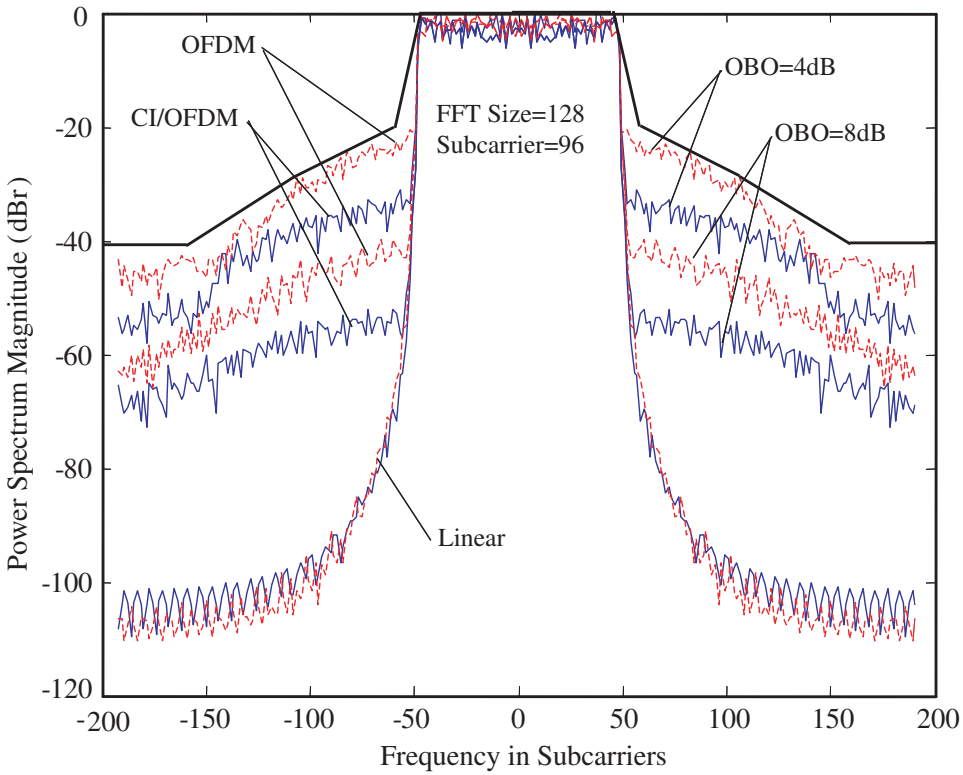

Figure 2.5. OOB spectrum radiation vs OBO for QPSK and 64QAM modulation

bandwidth. This phenomenon is often denoted as OOB spectrum radiation.

Fig. 2.5 shows the OOB radiation for OBO=4dB and OBO=8dB. It is shown that higher OBO is better to obtain lower OOB spectrum radiation. The higher OBO, however, decreases the efficiency of a HPA. With the same OBO=4dB, CI/OFDM has a better PSD i.e. about 15dB lower than the OOB spectrum of OFDM system. When the OBO increases to OBO=8dB, the CI/OFDM provides lower OOB spectrum than that od the OFDM system by 20dB. This figure confirms that the CI/OFDM system has better PSD performance (with lower OOB) over a nonlinear channel. This better performance is guaranteed by lower PAPR level than the PAPR of OFDM system.

2.4.2 Bit-Error-Rate

The BER performance is an important aspect to verify the effectiveness of a communication system design. The performance is usually drawn with signal-to-noise ratio (SNR or S/N) or energy bit per noise (E_b/N_0). Both of them are usually presented in decibel (dB). Relation of SNR and E_b/N_0 can be mathematically described as

$$\frac{S}{N} = \frac{E_b}{N_0} \cdot \log_2(Q) \cdot R \cdot L, \tag{2.16}$$

where Q is the number of constellation points, R is a coding rate, and L is an oversampling factor. The value of Q for quadrature phase shift keying (QPSK), 16-quadrature amplitude modulation (QAM), and 64QAM is 4, 16 and 64, respectively.

Binary data can be mapped into Q-QAM symbols based on a Gray mapping i.e. a mapping that based on only one bit difference. Therefore, we can derive a theoretical BER based on the assumption that data are mapped using a Gray mapping. It is important to note that the derived BER performances in this chapter are for BER $\leq 10^{-4}$. Thus the approximation of symbol error rate is valid for this purpose.

QPSK

QPSK has 4 constellation points i.e. $1+j$, $1-j$, $-1+j$, and $-1-j$ as shown in Fig. 2.6. Each QPSK symbol is a mapping of the 2 information bits. This figure shows the areas of symbol error rate ξ. The probability of one symbol error can be computed as

$$\begin{aligned} \xi &= \frac{1}{4} \cdot \frac{1}{\sigma\sqrt{2\pi}} e^{-\frac{(x+\delta)^2}{2\sigma^2}} \\ &= \frac{1}{8} \operatorname{erfc}\left(\sqrt{\frac{\delta^2/\sigma^2}{2}}\right). \end{aligned} \tag{2.17}$$

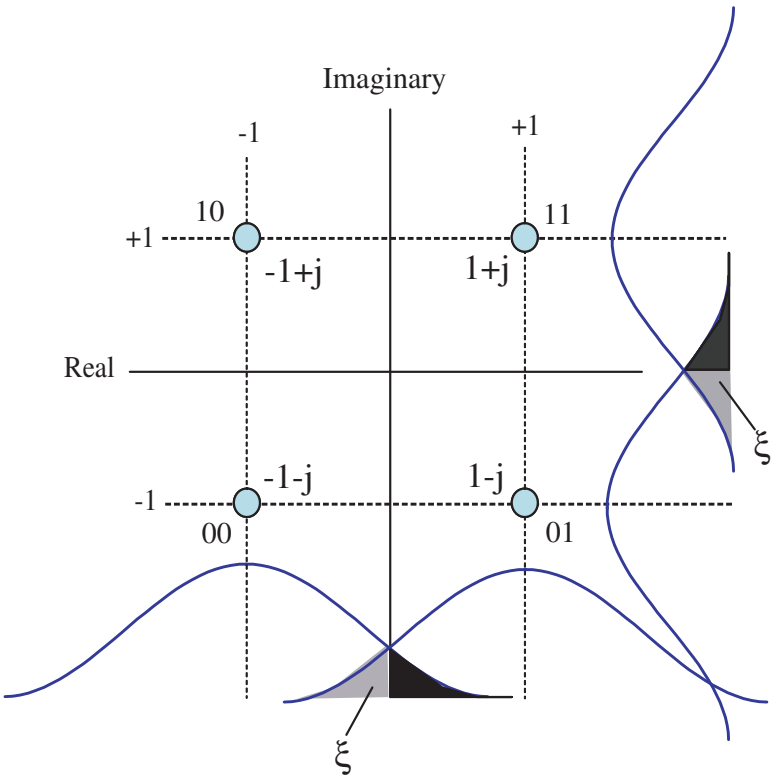

Figure 2.6. A QPSK constellation and the symbol error rate ξ

where $\text{erfc}(x) = \frac{2}{\sqrt{\pi}} \int_x^\infty e^{-u^2} du$. Now, the total BER of a QPSK modulation is

$$\begin{aligned} \text{BER}_{QPSK} &= \frac{1}{2} \cdot \xi \cdot 4 \cdot 2 \\ &= \frac{1}{2} \text{erfc} \left(\sqrt{\frac{\delta^2/\sigma^2}{2}} \right). \end{aligned} \tag{2.18}$$

Because in a QPSK, $S = \frac{1}{2} \left(\delta\sqrt{2}\right)^2$ and $N = \sigma^2$, the (2.18) can be expressed as

$$\text{BER}_{QPSK} = \frac{1}{2} \text{erfc} \left(\sqrt{\frac{S/N}{2}} \right). \tag{2.19}$$

From (2.16), S/N can be represented in E_b/N_0. Since the QPSK symbol has 2 information bits, it satisfy $S/N = E_b/N_0 \times 2$. Thus, the (2.19) can be expressed in E_b/N_0 as

$$\begin{aligned} \text{BER}_{QPSK} &= \frac{1}{2} \text{erfc} \left(\sqrt{2 \times \frac{E_b/N_0}{2}} \right) \\ &= \frac{1}{2} \text{erfc} \left(\sqrt{E_b/N_0} \right) \end{aligned} \tag{2.20}$$

64QAM

64QAM has 64 constellation points as a combinations of $\pm 7, \pm 5, \pm 3$, and ± 1. Each 64QAM symbol contains 6 information bits. The 64 constellations and symbol error rate are shown in Fig. 2.7. It is important to note that we assume a symbol is error detected just on the nearest neighbor symbols. This assumption is reliable for BER of less than 10^{-3}. Therefore, similar to the BER derivation of QPSK, we can derive a theoretical BER of 64QAM as follow. The probability of a 64QAM symbol error is

$$\begin{aligned} \xi &= \frac{1}{64} \cdot \frac{1}{\sigma\sqrt{2\pi}} e^{-\frac{(x+\delta)^2}{2\sigma^2}} \\ &= \frac{1}{128} \text{erfc} \left(\sqrt{\frac{\delta^2/\sigma^2}{2}} \right). \end{aligned} \tag{2.21}$$

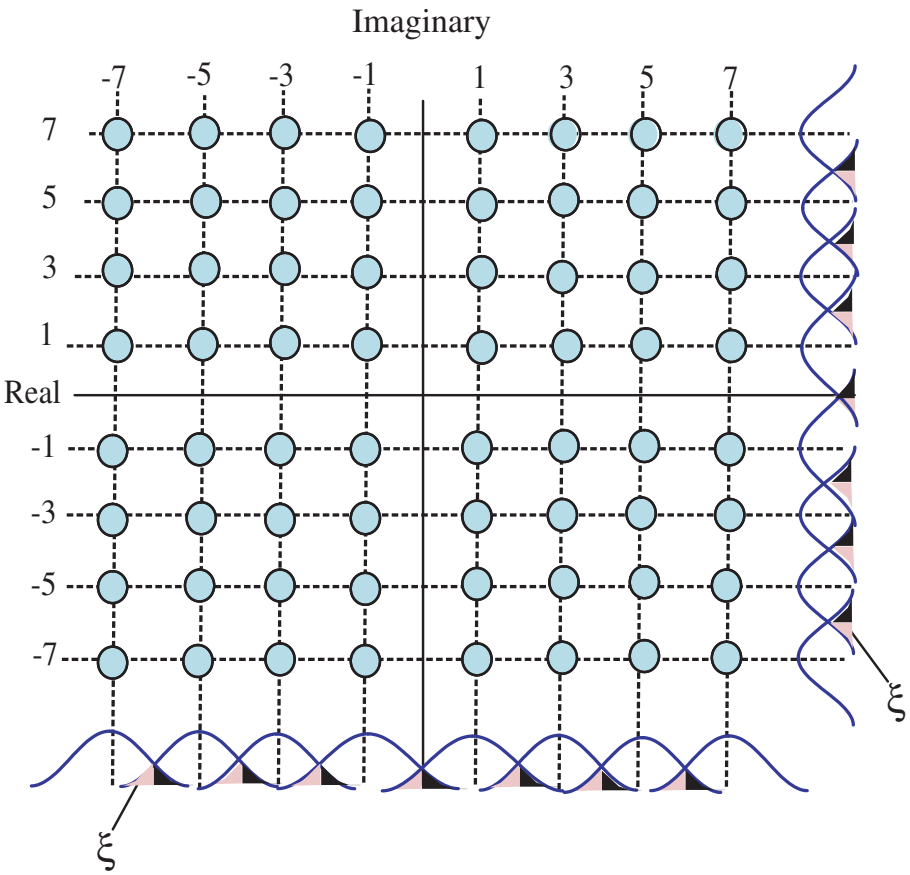

Figure 2.7. A 64QAM constellation and the symbol error rate ξ

The total BER of a 64QAM modulation becomes

$$\begin{aligned} \mathrm{BER}_{64QAM} &= \frac{1}{6} \cdot \xi \cdot 2 \cdot 7 \cdot 16 \\ &= \frac{7}{24} \operatorname{erfc}\left(\sqrt{\frac{\delta^2/\sigma^2}{2}} \right). \end{aligned} \tag{2.22}$$

Since in a 64QAM modulation, $S = \frac{1}{2}\left(\delta\sqrt{42}\right)^2$ and $N = \sigma^2$, the (2.22) can be expressed as

$$\mathrm{BER}_{64QAM} = \frac{7}{24} \operatorname{erfc}\left(\sqrt{\frac{S/N}{42}} \right). \tag{2.23}$$

From (2.16), S/N can be represented in E_b/N_0. Since a 64QAM symbol contains 6 information bits, thus it satisfies $S/N = E_b/N_0 \times 6$. Therefore, the (2.23) can be expressed in E_b/N_0 as

$$\begin{aligned} \mathrm{BER}_{64QAM} &= \frac{7}{24} \operatorname{erfc}\left(\sqrt{6 \times \frac{E_b/N_0}{42}} \right) \\ &= \frac{7}{24} \operatorname{erfc}\left(\sqrt{\frac{E_b/N_0}{7}} \right) \end{aligned} \tag{2.24}$$

Figs. 2.6 and 2.7 show that the 64QAM contains higher number of information bits than the QPSK i.e. 6 bits for 64QAM and 2 bits for QPSK. As a consequent of higher bits rate, the 64QAM is sensitive to the noise and the nonlinear distortion. On the other hand, it is a well-known that 64QAM modulation has smaller Euclidian distance so that the probability of error in 64QAM is higher than that of the QPSK.

The sensitivity of 64QAM to the noise is clearly shown by (2.23) or (2.24). By plotting the BER curves of (2.23) and (2.24), it is easy to find that about 12dB in E_b/N_0 (or S/N) is required by 64QAM to have the same BER as QPSK. The sensitivity of 64QAM due to the nonlinear channel such as clipping is shown in Fig. 2.8. The BER performance in Fig. 2.8 is plotted with clipping ratio (CR) of CR=1.6. The detail of clipping and CR value will be presented in Chapter 3 and Chapter 6.

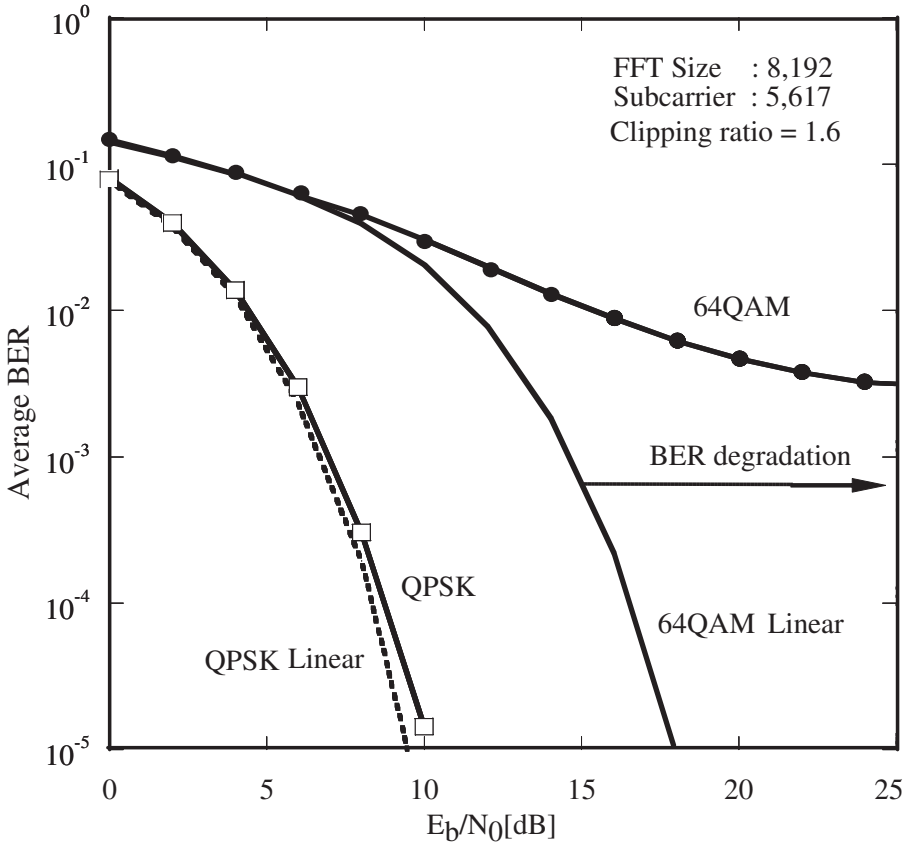

Figure 2.8. BER degradation of QPSK and 64QAM on the nonlinear channel due to the clipping

The BER degradation is defined as the difference between the required E_b/N_0 (or S/N) to ensure a fixed BER e.g. 10^{-3}) in the presence of nonlinear HPA and the linear channel as

$$\text{BER} = (E_b/N_0)_{HPA} - (E_b/N_0)_{linear}. \tag{2.25}$$

Fig. 2.8 shows the BER curves of QPSK and 64QAM symbols. It is shown that the BER degradation in QPSK with CR=1.6 is negligible, however, 64QAM has an unacceptable degradation (goes to infinity). The curve of 64QAM has a residual BER beyond the $BER = 10^{-3}$. Finally, we can conclude that a multilevel modulation, such as 16QAM and 64QAM, is more sensitive to the distortion caused by a nonlinear channel.

Chapter 3

OFDM-FM for Satellite Communication

THIS chapter describes a method for Japanese digital television transmission using satellite communications system related to the PAPR problem of OFDM signal transmission via the satellite. However, the method can be adapted for any digital television based on OFDM technology. Most of the ideas presented here were first described in literatures [42], [43] and more recently in [44]. The basic idea is to send the OFDM signals through FM modulation via the satellite link. The proposed system will not affect the configurations of existing broadcasting transmitters and widely used television receiver sets. Here, OFDM television signals are subjected to secondary modulation by the FM due to its characteristic of constant signal envelope. Thus, the efficient transmission via satellite is obtained.

For improving the transmission characteristic due to high PAPR level of the OFDM signal, it is suggested to use clipping as the simplest technique. By the clipping, the PAPR of OFDM signals can be limited so that unwanted expansion of the FM signal outside the desired bandwidth is reduced and FM gain can be increased. If the clipping of OFDM signal is deeper, the PAPR can be made smaller, but BER performance is degraded. On the other hand, the FM modulation index can be increased in effect by the clipping, so that FM gain can be increased. Therefore, this chapter presents the optimization of clipping ratio

considering the trade-off.

In this chapter, the relationship between the degree of clipping and the BER of the OFDM signals is derived and the FM gain, derived from the bandwidth of the OFDM signal and the bandwidth of the FM signals considering clipping, is computed. In this way, an optimum clipping level is derived. In the conventional theoretical calculation of the FM gain, the input signal is often assumed to be a sinusoidal wave with a small PAPR (3 dB) [45]. However, it is considered inappropriate to apply this approach directly to OFDM signals with a large PAPR, so that most of the power is concentrated at or below the average value. In this chapter, the concept of the PAPR of the OFDM baseband signal is introduced into the calculation of the FM gain. It is shown that the FM gain becomes larger even with the same bandwidth if the PAPR is reduced.

First, in Section 3.1 the configuration of the proposed system is described. The relationship between the peak voltage of the OFDM signal and the bandwidth of the FM signal is shown. In Section 3.2, the PAPR when the OFDM signals are clipped is derived by simulation and the spectral spreading of the OFDM signals due to clipping and the BER characteristics are evaluated. In Section 3.3, the transmission characteristics of the FM modulation scheme for a signal with large PAPR are theoretically analyzed. In Section 3.4, optimization of the clipping is discussed in terms of the FM gain determined from the bandwidth of the FM signal and the peak voltage of the OFDM signals. Also, in section 3.5, channel design assuming a real satellite is performed for both the OFDM/FM system proposed in this paper and the direct transmission of the OFDM, and the two are compared.

3.1. System Configuration

The proposed system configuration is shown in Fig. 3.1(a). On the transmitter side, the output of the existing OFDM modulator is applied to the FM modulator. The relay section is the satellite channel using FM signals. At the receiving ground station, the secondary modulation is removed by FM demodulation and then the signal is broadcasted by the terrestrial broadcast network. Hence, in

the present system, the path from FM modulation to FM demodulation via the satellite channel is transparent in function, although a certain effect on the overall transmission characteristics is permitted.

In [4], the bandwidth of the OFDM signals is specified as 5.572–5.575MHz. Here, it is assumed to be 6 MHz. The bandwidth of the FM signals in the present system depends on the peak voltage of the OFDM signal or the PAPR. The one-side maximum frequency shift of the FM signal is expressed by as follows [45]:

$$\Delta F = V_{max} \times \frac{k_f}{2\pi} \tag{3.1}$$

Here V_{max} is the peak voltage of the OFDM signal within one symbol and k_f is a system parameter. The relationship between V_{max} and the PAPR is given by

$$\begin{aligned} \underset{0 \leqslant t < T}{\text{PAPR}} &= \frac{P_{max}}{P_{avg}} \\ &= \frac{V_{max}^2}{\sigma^2} \end{aligned} \tag{3.2}$$

$$V_{max} = \sigma \times \sqrt{PAPR} \tag{3.3}$$

Here T denotes one symbol length of the OFDM and σ is the rms (root mean square) value of the OFDM signal. From (3.1) and (3.3), we obtain

$$\Delta F = \sigma \times \sqrt{PAPR} \times \frac{k_f}{2\pi} \tag{3.4}$$

Eq. (3.4) states that the maximum frequency shift of the FM signals is proportional to the root-mean-squared (rms) amplitude of the OFDM signals and the square root of the PAPR. Next, let us describe the clipping of the OFDM signals. Fig. 3.1(b) shows a configuration using filtering to produce out-of-band (OOB) spectral suppression, and clipping by oversampling (with a sampling factor of L).

When the PAPR of the analog signal is derived, the peaks to be clipped between the sample intervals may be overlooked if the number of samples is too small. Therefore, it is necessary to make this value as large as possible in realization. If L is large, the PAPR in the presence of clipping can be evaluated

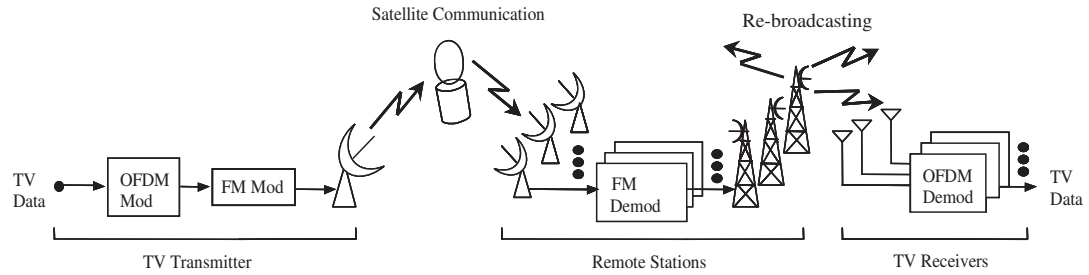

(a) OFDM/FM transmission over satellite communications system

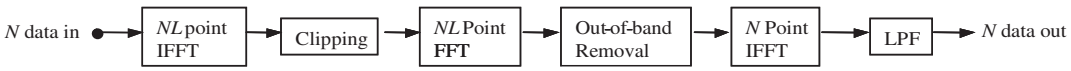

(b) OFDM clipping with oversampling factor of L and filtering

Figure 3.1. OFDM/FM transmission using satellite communications system

accurately. Hence, the PAPR of the clipped OFDM signals depends on the magnitude of the oversampling factor L. For instance, if $L = 1$, this becomes sampling at the Nyquist frequency [37, 46]. In Fig. 3.1(b), N denotes the number of carriers of the OFDM signals. After taking the inverse Fourier transform with $L \times N$ points, clipping is applied. Since clipping is a nonlinear operation, the OOB spectrum of the signal is broadened. Therefore, the results are reconverted by the FFT with $L \times N$ points. Then these components are suppressed by frequency domain filtering (FDF).

3.2. PAPR of OFDM Signals and Transmission Characteristics

3.2.1 PAPR

If the OFDM signal is $s(n) = r(n)e^{j\phi(n)}$ the amplitude component after clipping with voltage A_{max} are

$$r_c(n) = \begin{cases} r(n), & \text{for } r(n) \leqslant A_{max} \\ A_{max}, & \text{for } r(n) > A_{max} \end{cases} \tag{3.5}$$

Hence, the n-th sampled value of the clipped signal is given by $s_c(n) = r_c(n)e^{j\phi(n)}$. In this paper, a soft limiter in which phase rotation can be neglected is assumed as the element for clipping [46]. Also, as the degree of clipping, the clipping ratio (CR) is defined as follows:

$$CR = \frac{A_{max}}{\sigma} \tag{3.6}$$

where σ is the mean-square value of the OFDM signal level.

For instance, CR = 1.4 denotes the case in which the maximum level of the clipped signal is about 3dB higher than the average level. As described in section 3.1, a bandpass filter is used after the clipping to suppress the spectrum caused by clipping. Therefore, a peak larger than the clipping level appears due to the waveform response. Although clipping can reduce the PAPR, the PAPR of the filter output signal is larger than the value determined from CR.

Table 3.1 lists the parameters used in the computer simulation carried out for evaluation of various characteristics of the PAPR and those after clipping. As the modulation format for the OFDM signals, the 64QAM reference in the specification of the digital terrestrial broadcast services in Japan and the QPSK for comparison are used.

The PAPR after clipping and filtering is calculated by (3.2). Fig. 3.2(a) shows the complementary cumulative distribution function (CCDF) of the PAPR for the case of 64QAM for several values of CR, Also shown in Fig. 3.2(a) is the PAPR

Table 3.1. Simulation conditions of OFDM-FM

	Parameters	**Value(s)**
Transmitter	Modulation	QPSK, 64QAM
	FFT size	8,192
	Number of subcarriers	5,617
	Oversampling factor (L)	1,4587
	GI length (T_{GI})	1,024 (ISDB-T Mode 3)
	Clipping ratio (CR)	0.8 - 2.6
	BW of satellite transponder	36MHz
	BW of OFDM for Digital TV	6 MHz
Channel	SSPA, TWTA	Assumed to be operated in linear region
	AWGN	–
Receiver	Equalizer	perfect

distribution in the absence of clipping. We observe the PAPR level at CCDF of 10^{-4}. CCDF of 10^{-4} means that the probability of PAPR exceed a determined value (shown in its abscissa) is 10^{-4}. As a sampling factor L, we use a commonly employed value of $L = 1.4587$. As the clipping becomes deeper, the PAPR can be made smaller. Since the amplitude components contains information in back QAM format, increased deterioration of the BER is expected due to waveform distortion. This will be discussed later. Fig. 3.2(b) shows the PAPR values when QPSK is used as a modulation format. Since the amplitude components are smaller in QPSK than in QAM, it is possible to use deeper clipping (with a smaller CR) and a substantial improvement of the PAPR is expected.

3.2.2 Out-of-Band Radiated Power

By the nonlinear operation of clipping, the spectrum of the OFDM signal is spread outside the bandwidth, and the signal power within the bandwidth is decreased accordingly. Fig. 3.3 shows the signal spectrum power densities immediately after clipping and after filtering. From Fig. 3.3, it is found that the out-of-band power density increases to 33 dB at the maximum near the signal. When FM

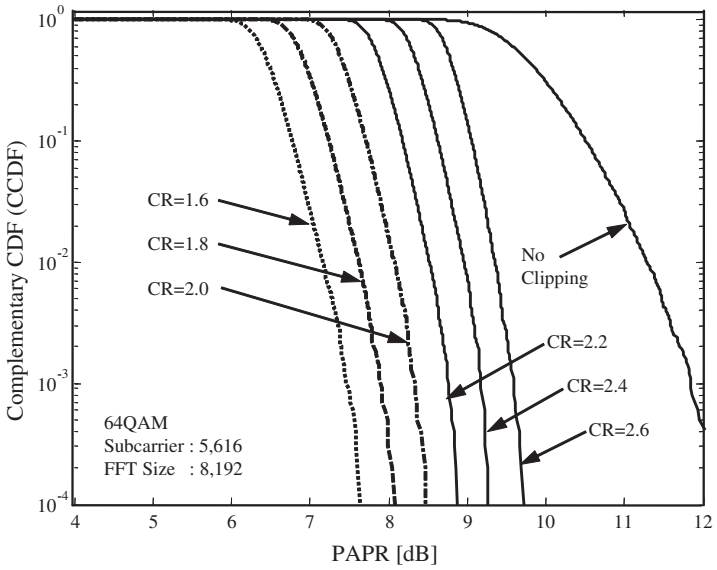

(a) PAPR performance of 64QAM

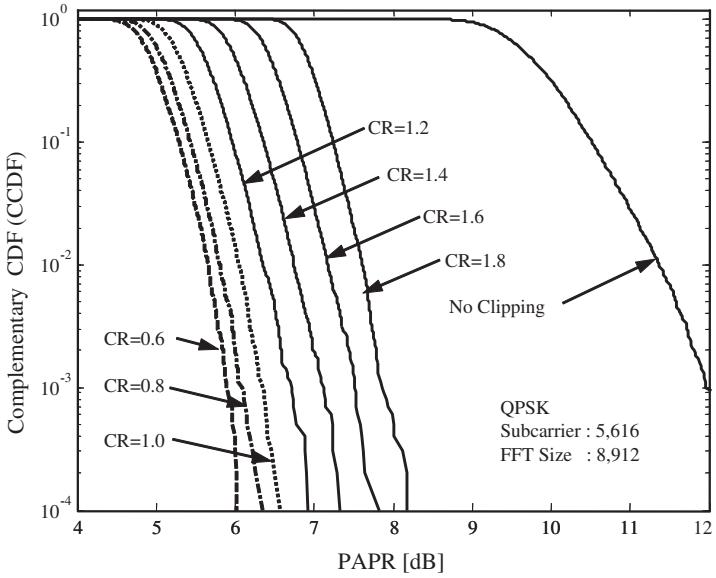

(b) PAPR performance of QPSK

Figure 3.2. Relationship between the PAPR and several CR values

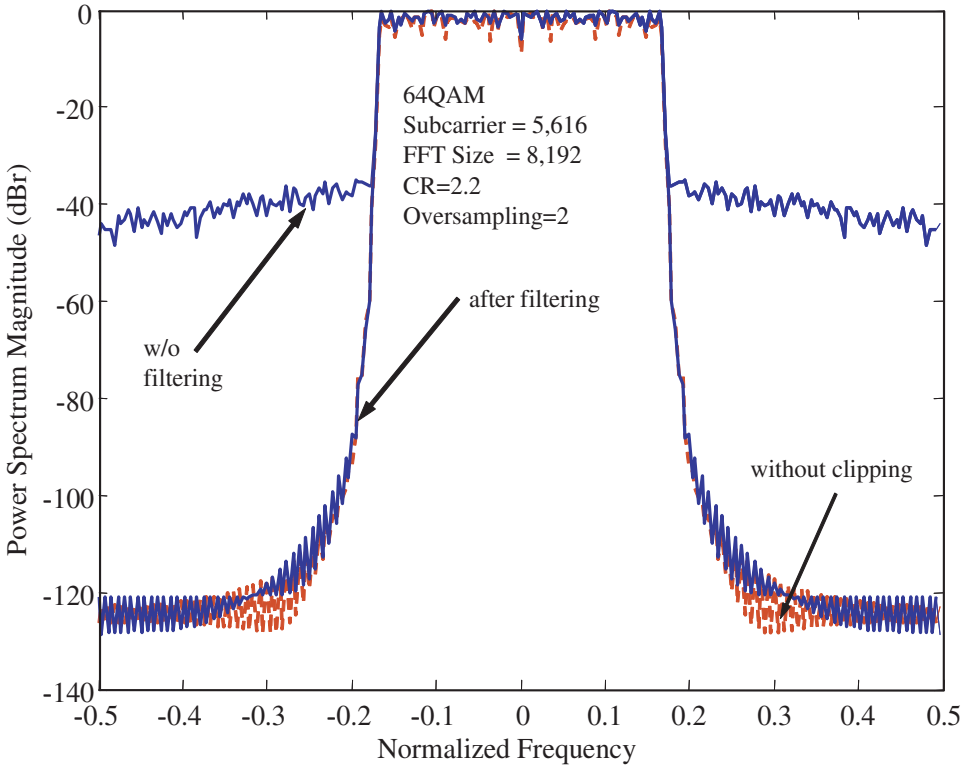

Figure 3.3. Power spectral density of a clipped OFDM

modulation is considered as secondary modulation, as in the present system, the bandwidth spread of the OFDM signal, which is the first modulated wave, equivalently decreases the FM modulation index and the FM gain is reduced. For suppression of the out-of-band power, use of an FIR (Finite Impulse Response) time domain filter with 103 taps is assumed in [37]. It is likely that the structure will be complicated in practice. On the other hand, the method used in this paper is to suppress the OOB components by filtering (a frequency domain filtering (FDF) [35], with an FFT size of 8,192). Since the FFT size is finite in real calculations, an ideal filter is not realized and power components outside the bandwidth still remain. However, a spectrum almost identical to that of without clipping can be obtained.

3.2.3 BER Characteristics

The transmission characteristics of the present system must be evaluated by the entire path sequence in the receiving system with OFDM-clipping, and FM modulation and demodulation. Of these, FM modulation and demodulation are essentially linear with regard to the waveform transmission. The BER deterioration due to the waveform distortion can be evaluated by the effect of clipping for the OFDM signal. The effect of FM modulation is evaluated, as noted later, from the relationship between the received C/N in the wireless channel and the S/N of the FM demodulator.

The OFDM signal is subject to waveform distortion as well as an increase in the out-of-band spectrum by clipping. Further, the BER characteristics are degraded by filtering. The BER characteristics are derived for several values of CR and the results are shown in Fig. 3.4. Fig. 3.4(a) presents the results for 64QAM and 3.4(b) the results for QPSK. From Fig. 3.4(a), it is seen that the effect of clipping is significant in 64QAM, as expected. The deterioration of the BER is very substantial when CR is less than 2.0. On the other hand, it is found from Fig. 3.4(b) that CR can be reduced to 1.4 in QPSK. This is because QAM contains much information in the amplitude.

3.3. FM Modulation and Demodulation

3.3.1 S/N and FM Demodulator

Fig. 3.5 shows an example of the waveform and instantaneous power when clipping is applied or not applied to the OFDM signal. In Fig. 3.5, A indicates the waveform with CR = 0.5, B indicates that with CR = 1.5. and C indicates that without clipping. As described above, the maximum frequency shift of the FM signal is dependent on the voltage peak of the input signal. According to (4.75) in [45], if the modulation signal is $m(t)$, the power of the demodulated signal is given by

$$S_0 = \left(\frac{k_f}{2\pi}\right)^2 \overline{m^2(t)}. \tag{3.7}$$

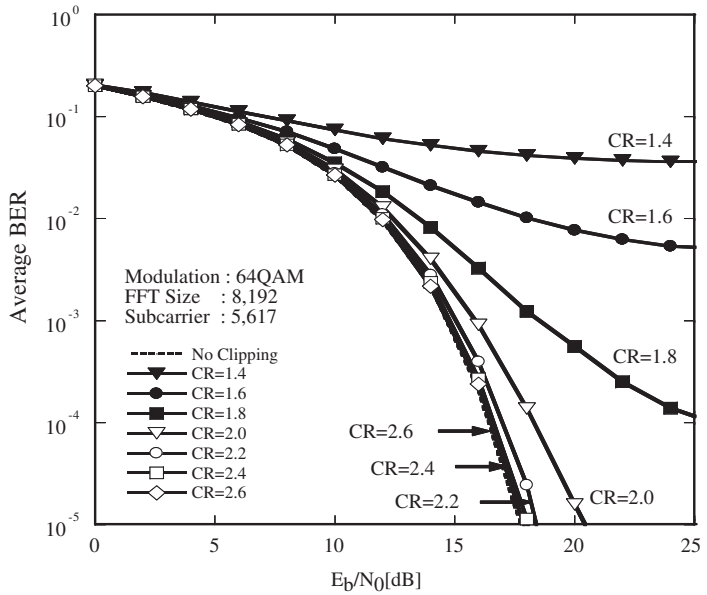

(a) BER performance of 64QAM

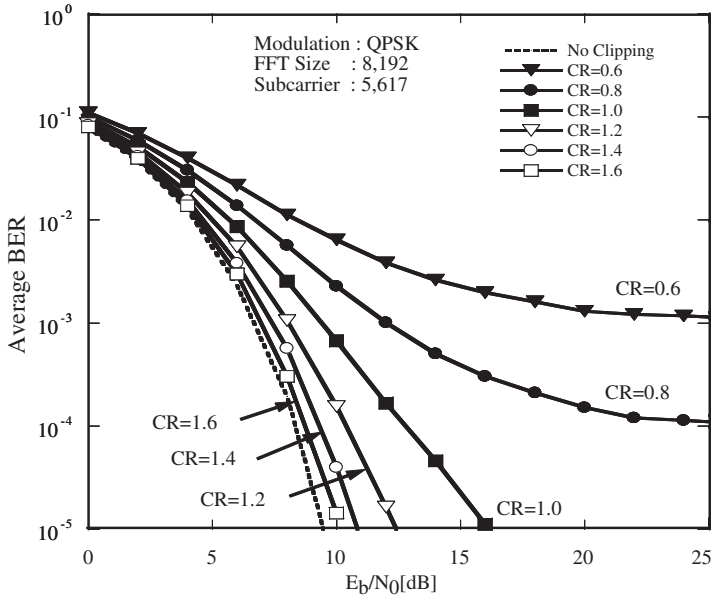

(b) BER performance of QPSK

Figure 3.4. BER performance of 64QAM and QPSK for several CR values

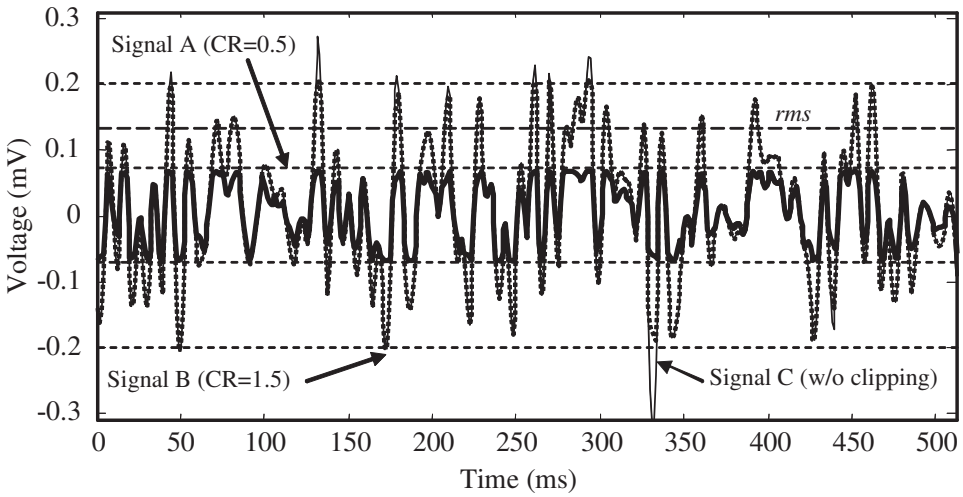

Figure 3.5. Waveform of OFDM signals with and without clipping

Here k_f is the system constant of the FM demodulator.

When the baseband signal is assumed to be sinusoidal, the signal power in the FM demodulator output is as follows, according to (4.91) of [45]:

$$S_0 = \frac{(\Delta F)^2}{2} \tag{3.8}$$

However, in the case of a waveform which has impulsive peaks, as in the OFDM, it is difficult to use (3.8) directly, and the following treatment is considered. With reference to (4.90) in [45], in which the modulation signal is treated as a sinusoidal wave, it is considered that the following equation holds in general for non-sinusoidal waves such as that of the OFDM as a modulation signal. Let us replace $\cos 2\pi f_m t$ on the right hand side of (4.90) in [45] with $A(t)$, obtaining

$$\begin{aligned} \frac{k_f}{2\pi} m(t) &= \Delta F \times A(t) \\ \text{that is} \quad m(t) &= \left(\frac{2\pi}{k_f}\right) \Delta F \times A(t). \end{aligned} \tag{3.9}$$

Here $A(t)$ is an OFDM modulation signal. Hence, the average power of the FM

demodulated signal is obtained from (3.7) and (3.9),

$$\begin{aligned} S_{0OFDM} &= \left(\frac{k_f}{2\pi}\right)^2 \overline{m^2(t)} \\ &= (\Delta F)^2 \times \overline{A^2(t)} \end{aligned} \tag{3.10}$$

From the definitions of the average power and peak power of the OFDM signal and the PAPR, we have

$$\overline{A^2(t)} = \frac{1}{PAPR}. \tag{3.11}$$

Here the peak voltage $A(t)$ is assumed to be normalized to 1.0. Therefore, by (3.10),

$$S_{0OFDM} = (\Delta F)^2 \times \frac{1}{PAPR}. \tag{3.12}$$

If it is taken into account that the PAPR of the sinusoidal wave is 2, the (3.12) may be considered as a generalization of (3.8) that is derived with the modulation signal as a sinusoidal wave. From (3.12) and (4.88) of [45], the signal-to-noise power ratio (SNR) of the OFDM signal of the FM demodulator output is

$$\begin{aligned} \frac{S}{N} &= \left(\frac{3B}{f_m^3}\right)\left(\frac{\Delta F^2}{PAPR}\right)\left(\frac{C}{N}\right) \\ &= \left(\frac{3 \times 2(\Delta F + f_m)}{f_m^3}\right)\left(\frac{\Delta F^2}{PAPR}\right)\left(\frac{C}{N}\right) \\ &= \frac{6}{PAPR}\beta^2(\beta+1)\left(\frac{C}{N}\right) \end{aligned} \tag{3.13}$$

where β is the modulation index, such that $\beta = \frac{\Delta F}{f_m}$, where f_m is the bandwidth of OFDM. Also the bandwidth B of FM signal is obtained from (4.46) in [45] as

$$B = 2\,(\Delta F + f_m) \tag{3.14}$$

The above can easily be predicted physically from the power distribution of the OFDM signal. However, in contrast to the conventional analysis of the FM gain using sinusoidal waves, which are easily treated, the present method considers the PAPR, so that the method is effective for quantitative evaluation of the FM

gain for arbitrary signals, such as OFDM.

3.3.2 Satellite Occupancy Bandwidth and the Received S/N

For ground stations installed on remote islands, it is desirable to make this size as small as possible for economy of operation. Also, if the high carrier-to-noise power ratio (C/N) required for the 64QAM demodulation is considered, the system is expected to be power limited. Under this assumption, secondary modulation by FM is used because it can increase the power by the use of the bandwidth. The case of using the total bandwidth of the satellite repeater per channel to make the FM gain greater is compared with the case in which half of the bandwidth is used.

In the FM modulation format, the modulation index can be made larger by taking a frequency shift that is larger with respect to the bandwidth of the input signal. In this way, a larger FM gain can be obtained.

On the other hand, the bandwidth B of the FM signal is expressed by (3.14). Therefore, ΔF becomes

$$\Delta F = \frac{B}{2} - f_m \tag{3.15}$$

The allowable FM bandwidth B is determined by the use condition of the satellite repeater. If the bandwidth of the satellite repeater is B=36MHz, and one FM signal wave is transmitted with the entire bandwidth of the repeater (**Case 1)**, B = 36MHz. If half bandwidth is used (**Case 2)**, B = 18 MHz. Therefore, ΔF is 12MHz in **Case 1** and 3 MHz in **Case 2**. Hence, the modulation index for each case is

$$\begin{aligned} \beta &= \frac{12}{6} = 2 \ (\textbf{Case 1}) \\ \beta &= \frac{3}{6} = 0.5 \ (\textbf{Case 2}) \end{aligned} \tag{3.16}$$

When the input C/N is sufficiently large (more than 10 dB), the relationship between the S/N in the FM demodulator output and the input C/N is shown above as being given by (3.13). From (3.16) and (3.13), the relationships between

the S/N and the C/N for Cases 1 and 2 above are

$$\textbf{Case 1}: \left(\frac{S}{N}\right)_1 = \frac{72}{PAPR} \times \frac{C}{N} = \left(\frac{C}{N}\right)_{dB} + 18.6 - PAPR(\text{dB}) \tag{3.17}$$

$$\textbf{Case 2}: \left(\frac{S}{N}\right)_2 = \frac{2.25}{PAPR} \times \frac{C}{N} = \left(\frac{C}{N}\right)_{dB} + 3.5 - PAPR(\text{dB}) \tag{3.18}$$

From (3.17) and (3.18), it is found that the S/N at the FM demodulator output, namely, the S/N of the OFDM receiver signal, is smaller by the magnitude of the PAPR in this system. Also, a difference of about 15 dB is noticed in different use conditions of the bandwidth of the satellite receiver, namely, one wave/all repeater, or one wave/half repeater. The ratio of (C/N) and (S/N) given by (3.17) or (3.18) is the FM gain in the proposed system.

3.4. System Optimization

In Section 3.2, the variations of the PAPR in the presence of the clipping to the OFDM signal and the degradation of the BER due to the waveform distortion are derived. It is found that the degradation of the BER is more significant though the PAPR is improved, if the clipping is deeper (or the CR is smaller). The effect is more significant in 64QAM than in QPSK. Further, in Section 3.3, the relationship between the output S/N of the FM demodulator and the PAPR is presented. It is shown that the S/N is reduced by the PAPR (called S/N loss and PAPR-FM loss). From these relationships, it is demonstrated that the magnitude of clipping is in contradiction with the BER and S/N characteristics.

Let us discuss how to select the CR for the entire system. Figs. 3.6(a) and 3.6(b) show the BER degradation, the S/N loss by the PAPR, and their sum for 64QAM and QPSK as functions of CR. As the BER degradation, that of the

equivalent E_b/N_0 is used at a BER of 10^{-3}, which is the threshold value of the bit error rate before error correction that is widely used for OFDM reception and mobile communication demodulation. First, it is found from Fig. 3.6(a) that the sum of the two quantities almost always tends to decrease with an increase in the CR up to the vicinity of CR = 2.4 in 64QAM. As Fig. 3.6(b) shows, the sum approaches the minimum at about CR = 1.4 for QPSK. Hence, in each system, CR = 2.4 is chosen for the former and CR = 1.4 for the latter for the minimum total deterioration. Then, the value of the PAPR directly affecting the FM gain described in Section 3.3 is about 9.3 dB for 64QAM and 7.4 dB for QPSK. When these values are assigned in (3.17) and (3.18), the FM gain for Case 1 is 9.3dB for 64QAM and 11.2dB for QPSK, while they are 5.8dB for 64QAM and 3.9dB for QPSK for Case 2.

The degradation of the BER is 0.1dB for 64QAM and about 0.5dB for QPSK for their optimum CR values.

3.5. Channel Design (Noise Budget)

By using the results up to Section 3.4, channel design was performed for an OFDM/FM system transmitting over a satellite channel and its effectiveness was verified. The channel design was performed only for 64QAM, which is actually used for digital terrestrial broadcasting. The satellite used for channel design was assumed by way of example to be JCSAT-1B. The case of one-wave transmission of OFDM/FM wave in the bandwidth of 36 MHz (Case 1) and the case of two-wave transmission (Case 2) were studied. In addition, channel design was performed for an OFDM signal transmitted directly without FM modulation (Case 3). Three cases were compared from the operational point of view. In order to perform comparison under the same conditions, the aperture of the transmitting antenna of the ground station was $4.5m\phi$ and the receiving antenna aperture was $3.6m\phi$ for all cases. With regard to the location of the station in the channel design, studies are needed for various locations over the country, including remote islands, based on the antenna beam shape and rainfall data. In the present design, calculations were performed for a transmitting station in Tokyo

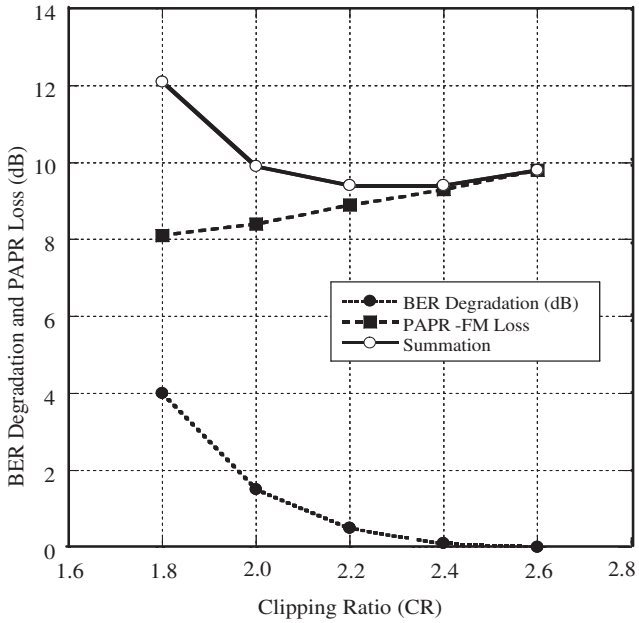

(a) 64QAM

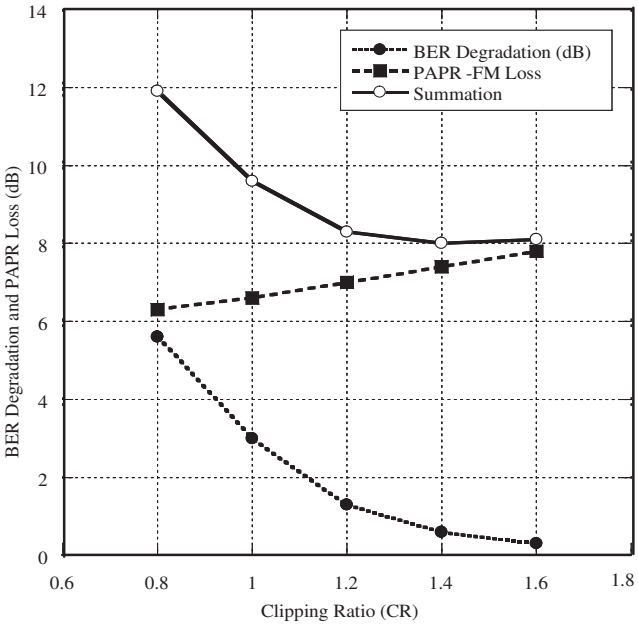

(b) QPSK

Figure 3.6. BER degradation and PAPR-FM loss as a function of CR

and a receiving station at Hachijojima Island as an example.

On the other hand, the satellite repeater amplifier can be operated at its saturation point by taking advantage of the constant amplitude for the FM signals in Case 1. Also, for Case 2, half of the satellite power (3dB) is assigned per wave. In order to reduce intermodulation due to multiple carrier transmission, a further back-off of 3dB (with a total output back-off (OBO) of 6 dB per wave) was assumed. Further, for Case 3, the output back-off was assumed to be that of the PAPR value (9.3dB at CCDF of 10^{-4}) of the OFDM signal after clipping. Note that in Case 3 the bandwidth of the repeater is only 6MHz. The total power other than the back-off was assigned. There are two conceivable ways to set the operating point of the satellite amplifier. In one approach, the satellite receiving power is made constant while the gain of the satellite amplifier is varied. In the other, the transmitting power of the ground station is reduced. Here, the latter method, which can be controlled for each carrier, was applied. Also, in this method, the transmitted power of the ground station can be made smaller at the time of back-off.

Table 3.2 shows the distribution of the signal power and the noise power from transmission at the ground station to reception by another ground station via a satellite. The present distribution is in accordance with the usual channel design method for satellite communications [47]. The upper portion of Table 3.2 indicates the uplink C/N, the middle portion shows the downlink C/N, and the lower portion presents the overall C/N and the S/N of the OFDM demodulator. Also shown in E2, in the lower portion is the downlink rainfall margin (according to the ITU-R Recommendation) needed to guarantee a non-operational rate of 0.05% (in terms of time, a total of about 4 hours in which the rain attenuation exceeds the specified margin over the year). The rain attenuation of the uplink is assumed to be compensated by the usual uplink power control.

In E3 of the lower portion, FM gain considering the PAPR of the OFDM signal are presented. Further, in E6 in the lower portion, the BER degradation of a 64QAM/OFDM signal due to clipping as derived in Section 3.2 is presented. The E7 shows the necessary S/N to obtain a BER of 64QAM with allowance for the deterioration in E6. The E8 shows the overall margin and represents the value of

Table 3.2. Comparison of three OFDM systems through a satellite communications

	1) OFDM-FM /Transponder	2) OFDM-FM /Half Transponder	3) OFDM /Transponder
Uplink (U)			
U1. ES. TX Power (dBW)	16.0	5.0	4.0
U2. ES. TX Losses (dB)	-2.9	-2.9	-2.9
U3. ES.Ant. Gain (dB)	56.4	56.4	56.4
U4. Uplink Loss (dB)	-206.9	-206.9	-206.9
U5. SAT G/T (dB/K)	12.2	12.2	12.2
U6. Bandwidth (dB-Hz)	-75.6 (36MHz)	-72.6(18MHz)	-67.8(6MHz)
U7. Boltz. Const(dBW)	228.6	228.6	228.6
U8. Uplink C/N (dB)	27.8	19.8	23.6
Downlink (D)			
D1. SAT. Power (dBW)	20.0	20.0	20.0
D2. Sat. Ant. Gain (dB)	36.0	36.0	36.0
D3. OBO (dB)	0	-6.0	-9.3
D4. Downlink Losses (dB)	-205.8	-205.8	-205.8
D5. ES.G/T(dB/K) (3.6m)	23.4	23.4	23.4
D6. Bandwidth(dB-Hz)	-75.6	-72.6	-67.8
D7. Boltz. Const(dBW)	228.6	228.6	228.6
D8. Downlink C/N (dB)	26.6	23.6	25.1
Evaluation (E)			
E1. Total C/N	24.1	18.4	21.3
E2. Rain Attenuation (0.05) (at Hachijojima)	-4.5	-4.5	-4.5
E3. FM Gain	9.3	-5.8	-
E4. FM Output S/N	28.9	8.1	-
E5. OFDM S/N	28.9	8.1	16.8
E6. BER degradation due to clipping (CR=2.4)	0.1	0.1	0.1
E7. Required S/N for	22.6	22.6	22.6
E8. Margin	6.3	×	×

- Satellite: JCSAT-1B, Ku-band (Up-link 14.25GHz, Down-link 12.5GHz)
- Earth Station Antenna : TX 4.5mϕ, RX 3.6mϕ
- Satellite Power Usage: 1. Saturation with one FM carrier, 2. OBO of 6dB with one FM carrier in half transponder, 3. OBO of 9.3dB with OFDM carrier
- Satellite Bandwidth: 1) 36MHz, 2) 18MHz, 3) 6MHz

E4 and to E7. For the present channel design, the following properties are found. (1) The scheme that enables transmission under the above conditions is limited to the case of one-wave/(all bandwidth of the repeater) with the OFDM/FM system. (2) Since the FM gain is small and the satellite power is 1/4 in the two-wave transmission scheme, transmission is not possible by itself. For transmission, a performance of at least 15dB is needed. This is unrealistic from the point of view of ground station size. (3) The OFDM direct transmission system has a large PAPR, so that the power use efficiency of the satellite repeater is poor (with a large back-off). The receiving S/N is about 12dB lower than that in the proposed system. Hence, the secondary modulation system using the FM proposed in this paper is found to be extremely effective for a system in which signals with a large PAPR such as OFDM are transmitted through a nonlinear amplifier.

Chapter 4

A New Design of Carrier Interferometry OFDM System

THE carrier interferometry OFDM (CI/OFDM) system has superior performance in terms of PAPR and BER performances in wireless environment. However, the complexity in practical implementation has been a major demerit. This chapter proposes a drastically low complexity design of CI/OFDM by utilizing FFT spreading instead of the current CI spreading. Also, to increase the throughput, we propose double FFT spreading with a *separator* for keeping the orthogonality between the code sets instead of pseudo-orthogonal carrier interferometry (POCI) codes in POCI/OFDM system. Our results show that the proposed technique is more efficient and has significant lower computational complexity than the current CI/OFDM system and POCI/OFDM system. First, we re-derive the concept of CI spreading rather than that has been introduced in the current system. It is found that CI/OFDM can be considered as an OFDM system that has a characteristic similar to a single carrier with cyclic prefix (SCCP) [48] though technically it is derived from the OFDM system. Second, we introduce a more realistic oversampling technique for CI/OFDM. As a consequence of this oversampling technique, our design has a small difference in signal waveforms compared with that of the conventional CI/OFDM and POCI/OFDM waveforms. Finally, we introduce the use of FFT to replace the conventional matrix multiplication of CI and POCI spreadings. We then call it as CI-FFT and POCI-FFT.

The results show significantly lower computational complexity of more than 90% compared with that of spreading using CI and POCI codes. The new design of CI/OFDM achieves a high frequency efficiency and very low computational complexity system while providing high BER performance in a frequency selective fading channel.

This chapter is organized as follows. Overview of CI Spreading in CI/OFDM system is presented in Section 4.1. Section 4.2 presents the proposed design. Comparison and possibility replacement of CI spreading with FFT spreading is presented in Section 4.3. Section 4.5 overviews the combiners. Numerical results of computational complexity reduction, PAPR and BER performances are presented in Section 4.7.

4.1. The Conventional CI Spreading

CI/OFDM was introduced in [5, 15, 16, 20, 29] and completely compiled in [14]. However, the spreading method in these references may result in a single carrier system with cyclic prefix (SCCP) [48] as commented in [49, 50]. As shown in (5)–(9) of [49], the CI spreading matrix in the conventional CI/OFDM can be expressed as

$$\mathbf{R} = \bar{\mathbf{W}}\,\bar{\mathbf{W}} = \begin{bmatrix} 1 & 0 & \cdots & 0 \\ 0 & 0 & & 1 \\ \vdots & & \ddots & \vdots \\ 0 & 1 & 0 & 0 \end{bmatrix}, \tag{4.1}$$

where $\bar{\mathbf{W}}$ is the inverse fast Fourier transform (IFFT) matrix.

For POCI/OFDM system, it was proven in (13)–(21) of [49] that the spreading with first code set can be shown as (4.1) while the spreading with the second code set is

$$\tilde{\mathbf{R}} = \mathbf{R}\,\Phi = \begin{bmatrix} 1 & 0 & \cdots & 0 \\ 0 & 0 & & \alpha^{(N-1)} \\ \vdots & & \ddots & \vdots \\ 0 & \alpha & 0 & 0 \end{bmatrix} \tag{4.2}$$

where $\alpha = e^{j\pi/N}$ and $\Phi = \text{diag}\left(1, \alpha, \alpha^2, \cdots, \alpha^{(N-1)}\right)$.

The facts in (4.1) and (4.2) show that the conventional CI spreading does not give any contributions results except just a re-arranging the input sequence. Therefore, it may lead to a conclusion that the conventional CI/OFDM has more computational complexity than SCCP [49] and may not give any improvements to the performance of OFDM system.

In this chapter, a new design of CI/OFDM system is proposed. The design results in a new OFDM system that has a similar characteristic to the SCCP. Observation on time domain response signal may show that the proposed new CI/OFDM is expected to have lower inter-carrier interference compared to the SCCP time domain response.

4.2. Proposed New Design of CI/OFDM and POCI/OFDM Systems

4.2.1 CI/OFDM system

The idea in the proposed method comes from the fact that guard-band is practically required to reduce the adjacent channel interference (ACI). Guard-band is also important to compensate an imperfect filter and spectral spreading due to the Doppler effect. Guard-band is simply done by zeroing the intended subcarrier (usually on each side of the band edges). In IEEE.802.11a [40], OFDM has 64 subcarriers to be generated, although only 48 subcarriers are actually used for the data transmission. The outer 12 subcarriers are zeroed as the guard-band while other 4 subcarriers used as pilot symbols for the channel estimation. In the proposed new CI/OFDM, we assume that generally the OFDM systems make some subcarriers to be zeroed as the guard-band. For further expression, this dissertation called the terms 'used subcarrier' as 'subcarrier' with symbol notation of N and the total generated subcarriers as the 'FFT size' with symbol notation of M.

As described model in Fig. 4.1, the incoming QAM data symbols stream are converted from serial to parallel just like in OFDM case. In CI/OFDM, however,

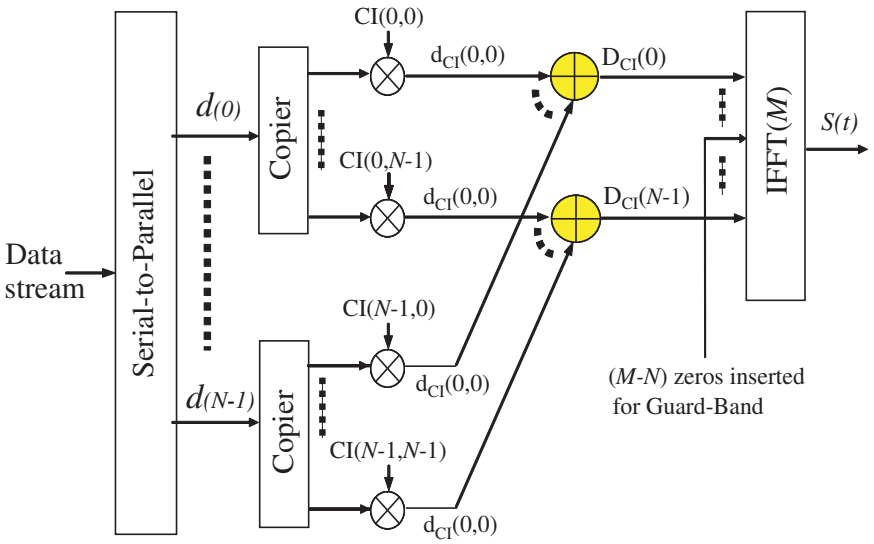

Figure 4.1. CI spreading in CI/OFDM system (transmitter side)

each data symbol is spread out onto all of the N subcarriers while in OFDM, each data symbol is modulated onto its own subcarrier and sent over the channel. Data symbol-k are separated from other $(N-1)$ data symbols by employing complex spreading codes called $CI(k,n)$ codes which is defined as

$$CI(k,n) = e^{j\left(\frac{2\pi}{N}\right)\cdot k\cdot n}, \quad \text{with} \quad \begin{cases} k = 0,1,2,\ldots,N-1 \\ n = 0,1,2,\ldots,N-1 \end{cases}, \tag{4.3}$$

where k is data symbol index and n is subcarrier index. We can construct the matrix of CI codes in (4.3) for all values of k and n as

$$\mathbf{CI} = \begin{pmatrix} 1 & 1 & \ldots & 1 & 1 \\ 1 & e^{j\frac{2\pi}{N}\cdot 1\cdot 1} & \ldots & e^{j\frac{2\pi}{N}\cdot(N-2)\cdot 1} & e^{j\frac{2\pi}{N}\cdot(N-1)\cdot 1} \\ \vdots & \vdots & \ddots & \vdots & \vdots \\ 1 & e^{j\frac{2\pi}{N}\cdot 1\cdot(N-2)} & \ldots & e^{j\frac{2\pi}{N}\cdot(N-2)\cdot(N-2)} & e^{j\frac{2\pi}{N}\cdot(N-1)\cdot(N-2)} \\ 1 & e^{j\frac{2\pi}{N}\cdot 1\cdot(N-1)} & \ldots & e^{j\frac{2\pi}{N}\cdot(N-2)\cdot(N-1)} & e^{j\frac{2\pi}{N}\cdot(N-1)\cdot(N-1)} \end{pmatrix}. \tag{4.4}$$

Since $P(n) = \sum_{k=0}^{N-1} CI(k,n) = N$, CI codes boost the power of k-th data

symbol. Therefore, a normalization is required. We should multiply (4.4) by $1/\sqrt{N}$ for obtaining a normalized power of CI/OFDM signals . The k-th data is multiplied by CI code for k-th data on n-th subcarrier, $CI(k,n)$, to obtain

$$d_{CI}(k,n) = d(k) \cdot e^{j\frac{2\pi}{N}k\cdot n} \tag{4.5}$$

With $d_{CI}(k,n)$ in (4.5), the result of CI spreading on n-th subcarrier in CI/OFDM can be expressed as

$$\begin{aligned} D_{CI}(n) &= \frac{1}{\sqrt{N}}\sum_{k=1}^{N-1} d_{CI}(k,n) \\ &= \frac{1}{\sqrt{N}}\sum_{k=1}^{N-1} d(k)e^{j\frac{2\pi}{N}k\cdot n}, \end{aligned} \tag{4.6}$$

where $d(k)$ is the k-th QAM data symbol. From (4.6), the total of a CI spread data stream that contains N data will be

$$\begin{aligned} \mathbf{D}_{CI} &= [D_{CI}(0) \quad D_{CI}(1) \quad \cdots \quad D_{CI}(N-1)]^T \\ &= \frac{1}{\sqrt{N}}\left[\sum_{k=0}^{N-1} d(k) \sum_{k=0}^{N-1} d(k)\, e^{j\frac{2\pi}{N}k\cdot 1} \quad \cdots \quad \sum_{k=0}^{N-1} d(k)\, e^{j\frac{2\pi}{N}k\cdot(N-1)}\right]^T . \end{aligned} \tag{4.7}$$

The guard-band is practically implemented by zeroing the edge bands. As shown in Chapter 2 (similar with an oversampling) the zero-ed subcarriers for guard-band are theoretically located at the middle of the spread data. Therefore, (4.7) with $(M-N)$ guard-band length, $N \leqslant M$ (subcarriers for pilots are removed for simplicity) can be described as

$$\widetilde{\mathbf{D}}_{CI} = [\underbrace{D_{CI}(0)\cdots D_{CI}(\tfrac{N}{2}-1)}_{\frac{N}{2}} \quad \underbrace{0\cdots 0}_{M-N} \quad \underbrace{D_{CI}(\tfrac{N}{2})\cdots D_{CI}(N-1)}_{\frac{N}{2}}]^T, \tag{4.8}$$

where M is the FFT size of the OFDM system. From (4.8), we can derive the total transmitted signals for a single CI/OFDM symbol that has N subcarriers

and M FFT size as

$$S(t) = \frac{1}{\sqrt{M}} \sum_{m=0}^{M-1} \widetilde{D}_{CI}(m)\ e^{j\frac{2\pi}{M}m\cdot t}, \tag{4.9}$$

where $t = 0, 1, 2, \cdots, M-1$.

However, for the case of without guard-band, we get $M = N$, so that $\widetilde{D}_{CI} = D_{CI}$ and the total CI/OFDM signal becomes

$$\begin{aligned} S(t) &= \frac{1}{\sqrt{N}} \sum_{m=0}^{N-1} d_{CI}(m)\ e^{j\frac{2\pi}{N}m\cdot t} \\ &= \frac{1}{N} \sum_{m=0}^{N-1} \left(\sum_{k=0}^{N-1} d(k) e^{j\frac{2\pi}{N}k\cdot m} \right)\ e^{j\frac{2\pi}{N}m\cdot t} \\ &= \begin{cases} d(t) & \text{for } t = 0, \\ d(N-1-t) & \text{otherwise} \end{cases}. \end{aligned} \tag{4.10}$$

Equation (4.10) shows that a matrix shown in (4.1), (4.2), and Eq. (9), (21) in [49] is just a special case of (4.9) when $M = N$ (without guard-band). Therefore, in this special case, CI spreading is useless as pointed out in [49]. The derivation in this dissertation is more acceptable and generally shows that CI spreading in the proposed CI/OFDM is meaningful.

Since an oversampling is needed for the practical design, we introduce the signal in (4.9) with the notation of $S[m/L]$ to denote an oversampled signal by factor of L. We then obtain the oversampled new CI/OFDM signals by following (2.5) of Chapter 2 (rectangular window $w(m/L)$ is removed for simplicity) as

$$\begin{aligned} S\,[t/L] &= \frac{1}{\sqrt{M}} \sum_{m=0}^{M-1} \widetilde{D}_{CI}(m) e^{j\left(\frac{2\pi}{ML}t\cdot p\right)} \\ &= \frac{1}{\sqrt{M}} \left(\sum_{m=0}^{\frac{M}{2}-1} \widetilde{D}_{CI}(m) e^{j\left(\frac{2\pi}{ML}m\cdot t\right)} + \sum_{m=ML-\frac{M}{2}}^{ML-1} \widetilde{D}_{CI}(m-(L-1)) e^{j\left(\frac{2\pi}{ML}m\cdot t\right)} \right) \\ &= IFFT(\sqrt{L}[\underbrace{\widetilde{D}_{CI}(0)\cdots\widetilde{d}_{CI}\left(\tfrac{N}{2}-1\right)}_{\frac{N}{2}}\ \underbrace{0\cdots 0}_{M(L-1)}\ \underbrace{\widetilde{D}(\tfrac{N}{2})\cdots\widetilde{D}(N-1)}_{\frac{N}{2}}]). \end{aligned} \tag{4.11}$$

Constant multiplier $\sqrt{L}$ is added for normalizing the output because of oversampling factor of L. However, the conventional CI/OFDM signals in [5, 15–17] and [14] may be obtained with another oversampling technique such as

$$S[p/L] = IFFT(\sqrt{L}[\underbrace{\widetilde{d}_{CI}(0)\cdots\widetilde{D}_{CI}(N-1)}_{N}\ \underbrace{0\ 0\ \cdots 0\ 0}_{M(L-1)}]), \quad (4.12)$$

which is basically incorrect. Consequently, the conventional oversampling in (4.12) gives a waveform as shown in Fig. 4.2(a), while the waveform of the proposed CI/OFDM with oversampling in (4.11) is shown in Fig. 4.2(b). In Chapter 2 of [1], it was also pointed out that in an IFFT matrix, the first half of rows corresponds to positive frequency, while second half corresponds to negative frequency. Hence, if oversampling is used, the zeros should be added in the middle of the data vector rather than appending them at the end. This ensures that the zeros data value are mapped onto frequency plus and minus half the sampling rate, while non zero data values are mapped onto the subcarriers around 0Hz (baseband).

The proposed CI/OFDM results in a new waveform which is different from the conventional CI signals as shown in Fig. 4.2(b). We will prove (by the simulation results) that it does not impact to the PAPR performances and the degradation of BER performances.

4.2.2 POCI/OFDM System

POCI code consists of two CI code sets. The second set is a copy of the first code set which is designed to have different phases of $\Delta\theta$. The codes in code set 1 are orthogonal to each other and the codes in code set 2 are also orthogonal to each other. However, the codes in code set 1 are non-orthogonal to the codes in code set 2. This problem has been solved by seeking $\Delta\theta$ that is able to minimize the cross-correlation value between these codes set.

In [16], it is reported that $\Delta\theta = \pi/N$ is the optimum value (however, it will be outperformed by the proposed LCI code in Chapter 5) for a minimum cross-correlation, especially for high N. With this value, the POCI code for k-th data

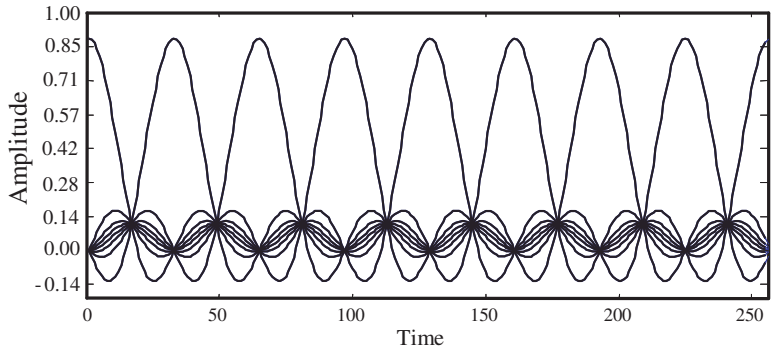

(a) Waveform of the conventional CI/OFDM signal

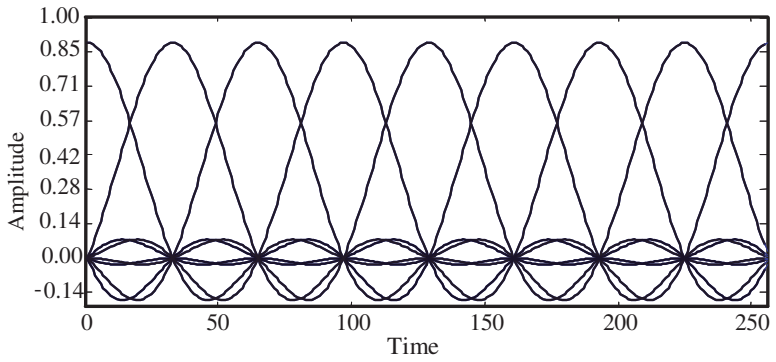

(b) Waveform of the proposed CI/OFDM signal

Figure 4.2. Waveforms of the conventional CI/OFDM and the proposed CI/OFDM signals

symbol on n-th subcarrier is then expressed as

$$POCI(k,n) = \begin{cases} e^{j\left(\frac{2\pi}{N}\right)\cdot k_1 \cdot n}, & \text{for } k_1 = 0, 1, 2, \cdots, N-1 \\ e^{j\left\{\left(\frac{2\pi}{N}\right)\cdot k_2 + \left(\frac{\pi}{N}\right)\right\}\cdot n}, & \text{for } k_2 = N, N+1, \cdots, 2N-1 \end{cases} . \quad (4.13)$$

Performing derivations similar to (4.6)– (4.11), it is found that (4.2) and (13)–(22) of [49] is just a special case when $M = N$ (without guard-band). We plot POCI signals in Figs. 4.3(a) and 4.3(b). Although the signals with the proposed design are different from those of the conventional system, the PAPR level remains almost similar (the result will be presented in Section 4.7.1). The reason of its similarity is that the superposition of all signals in Fig. 4.3(b) has a similar distribution as the distribution in Fig. 4.3(a), though the waveforms are different.

4.3. Replacement of CI Spreading by FFT

4.3.1 CI Spreading Using FFT

In this section, we analyze an FFT spreading, then compare it to the CI spreading and finally conclude that the CI spreading can be replaced by the FFT spreading. We also prove here that POCI spreading is also possible to be replaced by the double FFT spreadings of which its computational complexity is significantly low.

The conventional CI spreading (with matrix multiplication) requires about N^2 complex multiplications. However, in large number of subcarriers, the complexity will increase quadratically. If the CI/OFDM will be implemented on Japanese digital television broadcasting (ISDB-T) mode 3 with $K = 5,616$ [4], the number of complex multiplications will be $5,616 \times 5,616 = 31,539,456$. It seems impractical to be implemented. Therefore, another technique should be investigated to reduce the computational cost of the CI spreading.

By carefully observing (4.3) and (4.4), it is straightforward to realize that CI codes with N subcarriers can be replaced by IDFT matrixes with the same sample size N. For an example, CI codes of 8×8 can be replaced by IDFT with size of 8. It is also well known that IDFT can be performed faster and simpler by

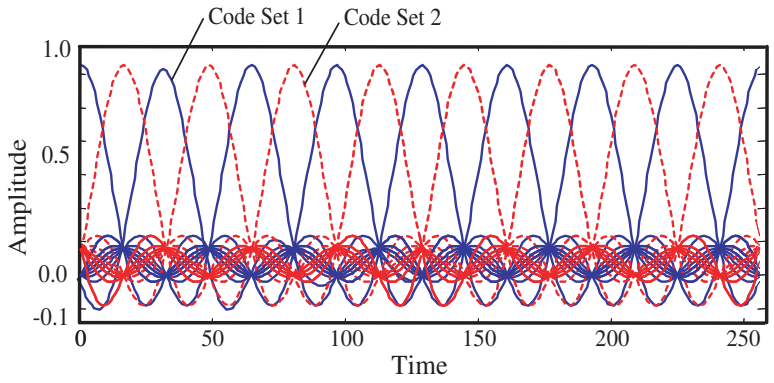

(a) Waveform of the POCI/OFDM signal

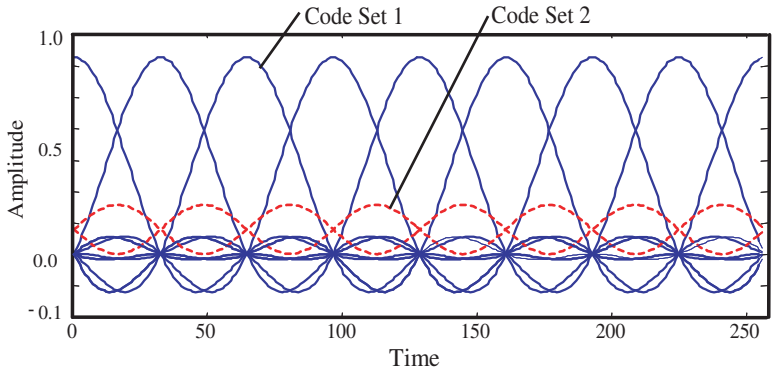

(b) Waveform of the proposed POCI/OFDM signal

Figure 4.3. The comparison of waveforms between the conventional POCI/OFDM and the proposed POCI/OFDM signal

an algorithm called inverse fast Fourier transform (IFFT), because the twiddle factors ($e^{j\frac{2\pi}{N}k\cdot n}$) have to be calculated only once for the two existing combinations of k and n as shown in [51].

At each stage of an FFT with radix-2, $N/2$ multiplications are required to combine the results of the previous stages. Since there are $\log_2(N)$ FFT stages, the number of multiplications is approximately $N/2\ \log_2(N)$. The number of additions/subtractions is $N\log_2(N)$ while the required memory is only N because it is not necessary to save all codes in a memory like in the conventional CI spreading.

With the benefit as described above, we propose FFT and IFFT for replacing the conventional CI spreading and de-spreading, called as CI-FFT and CI-IFFT. CI-FFT is a CI de-spreading using FFT with a size of N (at the receiver) and CI-IFFT is CI spreading using IFFT with a size of N (at the transmitter). It is, however, important to note that it is possible to locate CI-FFT at the transmitter and CI-IFFT at the receiver. Both of the designs are acceptable. The difference is only on the order of the modulated symbols as the output of CI spreading and de-spreading. Fig. 4.4 shows the sequences of the waveforms when CI-IFFT is located at the transmitter and the receiver. The waveforms $C_1, C_2, \cdots, C_8$, are the waveforms in OFDM with subcarriers $N = 8$ when CI-IFFT is located at the transmitter. The waveforms $D_1, D_2, \cdots, D_8$, are the waveforms in OFDM with subcarriers $N = 8$ when CI-IFFT is located at the receiver.

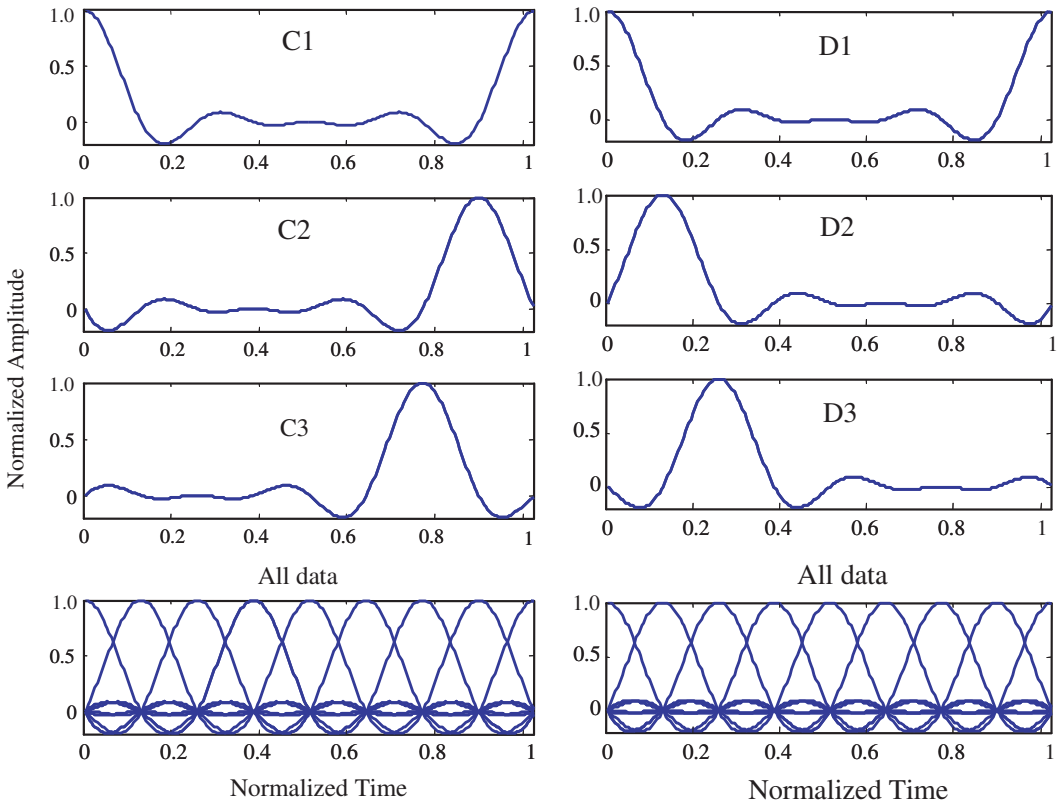

Figure 4.4. Comparison between the sequence waveforms of CI-FFT/OFDM when CI-IFFT is located at the transmitter and the receiver

4.3.2 POCI Spreading Using Double FFT

For POCI code, we can represent (4.13) in a POCI matrix as

$$\mathbf{CI}_1 = \begin{pmatrix} 1 & 1 & \dots & 1 & 1 \\ 1 & e^{j\frac{2\pi}{N}1\cdot 1} & \dots & e^{j\frac{2\pi}{N}(N-2)\cdot 1} & e^{j\frac{2\pi}{N}(N-1)\cdot 1} \\ \vdots & \vdots & \ddots & \vdots & \vdots \\ 1 & e^{j\frac{2\pi}{N}1\cdot(N-2)} & \dots & e^{j\frac{2\pi}{N}(N-2)\cdot(N-2)} & e^{j\frac{2\pi}{N}(N-1)\cdot(N-2)} \\ 1 & e^{j\frac{2\pi}{N}1\cdot(N-1)} & \dots & e^{j\frac{2\pi}{N}(N-2)\cdot(N-1)} & e^{j\frac{2\pi}{N}(N-1)\cdot(N-1)} \end{pmatrix}$$

$$\mathbf{CI}_2 = \begin{pmatrix} 1 & e^{j\left(\frac{2\pi}{N}(N+0)\cdot 1+\frac{\pi}{N}1\right)} & \dots & e^{j\left(\frac{2\pi}{N}(N+0)\cdot(N-1)+\frac{\pi}{N}(N-1)\right)} \\ 1 & e^{j\left(\frac{2\pi}{N}(N+1)\cdot 1+\frac{\pi}{N}1\right)} & \dots & e^{j\left(\frac{2\pi}{N}(N+1)\cdot(N-1)+\frac{\pi}{N}(N-1)\right)} \\ \vdots & \vdots & \ddots & \vdots \\ 1 & e^{j\left(\frac{2\pi}{N}(2N-2)\cdot 1+\frac{\pi}{N}1\right)} & \dots & e^{j\left(\frac{2\pi}{N}(2N-2)\cdot(N-1)+\frac{\pi}{N}(N-1)\right)} \\ 1 & e^{j\left(\frac{2\pi}{N}(2N-1)\cdot 1+\frac{\pi}{N}1\right)} & \dots & e^{j\left(\frac{2\pi}{N}(2N-1)\cdot(N-1)+\frac{\pi}{N}(N-1)\right)} \end{pmatrix}, \quad (4.14)$$

where $\mathbf{CI}_1$ and $\mathbf{CI}_2$ are matrixes for code set 1 and code set 2, respectively. To obtain a normalized power, a constant $\frac{1}{\sqrt{2N}}$ is multiplied to the spread data output.

The output signal for each subcarrier is obtained by summing all outputs of the spread data with code set 1 and 2. The number of row represents number of data while the number of column represents the number of subcarriers. The result of POCI spreading for both data set 1 and data set 2 for n-th subcarrier can be expressed as

$$D_{POCI}(n) = \underbrace{\sum_{k_1=0}^{N-1} d(k_1)e^{j\left(\frac{2\pi}{N}k_1\cdot n\right)}}_{\text{from code set 1}} + \underbrace{\sum_{k_2=N}^{2N-1} d(k_2)e^{j\left(\frac{2\pi}{N}k_2\cdot n+\frac{\pi}{N}\cdot n\right)}}_{\text{from code set 2}}. \quad (4.15)$$

Because this signal is periodic with period of N, we can further simplify the computation of (4.15) and obtain a new format of POCI code using double FFT

as

$$D_{POCI}(n) = \underbrace{\sum_{k_1=0}^{N-1} d(k_1) e^{j\left(\frac{2\pi}{N} k_1 \cdot n\right)}}_{IFFT_1} + \underbrace{e^{j\frac{\pi}{N}n}}_{separator} \cdot \underbrace{\sum_{k_1=N-1, k_2=2N-1}^{k_1=0, k_2=N} d(k_2) e^{j\left(\frac{2\pi}{N} \cdot k_1 \cdot n\right)}}_{IFFT_2}. \tag{4.16}$$

The first part of (4.16) can be represented by $IFFT_1$ (called CI-FFT$_1$) and the second part can be performed by $IFFT_2$ (called CI-FFT$_2$) followed by one multiplication with a constant value $e^{j\frac{2\pi}{N}n}$ per subcarrier which is called as the *separator* in this dissertation to separate the spread data 1 and spread data 2. With this separation, both of the data sets are detectable at the receiver side because inter-code interference can be minimized.

4.4. Proposed CI-FFT/OFDM and POCI-FFT/OFDM Systems

Based on the conclusion in Sections 4.2 and 4.3, to obtain an efficient design we propose FFT to replace CI spreading and double FFT to replace POCI spreading in CI/OFDM and POCI/OFDM system (called CI-FFT/OFDM and POCI-FFT/OFDM), respectively. Figs. 4.5 and 4.6 show the structures of the proposed design. Data streams d are modulated by binary phase shift keying (BPSK) or by QAM modulations and then converted from serial to a parallel format. Then the parallel data are spread out by CI-FFT in CI-FFT/OFDM and by double CI-FFT in POCI-FFT/OFDM system.

Spread signals are converted into the time domain by an IFFT with oversampling factor L. After the GI insertion, CI-FFT/OFDM and POCI-FFT/OFDM signals are transmitted. At the receiver, GI is removed and FFT-ed to obtain frequency domain signals, down-sampled and equalized. The signal are then are de-spread using CI-FFT de-spreading. Demodulation is then performed to obtain the received data ($\hat{d}$).

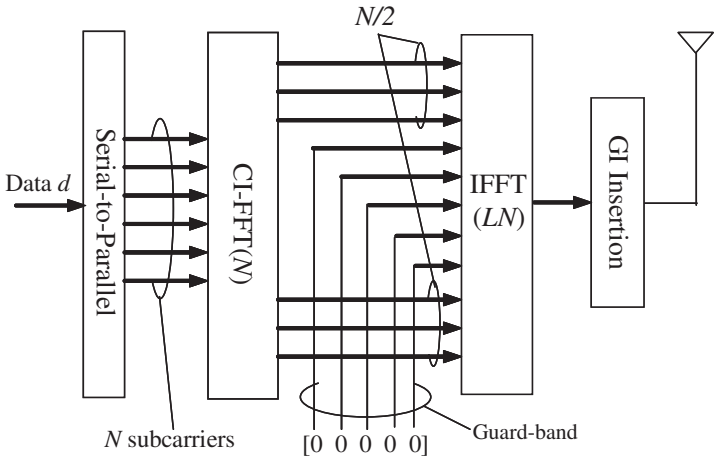

(a) Transmitter

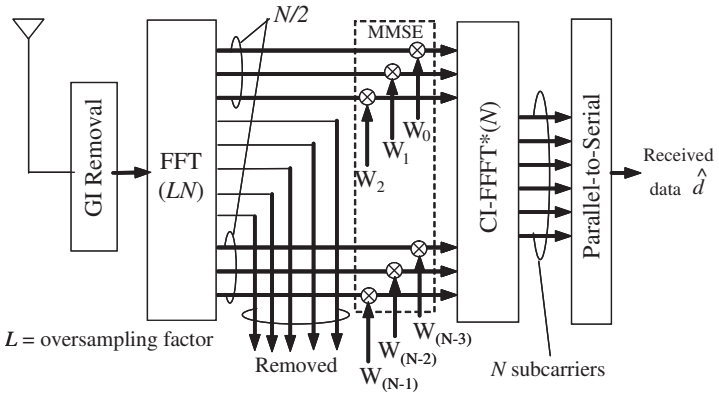

(b) Receiver

Figure 4.5. The proposed CI-FFT/OFDM structures

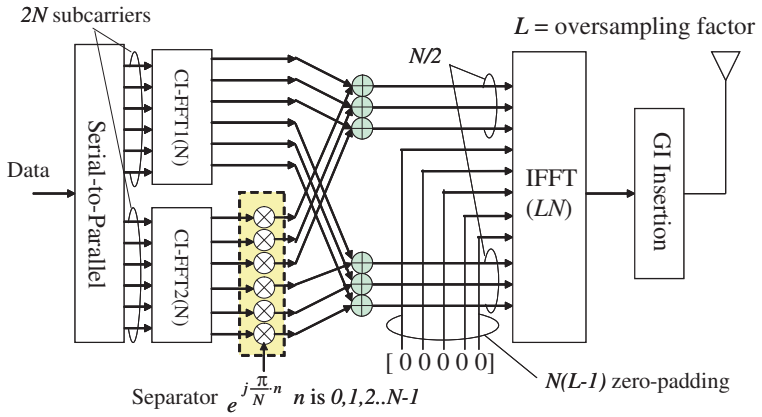

(a) Transmitter

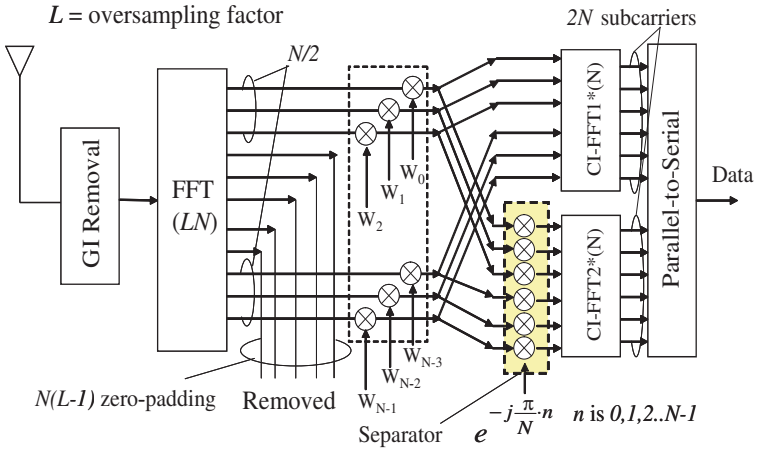

(b) Receiver

Figure 4.6. The proposed POCI-FFT/OFDM structures

4.5. Combiner Design at the Receiver

In the multipath fading environment, a combiner is required. Being different from the design in [5, 15, 16, 19] and [14], we propose a new design by locating the equalizer before the CI-FFT instead of that after the CI de-spreading as designed in the conventional combiner of CI/OFDM system [14]. The benefit is that our new combiner requires only N multiplications of combiner's weights, while the conventional CI/OFDM system requires $N \times N$ complex multiplications with the combiner's weights. Thus, the proposed new design is capable of reducing the computational complexity of equalization and combination significantly.

In this chapter, we select a minimum mean square error (MMSE) equalizer [21], a sub-optimum method for a performance close to maximum likelihood (ML) method in multipath fading channel. Weighting values derived from MMSE criteria for n-th subcarrier can be shown by

$$W_{MMSE}(n) = \frac{H^*(n)}{|H(n)|^2 + \sigma}, \tag{4.17}$$

where $H(n)$ is the channel impulse response (CIR). The CIR is obtained from the channel estimation module, for ease in presentation, in this chapter, we assume a perfect channel estimation is performed. $H^*(n)$ is a complex conjugate of $H(n)$, and σ is the variance of the noise.

4.6. Complexity Reduction by FFT Algorithm

4.6.1 Reduction by CI-FFT Spreading

Table 4.1 shows the computational complexity reduction of CI spreading by CI-FFT spreading. As shown in (4.4), it is not required to operate any multiplications for the $1, N/2, N/4, 3N/4$-th row/column of CI codes matrix because all values in both row and column are "$\pm 1 \pm j0$" or "$0 \pm j1$". Therefore, we can obtain a number of complex multiplications in CI spreading is $(N-4) \times (N-4)$ as well as the memory size of $(N-1) \times (N-1)$, while the number of addition is normally $(N-1) \times (N-1)$, independent of the value in the first row and column.

Table 4.1. Computational complexities of CI and CI-FFT spreading

The conventional CI spreading

Subc.	**Mult.**	**Add.+Subt.**	**Mem.**
16	144	225	255
32	784	961	961
64	3,600	3,969	3,969
128	15,376	16,129	16,129
256	63,504	65,025	65,025
512	258,064	261,121	261,121
1,024	1,040,400	1,046,529	1,046,529
⋮	⋮	⋮	⋮
N	$(N-4)(N-4)$	$(N-1)(N-1)$	$(N-1)(N-1)$

The proposed CI-FFT spreading

Subc.	**Multipl.**	**Saving**	**Add.+Sub.**	**Saving**	**Mem.**	**Saving**
16	32	77.8%	64	71.6%	15	93.3%
32	80	89.7%	160	83.4%	31	96.8%
64	192	94.7%	384	90.3%	63	98.4%
128	448	97.1%	896	94.4%	127	99.2%
256	1,024	98.4%	2,048	96.9%	255	99.6%
512	2,304	99.1%	4,608	98.2%	511	99.8%
1,024	5,120	99.5%	10,240	99.0%	1,023	99.9%
⋮	⋮	⋮	⋮	⋮	⋮	⋮
N	$\frac{N}{2}\log_2(N)$	MX_{CI-FFT}	$N\log_2(N)$	AD_{CI-FFT}	$(N-1)$	MS_{CI-FFT}

In CI-FFT spreading, the FFT algorithm does not calculate all twiddle factors. Therefore, the number of multiplications, additions/subtractions and memory size in CI-FFT can be reduced significantly. The number of multiplication (for radix-2) is $(N/2) \times \log_2(N)$ with the memory size of $(N-1)$ (the first row of "1" does not need to be stored). As a consequence of using twiddle factor many times, CI-FFT required some subtraction operations while it does not exist in the conventional CI spreading. Because the complexities of addition and subtraction are similar, we can express the total number $additions + subtractions$ in CI-FFT as $N\log_2(N)$.

The percentages of complexity reduction (saving cost) in multiplication MX, addition AD and memory size MS of CI-FFT/OFDM are derived as

$$MX_{CI-FFT} = \left(1 - \frac{(N/2) \times \log_2(N)}{(N-4) \times (N-4)}\right) \times 100\%, \tag{4.18}$$

$$AD_{CI-FFT} = \left(1 - \frac{N \times \log_2(N)}{(N-1) \times (N-1)}\right) \times 100\%, \tag{4.19}$$

$$MS_{CI-FFT} = \left(1 - \frac{N}{N \times N}\right) \times 100\%. \tag{4.20}$$

If the number of subcarriers N is not a power of two, the CI spreading (CI-IFFT) will not be a power of two. One may think that it is a small problem that causes a slower computation compared with that of IFFT with power of two. To solve this small problem, we can apply a parallel algorithm with different power of butterfly operation [52]. For example, we consider the subcarrier number of $N = 96$, FFT point with $M = 128$ and zero padding for guard-band of $Z = 32$.

Because $N = 96$ can be transformed to $N = 3^1 \times 2^5$. It means that the computation of CI-IFFT requires 5 stages power of two butterfly operation and 1 stage power of three butterfly operation. With this technique, we can perform faster CI spreading than that of the conventional CI spreading with matrix multiplications. The power of two butterfly operator is described as [52]

$$\begin{pmatrix} 1 & \\ & D_f \end{pmatrix} \begin{pmatrix} 1 & 1 \\ 1 & -1 \end{pmatrix} \tag{4.21}$$

where f-th stage element $D_f = e^{-j\frac{\pi}{F}f}$, $F = M/2$, and M is the FFT size. The power of three butterfly operator is [52]

$$\begin{pmatrix} 1 & & \\ & D_p & \\ & & {D_p}^2 \end{pmatrix} \begin{pmatrix} 1 & 1 & 1 \\ 1 & \alpha^2 & -\alpha \\ 1 & -\alpha & \alpha^2 \end{pmatrix} \tag{4.22}$$

where $P = M/3$, $\alpha = e^{-\frac{\pi}{3}}$, and $D_p = e^{-j\frac{\pi}{P}p}$ is the diagonal element of the p-th stage. It is shown in (4.21) and (4.22) that the computational complexity for

non-power of two is not a big problem on the CI-FFT computation. On the other hand, the CI-FFT computation for $N = 96$ in this chapter is not a problem.

4.6.2 Reduction by POCI-FFT Spreading

Table 4.2 shows the computational complexity reduction of the conventional POCI spreading by POCI-FFT spreading. Similar to CI codes and as shown in (13), it is not required to operate any multiplications for the $1, N/2, N/4, 3N/4$-th row/column of POCI codes matrix because the all values in both row and column are "$\pm 1 + j0$" or "$0 \pm j1$". POCI codes matrix has size of $2N \times N$, therefore, we can obtain the number of multiplications in POCI spreading is $2 \times (N-1) \times (N-1)$ as well as the memory size of $2 \times (N-1) \times (N-1)$. In POCI spreading, the number of additions increases by factor of N, i.e. the factor of subcarrier number, so the total number of additions is $2(N-1) \times (N-1) + N$.

In POCI-FFT spreading, instead of using single FFT, we utilize double FFT for performing POCI spreading. The number of multiplications (for radix-2) becomes $2(N/2) \times \log_2(N)$ with the memory size $2(N-1) + N$, where N additional memory for restoring the N separators. The total number of *additions* + *subtractions* in POCI-FFT is $2 \times N \log_2(N)$.

For the POCI-FFT/OFDM, the percentages of saving cost in multiplication MX, addition AD and memory size MS are derived as:

$$MX_{POCI-FFT} = \left(1 - \frac{2 \times (N/2) \times \log_2(N) + N}{2 \times (N-4) \times (N-4) + N}\right) \times 100\%, \tag{4.23}$$

$$AD_{POCI-FFT} = \left(1 - \frac{2 \times N \times \log_2(N) + N}{2 \times (N-1) \times (N-1) + N}\right) \times 100\%, \tag{4.24}$$

$$MS_{POCI-FFT} = \left(1 - \frac{2 \times N + N}{2 \times N \times N}\right) \times 100\%. \tag{4.25}$$

As presented in Table 4.1 and 4.2, for $N \geq 64$ we can save more than 95% of multiplications, 90% of additions and 98% of memory size. As the increasing of N more than 8,192, the saving cost for all of additions/subtractions, multiplications

TABLE 4.2. COMPUTATIONAL COMPLEXITIES OF THE POCI AND THE POCI-FFT SPREADING

THE CONVENTIONAL POCI SPREADING

Subc.	**Mult.**	**Add. + Subt.**	**Mem.**
16	288	466	450
32	1,568	1,954	1,922
64	7,200	8,002	7,938
128	30,752	32,386	32,258
256	127,008	130,306	130,050
512	516,128	522,754	522,242
1,024	2,080,800	2,094,082	2,093,058
⋮	⋮	⋮	⋮
N	$2(N-4)(N-4)$	$2(N-1)(N-1)+N$	$2(N-1)(N-1)$

THE PROPOSED POCI-FFT SPREADING

Subc.	**Mul.**	**Saving**	**Add.+Sub.**	**Saving**	**Mem.**	**Saving**
16	80	72.2%	144	69.1%	46	89.9%
32	192	87.8%	352	82.0%	94	95.1%
64	448	93.8%	832	89.6%	190	97.6%
128	1,024	96.7%	1,920	94.1%	382	98.8%
256	2,304	98.2%	4,352	96.7%	766	99.4%
512	5,120	99.0%	9,728	98.1%	1,534	99.7%
1,024	11,264	99.5%	21,504	99.0%	3,070	99.9%
⋮	⋮	⋮	⋮	⋮	⋮	⋮
K	$K\log_2(N)+N$	MX	$2N\log_2(N)+N$	AD	$2(N-1)+N$	MS

and memory size will be more than 99.9%.

CI-FFT/OFDM and POCI-FFT/OFDM complexities will depend only on the complexity of FFT algorithm. If there is a DFT algorithm that is faster and more efficient than the current FFT algorithm, the proposed design will also be better and faster.

Fig. 4.7 shows the curves of complexity reductions for CI spreading and POCI spreading using the proposed method. Number of effective subcarriers is the number of CI codes or the number of non-zeroed subcarriers of CI/OFDM and POCI/OFDM systems. Curves of CI code and POCI codes grows quadratically, while CI-FFT and POCI-FFT grows almost linearly. This figure expresses how significant reduction can be obtained by the use of CI-FFT or POCI-FFT spreading instead of the current CI and POCI spreading.

4.7. Numerical Results

In this section, we discuss the PAPR and BER performance of the proposed CI-FFT/OFDM and POCI-FFT/OFDM in additive white Gaussian noise (AWGN) channel and multipath fading channel. The simulation parameters are shown in Table 4.3. Hadamard code, which is famous in the area of spread OFDM, is considered in this evaluation to obtain more beneficial comparison. For multipath fading channel, we use bad urban (BU) of COST-207 channel model [53] with the delay profile shown in Fig. 4.8. T_s is the time symbol duration of one CI/OFDM or POCI/OFDM symbols.

4.7.1 PAPR Performances

To produce the graph, we used 100,000 randomly distributed OFDM symbols to measure the PAPR performance at CCDF of 10^{-4}. Increasing the number of symbols beyond it, however, shall not drastically change the curves. PAPR performances of the proposed system with an oversampling factor of $L = 4$ for BPSK modulated symbols are shown in Figs. 4.9 and 4.10. It is shown in Fig. 4.9 that CI-FFT outperforms Hadamard code by about 1.3dB at CCDF of 10^{-4}. The PAPR of the proposed technique is almost equal with the PAPR of original

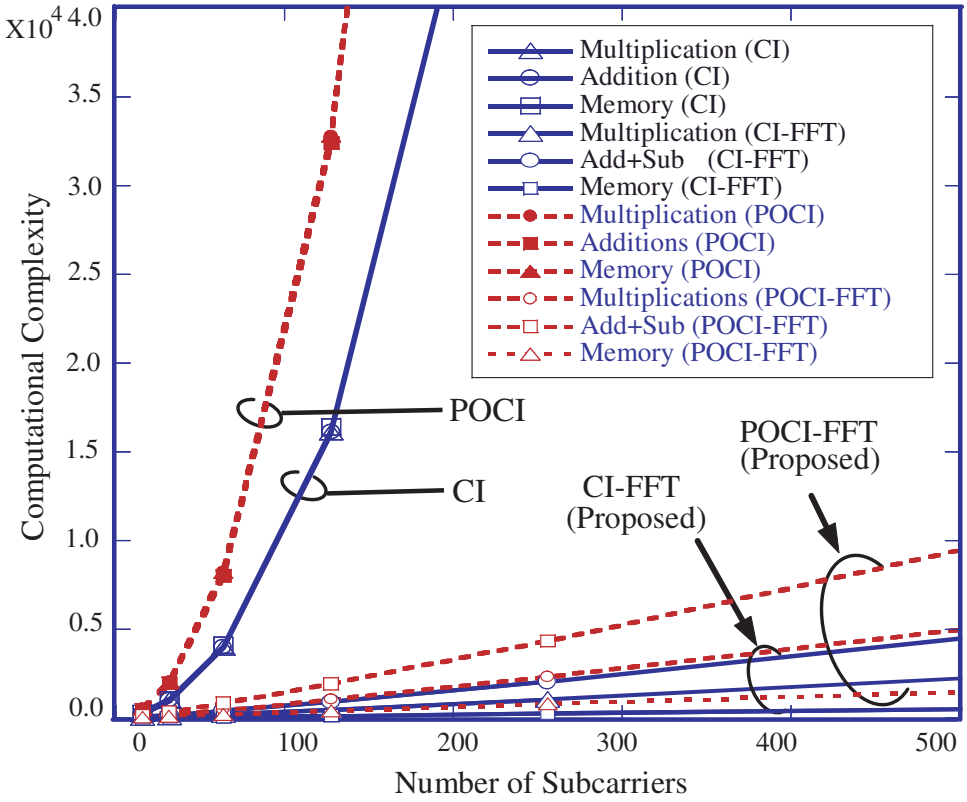

Figure 4.7. Complexity reduction of CI and POCI spreading by CI-FFT and POCI-FFT

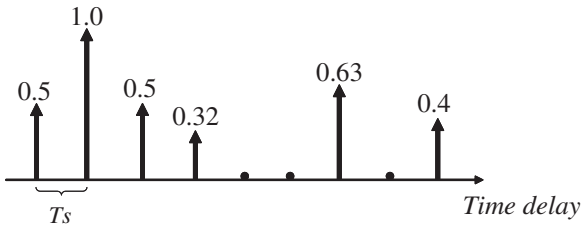

Figure 4.8. Power delay profile of Bad Urban (BU) COST-207 fading model

Table 4.3. Simulation parameters

	Parameter	Value(s)
Transmitter	Modulation	BPSK
	Subcarrier number (S)	96
	FFT size (N)	128
	Oversampling factor (L)	4
	Error correction coding	Convolutional coding, $R = 1/2$, Soft
Decision	GI length	16
	Spreading ($C(k, n)$)	CI, POCI and Hadamard
Channel	AWGN	–
	Fading	Bad Urban of COST207 model [53]
Receiver	Equalizer	MMSE

CI/OFDM though the symbol waveform is different (see Section 4.2). A large difference by about 0.25dB at CCDF of less than 10^{-3} is negligible.

For the case of POCI/OFDM and POCI-FFT/OFDM in Fig. 4.10, the degradation is about 1.2dB from the PAPR level of the conventional POCI/OFDM. However, the oversample in the conventional POCI/OFDM as shown in Section 4.2 is incorrect. Thus, it can be confirmed that the true PAPR of POCI/OFDM is as shown in Fig. 4.10.

Generally, we can conclude that CI-FFT/OFDM and POCI-FFT/OFDM is capable of reducing the PAPR of OFDM to 8dB or 9dB from the original PAPR of 12dB.

4.7.2 BER Performances

Figs. 4.11 and 4.12 only show the performance of CI-FFT/OFDM, POCI-FFT/OFDM and OFDM with and without error correction code. We assume that the BER performance of CI-FFT/OFDM and POCI-FFT/OFDM are similar to that of conventional CI/OFDM and POCI/OFDM systems, due to the similar frequency diversity benefits. Therefore, it is interesting to compare them with OFDM system (without spreading) in frequency selective fading channel.

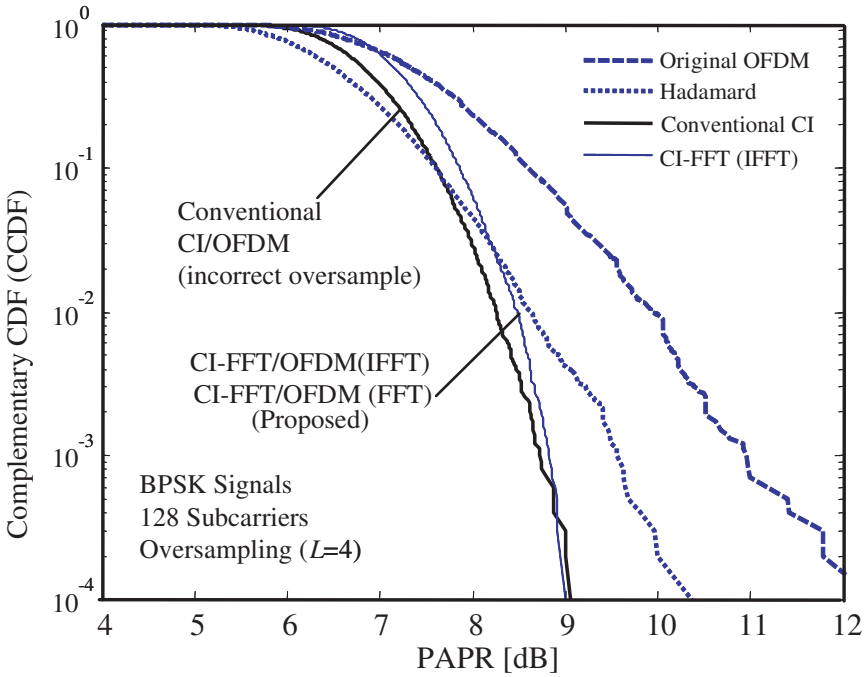

Figure 4.9. PAPR performance of CI-FFT/OFDM, CI/OFDM and OFDM signals

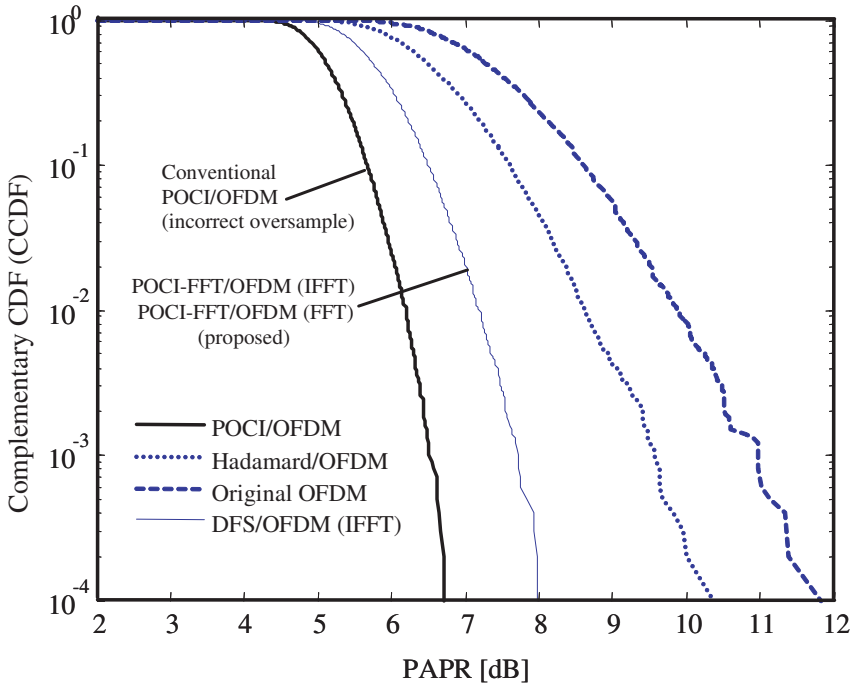

Figure 4.10. PAPR Performances of POCI-FFT/OFDM, POCI/OFDM and OFDM signals

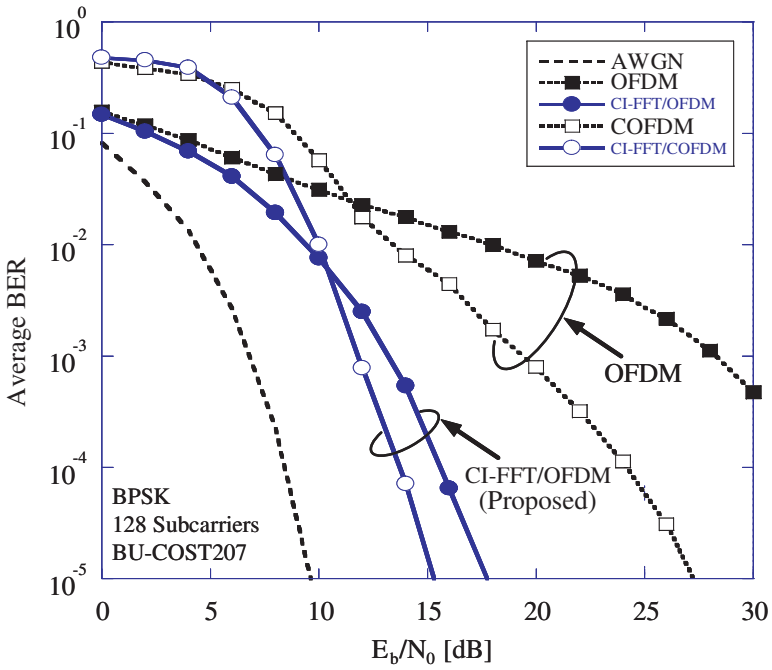

Figure 4.11. BER performance in Bad Urban COST-207 fading model

BER performance of CI-FFT/OFDM is shown in Fig. 4.11. In the case of without error correction coding, CI-FFT/OFDM outperforms OFDM by about 15dB at BER level of 10^{-3}. When error correction coding is employed, coded CI-FFT/OFDM (called CI-FFT/COFDM) still outperforms the coded OFDM (COFDM) by about 6dB at BER level of 10^{-3}.

Fig. 4.12 shows the BER performance of POCI-FFT/OFDM and OFDM system. In the case of without error correction coding, POCI-FFT/OFDM outperforms OFDM by about 11dB at BER level of 10^{-3}. The convolutional coding improved the BER by about 5dB better than coded OFDM (COFDM) system. Generally, we can conclude that both CI-FFT/OFDM and POCI-FFT/OFDM outperform OFDM and COFDM systems.

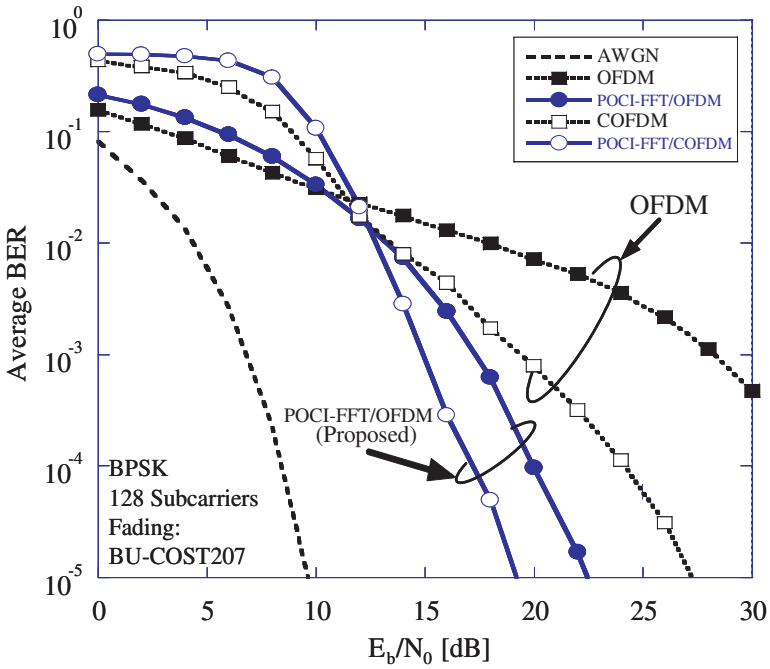

Figure 4.12. BER performance of BPSK OFDM and BPSK POCI-FFT/OFDM systems

Chapter 5

A Novel Large Code Set for Low PAPR and Double User Capacity

THIS chapter proposes a novel spreading code set, called large carrier interferometry (LCI), to reduce the PAPR while increasing the number of user capacity to the system at the same time. The user capacity can be increased because the proposed spreading code set is large. A code is large if the number of codes (code-number) is larger than the length of code (code-length), while generally the code-number is equal with the code-length. As a consequence of large code, errors may increase due to higher interference between the codes.

With some difficulties and limitations, the proposed LCI code set is designed to have a uniform low cross-correlation property for reducing the additional error due to the inter-symbol(-user) interference. The proposed code set is capable of (1) increasing more than twice the user/bit capacity and at the same time (2) reducing the peak-to-average power ratio (PAPR) of the MC-CDMA and OFDM systems.

This chapter derives the proposed LCI code set mathematically and presents an example to demonstrate its improvements on OFDM and MC-CDMA systems. The proposed code set with code-length of N has code-number $K = 2N + 1$ for supporting up to $(2N + 1)$ users and exhibits lower cross-correlation properties compared with the existing spreading code sets. The capacity of $(2N + 1)$ means that $(2N + 1)$ users or data symbols are successfully separated over the N sub-

carriers.

The remainder of this chapter is as follows. Section 5.1 describes the considered system model of OFDM and MC-CDMA systems. The derivation of the proposed spreading code is presented in Section 5.2 followed by its cross-correlation analysis. The performance evaluation of the PAPR is presented in Section 5.4, followed by the BER performance evaluations for both OFDM and MC-CDMA systems.

5.1. Spreading Codes in OFDM and MC-CDMA Systems

Fig. 5.1(a) shows the transmitter structure of the OFDM with a spreading code and Fig. 5.1(b) shows that of MC-CDMA system. The incoming data symbols are converted from serial to a parallel data stream format. In the current OFDM system, each data symbol is modulated onto its own subcarrier and sent over the channels. Here, in OFDM with spreading code, each data symbol is multiplied by spreading code $C(k, n)$, then spread-out onto all subcarriers, where k is data index of OFDM (or user index in MC-CDMA system) and n is the subcarrier index.

As shown in Fig. 5.1(a), one subcarrier holds N different data symbols. To separate data symbol-k ($d(k)$ from other $(N-1)$ symbols in N subcarriers, the spreading codes $C(k, n)$ with low cross-correlation properties should be selected. In current OFDM and MC-CDMA systems, the $C(k, n)$ is Hadamard spreading code with the size of $N \times N$ and noted as $C(k, n)_{(N\times N)}$. However, to increase the user capacity or additional data symbols, the size of spreading code should be $K \times N$, where $K > N$ and noted as $C(k, n)_{(K\times N)}$. Further, these $C(k, n)_{(K\times N)}$ code set is called as large spreading code in this chapter.

We substitute $C(k, n)_{(N\times N)}$ with larger code $C(k, n)_{(K\times N)}$ i.e. POCI code and our proposed LCI code to achieve higher capacity of $K > N$. Further, $C(k, n)_{(K\times N)}$ is noted as $C(k, n)$ for simple expression. Using $C(k, n)$, we spread

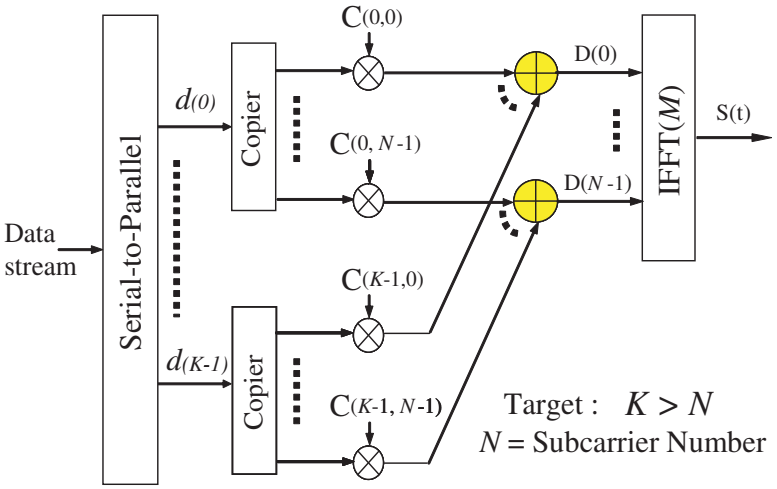

(a) The transmitter of an OFDM with a spreading code

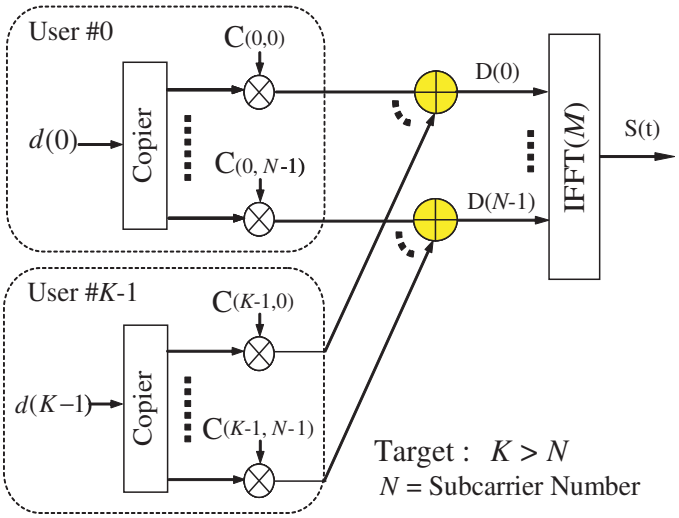

(b) The transmitter of an MC-CDMA system

Figure 5.1. The transmitter structures of a spread OFDM and MC-CDMA systems

the input data symbols to obtain spread data $D(i)$ and generally expressed as

$$D(i) = \frac{1}{\sqrt{K}} \sum_{k=0}^{K-1} d(k) \cdot C(k,i), \tag{5.1}$$

where $d(k)$ is the k-th data symbol and $i = 0, 1, \cdots, N-1$. It is important to note that in the current OFDM system with a non-large spreading code, K will always equal to the length of spreading code N. Therefore, the spread data $D(i)$ for the current OFDM system can be derived from (5.1) as

$$D_{\text{OFDM}}(i) = \frac{1}{\sqrt{N}} \sum_{k=0}^{N-1} d(k) \cdot C(k,i). \tag{5.2}$$

On the other hand, in the MC-CDMA system, K is the number of active user that vary between 1 to K_{user}. Thus, the spread data $D(i)$ for the MC-CDMA system can be obtained from (5.1) as

$$D_{\text{MC-CDMA}}(i) = \frac{1}{\sqrt{N}} \sum_{k=0}^{K_{\text{user}}-1} d(k) \cdot C(k,i). \tag{5.3}$$

To simplify the presentation in this chapter, we will use the term $D(i)$ as in (5.1) to express both spread data $D_{\text{OFDM}}(i)$ and $D_{\text{MC-CDMA}}(i)$.

An oversampling is required to obtain an accurate result of the PAPR evaluation. In addition, a guard-band is practically used to reduce the ACI such as IEEE.802.11a [40]. When the spreading code is CI or POCI code, the use of guard-band (by nulling the unused subcarriers) results in a new system as presented in Chapter 4 which is different from that pointed out in [49, 50]. A signal with a guard-band and an oversampling can be obtained by performing a zero padding into the $D(i)$ and obtain D_{zp} as

$$\mathbf{D_{zp}} = [\underbrace{D(0)\, D(1)\, \cdots\, D(\tfrac{N}{2}-1)}_{N/2}\ \underbrace{0\, 0\, \cdots 0}_{L}\ \underbrace{D(\tfrac{N}{2})\, \cdots\, D(N-1)}_{N/2}]^T, \tag{5.4}$$

where $M = L + N$ is the IFFT size. The n-th component of the zero-padded

spread data D_{zp} is noted as $D_{zp}(n)$, where $n = 0, 1, \cdots, M-1$.

The spread data $\mathbf{D_{zp}}$ are then converted to a time domain by IFFT with a size of M to obtain time-discrete transmit signals (baseband)

$$S(t) = \frac{1}{\sqrt{M}} \sum_{n=0}^{M-1} D_{zp}(n) \cdot e^{j(\frac{2\pi}{M} \cdot n \cdot t)}, \tag{5.5}$$

where $t = 0, 1, \cdots, M-1$. The GI with cyclic extension [1] is then added to the signal $S(t)$.

We assume a slowly varying Rayleigh fading channel and 2-rays Rayleigh fading with equal power as the considered fading model. We also assume that synchronization is perfectly carried out. It is also assumed that the delay spreading is less than the GI length in order to maintain the orthogonality amongst the subcarriers.

Figs. 5.2(a) and 5.2(b) show the receiver structure of the OFDM system with a spreading code and MC-CDMA system, respectively. Accompanied by the noise, the received signal $R(t)$ is expressed as

$$\begin{aligned} R(t) &= \hat{S}(t) + \eta(t) \\ &= \frac{1}{\sqrt{M}} \sum_{n=0}^{M-1} H(n) \cdot D_{zp}(n) \cdot e^{j\left(\frac{2\pi}{M} \cdot n \cdot t\right)} + \eta(t), \end{aligned} \tag{5.6}$$

where $\hat{S}(t)$ is the multipath faded signal $S(t)$, $H(n)$ is the channel impulse response (CIR) of n-th subcarrier (will be cancelled by the equalizer) and $\eta(t)$ is noise. Signal $R(t)$ is performed by the FFT to obtain the frequency domain signals $\hat{D}(r)$ as

$$\begin{aligned} \widehat{D}(r) &= \frac{1}{\sqrt{M'}} \sum_{t=0}^{M'-1} R(t) \cdot e^{-j\left(\frac{2\pi}{M} \cdot t \cdot r\right)} \\ &= \frac{1}{\sqrt{M'}} \sum_{t=0}^{M'-1} \left(\frac{1}{\sqrt{M}} \sum_{n=0}^{M-1} H(n) \cdot D_{zp}(n) \cdot e^{j\left(\frac{2\pi}{M} \cdot n \cdot t\right)} + \eta(t) \right) \cdot e^{-j\left(\frac{2\pi}{M'} \cdot t \cdot r\right)} \\ &= H(r) \cdot D_{zp}(r) + Z(r), \end{aligned} \tag{5.7}$$

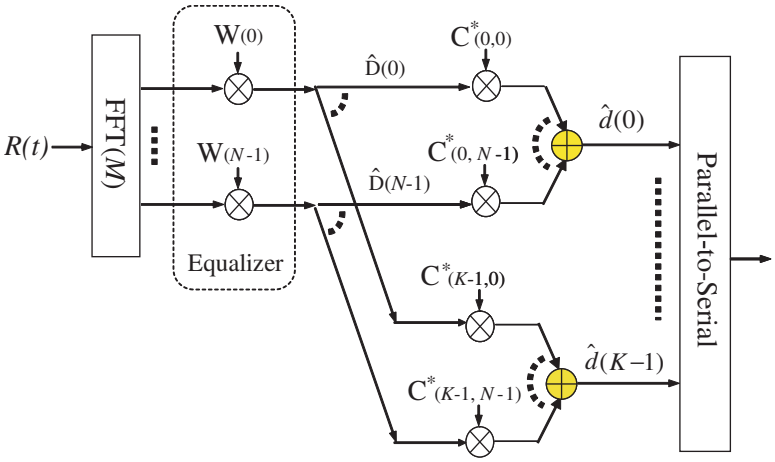

(a) The receiver of an OFDM with a spreading code

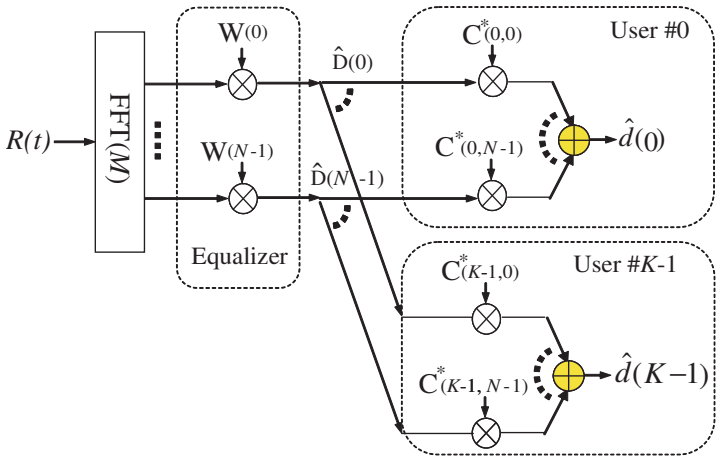

(b) The receiver of an MC-CDMA system

Figure 5.2. The receiver structures of an OFDM system with a spreading code and MC-CDMA system

where $r = 0, 1, \cdots, M' - 1$, M' is the size of FFT and $Z(r) = \frac{1}{\sqrt{M'}} \sum_{t=0}^{M'-1} \eta(t) \cdot e^{-j\left(\frac{2\pi}{M'} \cdot t \cdot r\right)}$ is the noise. The useful subcarrier components can be obtained as

$$\widehat{D}(i) = H(i) \cdot D(i) + Z(i), \tag{5.8}$$

where $i = 0, 1, \cdots, N - 1$.

This $\widehat{D}(i)$ is then equalized with weight values $W(i)$. We select minimum mean square error (MMSE) equalizer [21], a sub-optimal method for a performance which is close to the maximum likelihood (ML) method on multipath fading channel. As shown in Fig. 5.2, the MMSE equalization is located just after the FFT rather than between the de-spreading and combiner as in [14, 16]. Therefore, the computational complexity of the proposed design is similar to the equalization of the OFDM system. The conventional structure in [14, 16] may increase the computation complexity because of $K \times N$ complex multiplications should be performed.

Weighting values are derived from MMSE criteria as

$$W(i) = \frac{H^*(i)}{|H(i)|^2 + \sigma}, \tag{5.9}$$

where $H^*(i)$ is the complex conjugate of the CIR $H(i)$, and σ is the variance of noise. We assume that σ is uniform over the all subcarriers.

The MMSE equalized signals are then de-spread using the complex conjugate code $C^*(k, i)$ to obtain received data $\widehat{d}(k)$ (note that the length of $\widehat{D}(i)$ is now

N) as

$$\begin{aligned}
\widehat{d}(k) &= \frac{1}{\sqrt{K}} \sum_{i=0}^{K-1} W(i) \cdot \widehat{D}(i) \cdot C^*(k,i) \\
&= \frac{1}{\sqrt{K}} \sum_{i=0}^{K-1} W(i) \cdot \left\{ (H(i) \cdot D(i) + Z(i) \right\} \cdot C^*(k,i) \\
&\quad \text{(with } \widehat{D}(i) \text{ from (5.8))} \\
&= \frac{1}{\sqrt{K}} \sum_{i=0}^{K-1} W(i) \cdot H(i) \left(\frac{1}{\sqrt{K}} \sum_{u=0}^{K-1} d(u) \cdot C(u,i) \right) \cdot C^*(k,i) \\
&\quad + \frac{1}{\sqrt{K}} \sum_{i=0}^{K-1} W(i) \cdot Z(i) \cdot C^*(k,i) \\
&\quad \text{(with } D(i) \text{ from (5.1) but } k \text{ is changed to } u \text{ to avoid redundant parameters} \\
&= \frac{1}{K} \sum_{i=0}^{K-1} \sum_{u=0}^{K-1} W(i) \cdot H(i) \cdot d(u) \cdot C(u,i) \cdot C^*(k,i) \\
&\quad + \frac{1}{\sqrt{K}} \sum_{i=0}^{K-1} W(i) \cdot Z(i) \cdot C^*(k,i). \qquad (5.10)
\end{aligned}$$

To simplify the presentation, it is assumed that the output of the equalizer is $Y(i) = W(i) \cdot H(i)$, while element of the correlation of the spreading code is $X(u,k,i) = C(u,i) \cdot C^*(k,i)$. Thus, the (5.10) can be simplified as

$$\begin{aligned}
\widehat{d}(k) &= \frac{1}{\sqrt{NK}} \sum_{i=0}^{N-1} \sum_{u=0}^{K-1} d(u) \cdot X(u,k,i) \cdot Y(i) + \frac{1}{\sqrt{N}} \sum_{i=0}^{N-1} W(i) \cdot Z(i) \cdot C^*(k,i) \\
&= \frac{1}{\sqrt{NK}} \sum_{i=0}^{N-1} \sum_{u=0}^{K-1} d(u) \cdot X(u,k,i) \cdot Y(i) + \Gamma(k), \qquad (5.11)
\end{aligned}$$

where where $\Gamma(k) = \frac{1}{\sqrt{N}} \sum_{i=0}^{N-1} W(i) \cdot Z(i) \cdot C^*(k,i)$ is the noise. From (5.11), we conclude that the element of the correlation $X(u,k,i)$ should be minimized when $u \neq k$.

5.2. The Proposed Large Spreading Code

A large spreading code with a large code-number than its code-length is interesting in the view point of spreading code design. Some examples of the current existing codes for class of large code are TOCS, quadriphase code, POGC and POCI code. The proposed code has two purposes i.e. (1) provides larger number of codes with uniform low cross-correlation properties and (2) has ability to reduce the PAPR level.

To satisfy a low PAPR level, the code is designed in a complex form with phase $\theta \in [0, 2\pi]$ and has energy of unity. The code is then generally constructed as

$$C(k,n) = e^{j\theta(k,n)}. \tag{5.12}$$

The next problem is how to select the best phase $\theta(k,n)$ to satisfy the correlation properties of a good code i.e. low cross-correlation (by keeping the auto-correlation is always 1.0). By redefining the element of the correlation $X(u,k,i)$ in (5.11) as $X(p,q,n) = C(p,n) \cdot C^*(q,n)$. The real part of the correlation for N subcarriers can be derived as

$$\begin{aligned} \rho(p,q) &= \frac{1}{N}\sum_{n=0}^{N-1} C(p,n)\cdot C^*(q,n) \\ &= \frac{1}{N}\sum_{n=0}^{N-1} e^{j(\theta(p,n)-\theta(q,n))} \\ &= \frac{1}{N}\sum_{n=0}^{N-1} e^{j\cdot n\Delta\theta}; \quad (n\Delta\theta = \theta(p,n) - \theta(q,n)). \end{aligned} \tag{5.13}$$

We are interested in designing a code that has all elements are complex (except the first codeword), therefore it is acceptable to change the index n from $n = 0, 1, \cdots, N-1$ to $n = 1, 2, \cdots, N$ of (5.13) and obtain

$$\rho(p,q) = \frac{1}{N}\sum_{n=1}^{N} e^{j\cdot n\Delta\theta} \tag{5.14}$$

Now it is becoming easy to be solved using Geometric series for the total sum-

mation up to N as

$$S_N = \frac{r(1-r^N)}{1-r}, \tag{5.15}$$

where r is the ratio of the Geometric series. From (5.14), we got $r = e^{j\Delta\theta}$ to obtain

$$\begin{aligned}
\rho(p,q) &= \frac{1}{N} S_N \\
&= \frac{1}{N} \frac{e^{j\Delta\theta}(1-e^{j\Delta\theta\cdot N})}{1-e^{j\Delta\theta}} \\
&= \frac{1}{N} \frac{e^{j\frac{1}{2}\Delta\theta}(1-e^{j\Delta\theta\cdot N})}{e^{-j\frac{1}{2}\Delta\theta}-e^{j\frac{1}{2}\Delta\theta}} \\
&= \frac{1}{N} \frac{e^{j(N+1)\frac{1}{2}\Delta\theta}(e^{-j\frac{1}{2}\Delta\theta\cdot N}-e^{j\frac{1}{2}\Delta\theta\cdot N})}{e^{-j\frac{1}{2}\Delta\theta}-e^{j\frac{1}{2}\Delta\theta}} \\
&= \frac{1}{N} e^{j(N+1)\frac{1}{2}\Delta\theta} \cdot \left(\frac{e^{-j\frac{1}{2}\Delta\theta\cdot N}-e^{j\frac{1}{2}\Delta\theta\cdot N}}{e^{-j\frac{1}{2}\Delta\theta}-e^{j\frac{1}{2}\Delta\theta}} \right) \\
&= \frac{1}{N} \left(\cos(N+1)\tfrac{1}{2}\Delta\theta + j\sin(N+1)\tfrac{1}{2}\Delta\theta\right) \cdot \frac{\sin N\frac{1}{2}\Delta\theta}{\sin\frac{1}{2}\Delta\theta}.
\end{aligned} \tag{5.16}$$

where integers $p, q \in [1, K_{\max}]$ and $\Delta\theta = \theta(p,n) - \theta(q,n)$. The auto-correlation is obtained when $p = q$, noted as $\rho(p,p)$, i.e.

$$\begin{aligned}
\rho(p,p) &= \frac{1}{N}\sum_{n=1}^{N}(\cos n\cdot 0 + j\sin n\cdot 0) \\
&= N/N \\
&= 1
\end{aligned} \tag{5.17}$$

while the cross-correlation is obtained with $p \neq q$ and noted as $\rho(p,q)$.

To obtain a good spreading code, the cross correlation $\rho(p,q)$ should be minimized. Phase for perfect orthogonality $\rho(p,p) = 0$ can be obtained easily by solving (5.16) and obtain equality of $\sin\frac{1}{2}N\Delta\theta = 0$ by keeping $\sin\frac{1}{2}\Delta\theta \neq 0$. Finally, we will get $\Delta\theta = \frac{2\pi}{N}$ which is the basic phases of the CI code. However,

it does not meet our purpose to increase the capacity up to $K > N$ because the number of different phases is equal to the number of subcarriers. Consequently, it results in a spreading code with size of $N \times N$.

In this chapter, we consider a binary phase shift keying (BPSK) symbols. Therefore, it is acceptable to consider only the real part of (5.16) in this chapter. Code design that considers real and imaginary parts is left for future work. Thus, now we can only focus on the real parts of (5.16). Let us note the real parts with $R(p, q)$ as

$$\begin{aligned} R(p,q) &= \mathrm{Re}\{\rho(p,q)\} \\ &= \frac{1}{N}\cos\left(N+1\right)\tfrac{1}{2}\Delta\theta \cdot \frac{\sin\tfrac{1}{2}N\Delta\theta}{\sin\tfrac{1}{2}\Delta\theta} \\ &= \frac{1}{N}\left(\frac{\sin\left(2N+1\right)\tfrac{1}{2}\Delta\theta}{2\sin\left(\tfrac{1}{2}\Delta\theta\right)} - \frac{1}{2}\right) \\ &= \frac{1}{2N}\left(\frac{\sin\tfrac{1}{2}(2N+1)\Delta\theta}{\sin\tfrac{1}{2}\Delta\theta} - 1\right). \end{aligned} \tag{5.18}$$

By setting $\Delta\theta$ is low enough, we can approximate $\sin\frac{1}{2}\Delta\theta \cong \frac{1}{2}\Delta\theta$, because the difference is only about 36% even $\Delta\theta = \pi$. Therefore, we can approximate the $\sin(2N+1)\frac{1}{2}\Delta\theta / \sin\frac{1}{2}\Delta\theta$ in (5.18) as

$$\frac{\sin(2N+1)\frac{1}{2}\Delta\theta}{\sin\frac{1}{2}\Delta\theta} \approx \frac{\sin(2N+1)\frac{1}{2}\Delta\theta}{\frac{1}{2}\Delta\theta}. \tag{5.19}$$

Fig. 5.3 plots the curves of (5.19) to confirm the accuracy of the approximation on the number of subcarriers $N = 8$. Since a sinusoid is a periodical function, the (5.19) starts to enter the aliasing area at $\Delta\theta \geqslant 8\pi$. The figure indicates that phases with equal spaces (and capable of providing a uniform cross-correlation) are found when the (5.19) is equal to zero and mathematically expressed as

$$\frac{\sin(2N+1)\frac{1}{2}\Delta\theta}{\frac{1}{2}\Delta\theta} = 0. \tag{5.20}$$

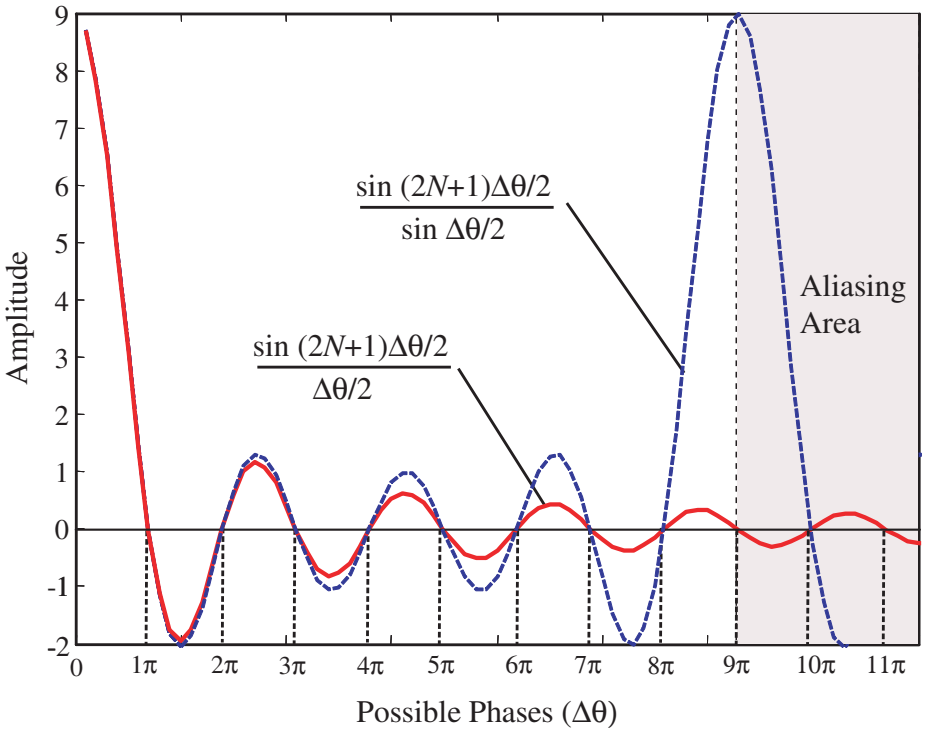

Figure 5.3. The accuracy of approximation in equation (5.19) and phases with equal spaces

Using the result of (5.20), we can get (5.18) as

$$R(p,q) = \frac{1}{2N}(0-1). \tag{5.21}$$

This cross-correalation is close to $R(p,q) \approx 0$, for a large N.

Phases with equal spaces is very important to guarantee a uniform cross correlation. By keeping $\sin\left(\frac{1}{2}\Delta\theta\right) \neq 0$, we can obtain new phases which have equal spaces by solving (5.20). The phases that satisfy the equality in (5.20) are

$$(2N+1)\tfrac{1}{2}\Delta\theta \;\; = \;\; \pi k, \;\; k = 1, 2, \cdots, 2N. \tag{5.22}$$

The value of k is limited to $2N$ because the $\sin(2N+1)\frac{1}{2}\Delta\theta$ is an alias of $\sin\frac{1}{2}\Delta\theta$ when $k > 2N$. Now, we obtain new $(2N+1)$ phases (phase 0 is included) for N subcarriers as

$$\Delta\theta = \frac{2\pi k}{(2N+1)}. \tag{5.23}$$

As an example for subcarrier number $N = 4$, we get 9 phases with equal space as illustrated in Fig. 5.3 i.e. $\{0,1,2,3,4,5,6,7,8\} \times \frac{2\pi}{9}$. Fig. 5.4 plots the phases of (5.23) and phases of the CI code. This figure also shows the real and imaginary parts of (5.16) for subcarrier $N = 4$.

Finally, from (5.12) and (5.14) which shows the considered index n from $n = 0, 1, \cdots, N-1$ to $n = 1, 2, \cdots, N$ or simply the index n should be $n+1$, the proposed code can be constructed as

$$C(k,n) = e^{j\left(\frac{2\pi}{2N+1}\right)\cdot k\cdot(n+1)}, \text{ for } \begin{cases} k = 0, 1, \cdots, 2N \\ n = 0, 1, \cdots, N-1 \end{cases}. \tag{5.24}$$

Equation (5.24) shows that the proposed code has code-number of $(2N+1)$ while its code-length is N. Consequently, the size is becoming $(2N+1)\times N$. Now, the designed spreading code meets the condition of a code where its code-number is larger than its code-length. It means that the user capacity or number of bits can be extended up to $(2N+1)$ users in multiuser multicarrier system with N subcarriers. In the OFDM system, $(2N+1)$ data symbols can be assigned on N

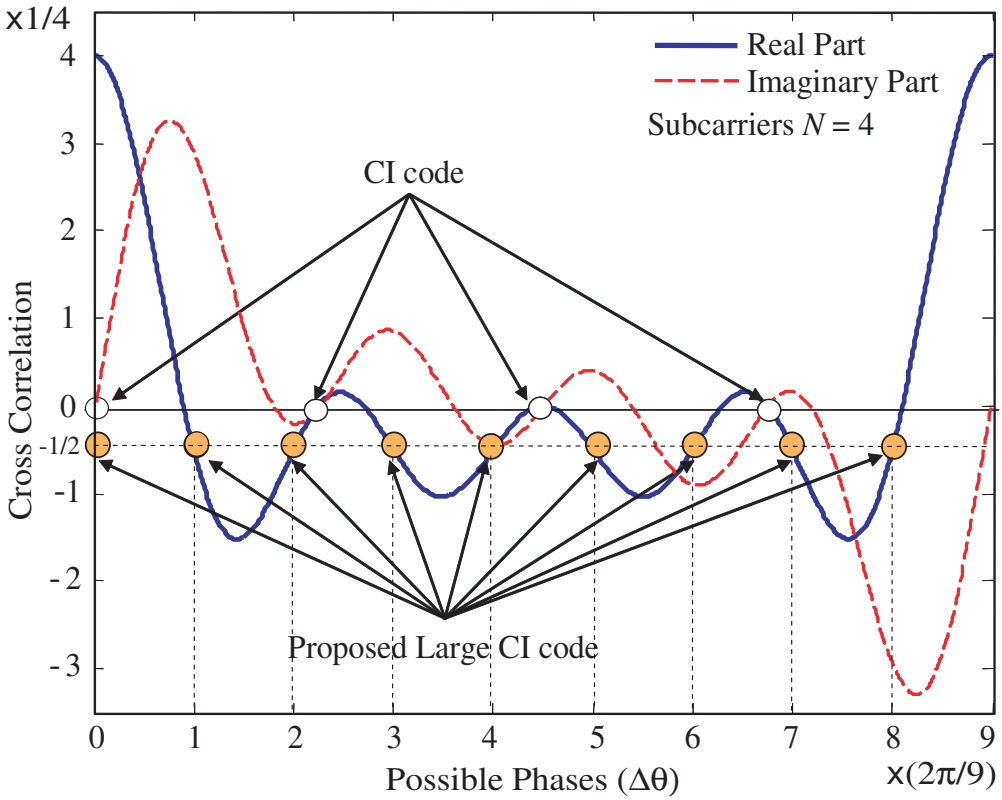

Figure 5.4. The real parts and imaginary parts of the correlation $\rho(p, q)$ of the proposed LCI code

subcarriers.

5.3. Cross-Correlations Analysis

This section analyzes the cross-correlation of the proposed LCI code and the POCI code. Uniform/equal cross-correlation code is interesting because of its assurance in the linearly independent of signals set that provides a minimum BER degradation. A code is said to have a uniform cross-correlation if the cross-correlation between different signals are all equal so we have the correlation matrix of that code as

$$R = \begin{bmatrix} 1 & & & & \\ & 1 & & \varphi & \\ & & \ddots & & \\ & \varphi & & 1 & \\ & & & & 1 \end{bmatrix}. \tag{5.25}$$

The matrix has all elements on the main diagonal equals to unity while the other parts equal to φ. It was also proven in [31] that this matrix has only two distinct eigenvalues i.e. $1-\varphi$ and $1+(K-1)\varphi$ for a matrix with a size of $K \times K$. Consequently, the value of φ is in the range of

$$-\frac{1}{K-1} \leq \varphi \leq 1. \tag{5.26}$$

where, K is the code-number. Recalling (5.18), the cross-correlation of the proposed LCI code with its equal cross-correlation can be formulated as

$$R_{LCI}(p,q) = \begin{cases} 1, & \text{for } p = q \\ -\dfrac{1}{2N}, & \text{for } p \neq q \end{cases}. \tag{5.27}$$

Here, we find that $\varphi = -\frac{1}{2N}$ for $K = 2N+1$. Now, it is clear that (5.26) can be satisfied by the proposed LCI code.

The POCI code for N subcarriers comprises two code sets of the CI code

(phase $\frac{\pi}{N} \cdot n$ is added for modifying the second code set) as

$$\mathrm{POCI}(k,n) = \begin{cases} e^{j\left(\frac{2\pi}{N}k \cdot n\right)}, & \text{for } k = 0, 1, \cdots, N-1 \\ e^{j\left(\frac{2\pi}{N}k \cdot n + \frac{\pi}{N} \cdot n\right)}, & \text{for } k = N, N+1, \cdots, 2N-1 \end{cases} . \quad (5.28)$$

Therefore, the POCI code has two distinct cross-correlation values i.e. zero and non-zero (ψ) as derived below. Zero cross-correlation exists if and only if $p, q \in [0, N-1]$ or $p, q \in [N, 2N-1]$. Generally, the cross-correlation of POCI can be derived as

$$\left|\rho^{\mathrm{POCI}}(p,q)\right| = \begin{cases} 0, & p, q \in [0, N-1], p, q \in [N, 2N-1] \\ \psi, & \text{otherwise} \end{cases} \quad (5.29)$$

where

$$
\begin{aligned}
\psi &= \frac{1}{N}\sum_{n=0}^{N-1} e^{j\left(\frac{2\pi}{N}k+\frac{\pi}{N}\right)\cdot n} \\
&= \frac{1}{N}\left(\frac{1-e^{j\left(\frac{2\pi}{N}k+\frac{\pi}{N}\right)\cdot N}}{1-e^{j\left(\frac{2\pi}{N}k+\frac{\pi}{N}\right)}}\right) \\
&= \frac{1}{N}\left(\frac{e^{-j\frac{1}{2}\left(\frac{2\pi}{N}k+\frac{\pi}{N}\right)}-e^{j\ N-\frac{1}{2}\ \left(\frac{2\pi}{N}k+\frac{\pi}{N}\right)}}{e^{-j\frac{1}{2}\left(\frac{2\pi}{N}k+\frac{\pi}{N}\right)}-e^{j\frac{1}{2}\left(\frac{2\pi}{N}k+\frac{\pi}{N}\right)}}\right) \\
&= \frac{1}{N}\left(\frac{e^{-j\frac{1}{2}\left(\frac{2\pi}{N}k+\frac{\pi}{N}\right)}-e^{j(N-\frac{1}{2})\left(\frac{2\pi}{N}k+\frac{\pi}{N}\right)}}{-2j\sin\frac{1}{2}\left(\frac{2\pi}{N}k+\frac{\pi}{N}\right)}\right) \\
&= \frac{1}{N}\left(\frac{j\left(e^{-j\frac{1}{2}\left(\frac{2\pi}{N}k+\frac{\pi}{N}\right)}-e^{j(N-\frac{1}{2})\left(\frac{2\pi}{N}k+\frac{\pi}{N}\right)}\right)}{2\sin\frac{1}{2}\left(\frac{2\pi}{N}k+\frac{\pi}{N}\right)}\right) \\
&= \frac{1}{N}\left(\frac{\sin\frac{1}{2}\left(\frac{2\pi}{N}k+\frac{\pi}{N}\right)+\sin\left(\left(N-\frac{1}{2}\right)\left(\frac{2\pi}{N}k+\frac{\pi}{N}\right)\right)}{2\sin\frac{1}{2}\left(\frac{2\pi}{N}k+\frac{\pi}{N}\right)}\right) \\
&\quad +j\cdot\frac{1}{N}\left(\frac{\cos\frac{1}{2}\left(\frac{2\pi}{N}k+\frac{\pi}{N}\right)-\cos\left(\left(N-\frac{1}{2}\right)\left(\frac{2\pi}{N}k+\frac{\pi}{N}\right)\right)}{2\sin\frac{1}{2}\left(\frac{2\pi}{N}k+\frac{\pi}{N}\right)}\right) \qquad (5.30)
\end{aligned}
$$

With the same assumption that the data symbols are in BPSK, we only focus on the real components of the cross-correlations. The real part of cross-correlation

of POCI code as proven above can be expressed as

$$\begin{aligned}
R_{POCI} &= \mathrm{Re}(\psi) \\
&= \frac{1}{N}\frac{\sin\frac{1}{2}\left(\frac{2\pi}{N}k+\frac{\pi}{N}\right)+\sin\left(\left(N-\frac{1}{2}\right)\left(\frac{2\pi}{N}k+\frac{\pi}{N}\right)\right)}{2\sin\frac{1}{2}\left(\frac{2\pi}{N}k+\frac{\pi}{N}\right)} \\
&= \frac{1}{N}\left(\frac{1}{2}+\frac{\sin\left(\left(N-\frac{1}{2}\right)\left(\frac{2\pi}{N}k+\frac{\pi}{N}\right)\right)}{2\sin\left(\frac{1}{2}\left(\frac{2\pi}{N}k+\frac{\pi}{N}\right)\right)}\right) \\
&= \frac{1}{N}\left(\frac{1}{2}+\frac{\sin(2\pi k+\pi)\cos\left(\frac{1}{2}\left(\frac{2\pi}{N}k+\frac{\pi}{N}\right)\right)-\cos(2\pi k+\pi)\sin\left(\frac{1}{2}\left(\frac{2\pi}{N}k+\frac{\pi}{N}\right)\right)}{2\sin\left(\frac{1}{2}\left(\frac{2\pi}{N}k+\frac{\pi}{N}\right)\right)}\right) \\
&\quad \text{(Here for any integer } k,\ \sin(2\pi k+\pi)=0 \text{ and } \cos(2\pi k+\pi)=-1) \\
&= \frac{1}{N}\left(\frac{1}{2}+\frac{1}{2}\right), \qquad (5.31)
\end{aligned}$$

and generally as

$$R_{POCI}(p,q)=\begin{cases} 1, & \text{for } p=q \\ 0, & \text{for } p\neq q,\ p,q\in[0,N-1], p,q\in[N,2N-1] \\ \frac{1}{N}, & \text{otherwise} \end{cases} . \quad (5.32)$$

Now, we can compare the cross correlation of the proposed LCI code in (5.27) and the POCI code in (5.32). For an example with $N = 4$, Fig. 5.5 illustrates the shape of the correlation of LCI and POCI codes. We can fairly compare the orthogonality of both codes using this figure. POCI code 1 up to 4 are correlated to code 5 up to 8 (indicated by gray area), while the proposed LCI code has lower and equal correlation with code 5 up to 9 (indicated by a similar white color that covers overall the whole area). It means that the proposed LCI codes are capable of providing low and uniform cross-correlation which ensures user fairness and lower error probability.

Revisiting (5.32) and (5.27), we get maximum cross-correlation R_{max} of the POCI code and the proposed LCI code as

$$I_{max}(POCI)=\sqrt{\frac{1}{N}}, \qquad (5.33)$$

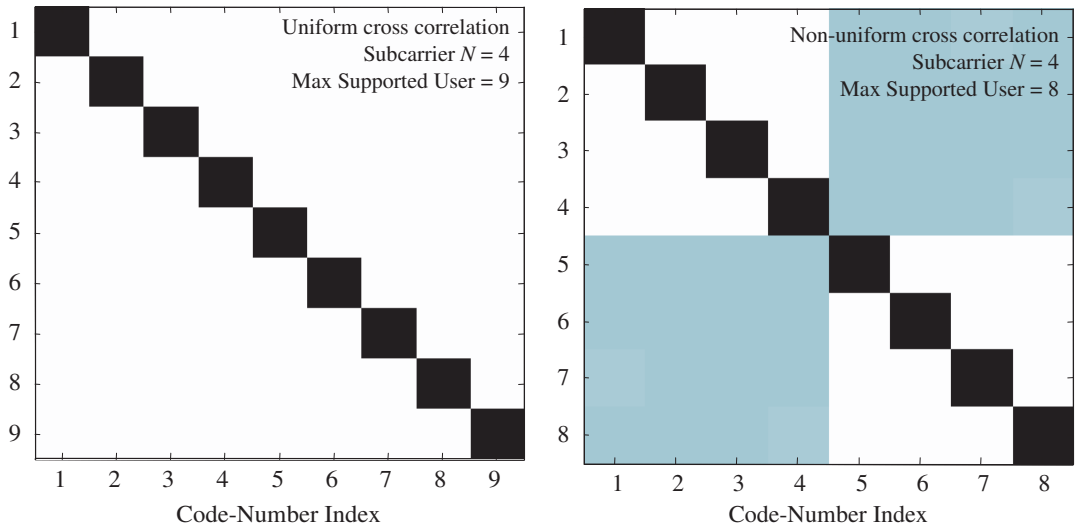

(a) The proposed LCI code

(b) The POCI code

Figure 5.5. The cross-correlation's shape of (a) the proposed LCI code and (b) the POCI code.

and

$$I_{max}(LCI) = \sqrt{\frac{1}{2N}}. \tag{5.34}$$

The results are plotted in Fig. 5.6 for any N (up to $N = 32$). It can be observed that for any value of N the R_{max} of the proposed LCI code is always equal to half of the cross-correlation of POCI code. For $N = 16$, we get $R_{max}(LCI) = \sqrt{\frac{1}{2N}} = 0.1768$ while $R_{max}(POCI) = \sqrt{\frac{1}{N}} = 0.2500$.

5.4. PAPR and Instantaneous Normalized Power Evaluations

The superposition of N signals to obtain the OFDM symbol may generate a high peak signal level. The PAPR is obtained by taking into account only one sample (the highest peak) per OFDM symbol. However, from a practical point of view, it is not interesting to evaluate only one sample of that maximum peak,

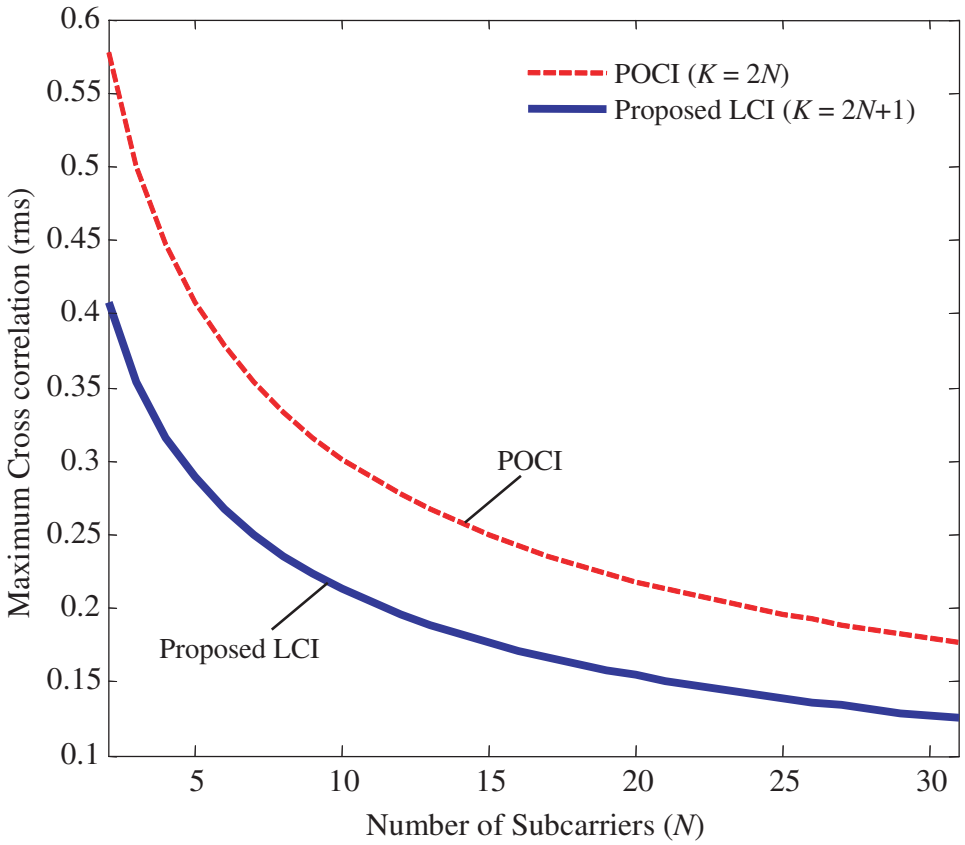

Figure 5.6. The maximum cross-correlation of the POCI and the proposed LCI code for several number of subcarriers.

but investigating all samples will give a better evaluation of peak power distributions. Therefore, beside the PAPR evaluation we present an INP performance to describe the power distribution in all samples.

The superpositions of signals that cause a high PAPR level are expected to be avoided by employing a complex spreading code. To meet this condition, the code should be composed of complex components with phases $\theta \in [0, 2\pi]$ and energy of unity. Thus, our proposed code which was designed to satisfy this condition will be evaluated in this section.

We consider OFDM and MC-CDMA with number of subcarriers $N = 16$ and BPSK symbols. As a consequence, both of the code-length of POCI and the proposed LCI code are equal to 16, while the code-number of the POCI and the proposed LCI code is 32 and 33, respectively. It means that in one OFDM symbol with the POCI code, 32 BPSK symbols can be assigned, while in one OFDM symbol with the proposed LCI code, 33 BPSK symbols are able to be assigned. With number of OFDM symbols $N_{OS} = 10,000$, we plot the PAPR and INP performances of both the POCI and the proposed LCI code. Considering to oversampling factor of $L = 4$, the samples obtained for the INP analysis are about $100,000$ samples.

The results of PAPR evaluations are plotted in Fig. 5.7(a) at CCDF of 10^{-4}. It is shown that PAPR level of OFDM is about 11.5dB, while OFDM with POCI codes is 7.5dB. Thus, a significant reduction about 4dB is obtained. It is interesting to note that the proposed LCI code also achieved a similar PAPR performance with that of the POCI code about 7.5dB at CCDF of CCDF of 10^{-4}.

Fig. 5.7(b) shows the INP performances of OFDM with the POCI and the proposed LCI and that of OFDM without spreading code. At CCDF of 10^{-4} the INP of OFDM is more than 10dB, while the INP of the POCI and the proposed LCI codes are similar in about 7.2dB. The proposed LCI code has similar performance as that of POCI code for both in PAPR and INP performances because LCI has been constructed from complex element with phase of $\theta \in [0, 2\pi]$ and energy of unity. Here, we can conclude that the proposed spreading code is capable of reducing significantly the PAPR and the INP of OFDM system similar as that of the POCI code.

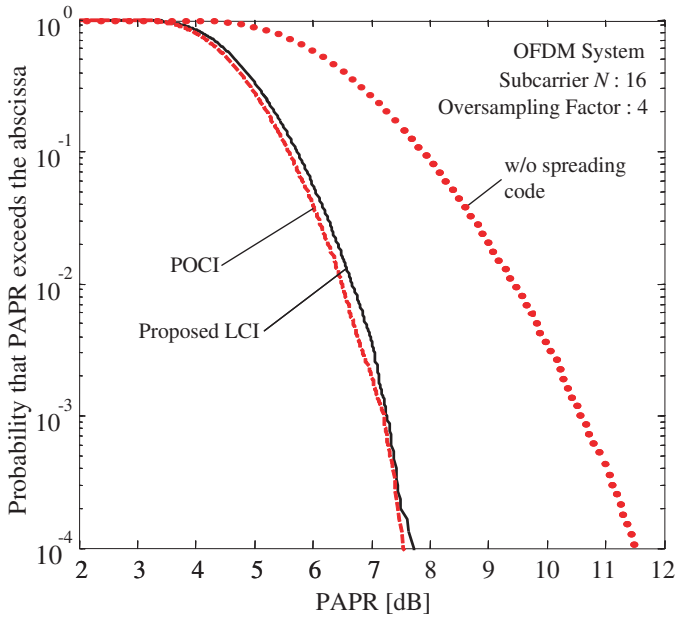

(a) PAPR Performance

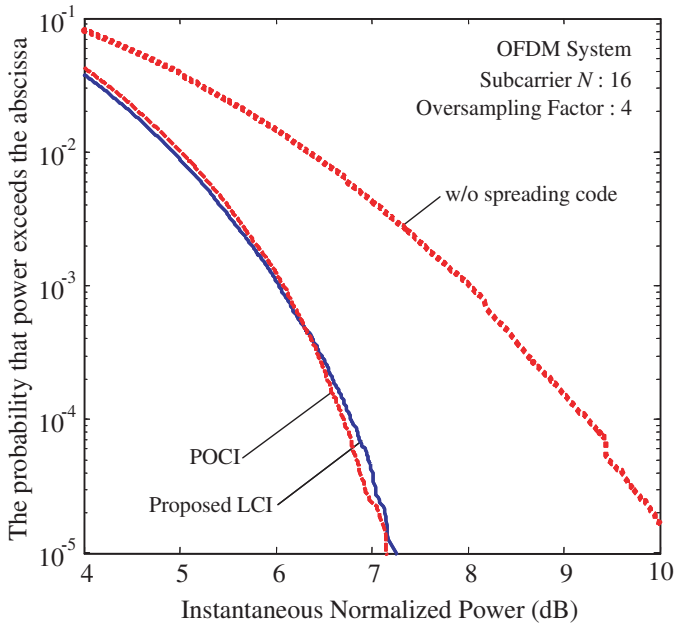

(b) INP Performance

Figure 5.7. PAPR and instantaneous normalized power (INP) performances of OFDM signals using the POCI code and the proposed LCI code

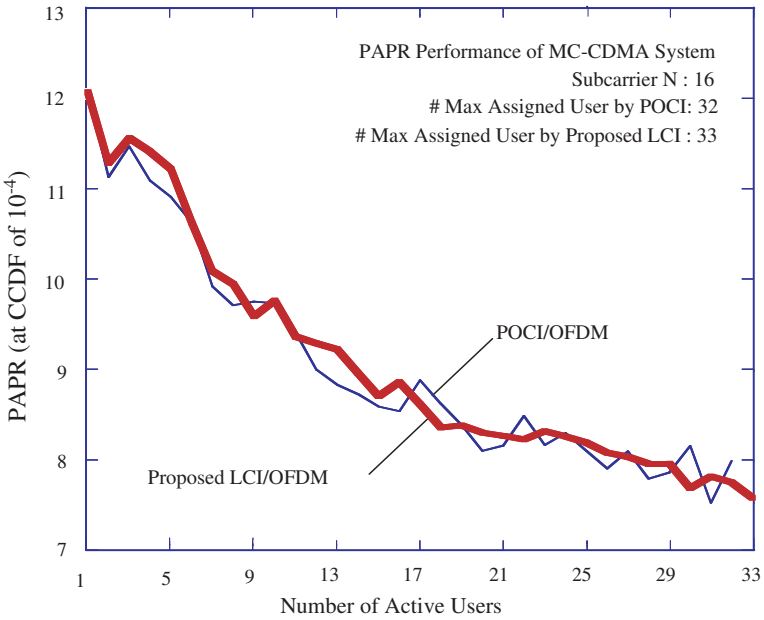

Figure 5.8. PAPR performance of MC-CDMA signals using POCI and the proposed LCI codes

In MC-CDMA system which the performance of peak power depends on the number of active users, we prefer to investigate the peaks with PAPR rather than with the INP for the reason of simplicity since PAPR only measures the maximum peak power. The results of PAPR evaluations are shown in Fig 5.8 for several numbers of active users. The results were obtained from 10,000 MC-CDMA symbols (downlink) with number of active users is varied from 1 to 32 for the POCI code and 1 to 33 for the proposed LCI code. The PAPR performances of the proposed LCI and POCI code are very similar for any number of active users, where both the PAPRs of the POCI and the proposed LCI codes decrease as the number of active users increases.

5.5. BER Performances Evaluation

This section evaluates the BER performance of the proposed LCI code in AWGN and a multipath fading channel for both OFDM and MC-CDMA systems with parameters as shown in Table 5.1.

Table 5.1. Simulation parameters for performances evaluation of the proposed LCI code

	Parameters	**Values**
Transmitter	Modulation of POCI	BPSK
	Modulation of LCI	BPSK
	Modulation of OFDM	QPSK
	Code-length	16
	Subcarrier (N)	16
	Oversampling factor (L)	4
	GI length	25%
	Error correction coding	–not applied–
Channel	AWGN	–
	Fading	2-rays Rayleigh, equal power
Receiver	Equalizer	MMSE

5.5.1 The BER Performance in AWGN Channel

We evaluate the BER performance of OFDM system with the number of subcarriers $N = 16$. It means that one OFDM symbol contains 32 BPSK data symbols for POCI and 33 BPSK data symbols for the proposed LCI. For a fair comparison we also plot the BER performance of QPSK in OFDM (without spreading code) by expecting the number of information bits is similar i.e. 32 bits in QPSK, 32 bits in POCI code and 33 bits in the proposed LCI code. The results are plotted in Fig. 5.9. Although the LCI code has BER degradation about 1.4dB compared to that of QPSK OFDM, the LCI code outperforms the POCI code about 5dB at average BER of 10^{-4}. This improvement comes from the benefit of uniform cross-correlation by the value of $\varphi = -\frac{1}{2N}$ presented by the proposed LCI code. However, the degradation of the LCI code comes from the non-zero cross-correlation especially when N is small. We expect that the degradation will diminish as the number of subcarriers N increases, because $\varphi = |-\frac{1}{2N}| \simeq 0$ for a large N.

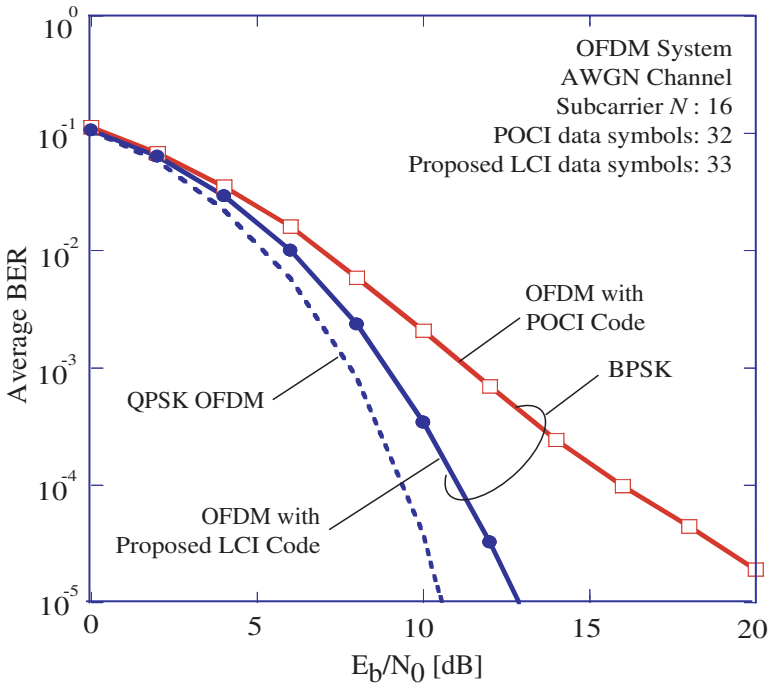

Figure 5.9. BER performance of POCI and the proposed code in AWGN channel

5.5.2 BER Performance in a Multipath Fading Channel

In multipath fading environment evaluation, 2-ray Rayleigh fading is considered. We evaluate the OFDM with subcarriers of $N = 16$. The BPSK data symbols is considered for POCI code and the LCI code, while QPSK data symbol for the OFDM without spreading code to obtain a fair comparison. For the MC-CDMA evaluation, we plot the BER with two conditions of active users i.e. below $N(K_{\text{user}} = 10)$ and above N $(K_{\text{user}} = 30)$.

Fig. 5.10 shows the BER of the OFDM system versus the E_b/N_0. Three curves are presented i.e. BER of QPSK OFDM (without spreading code), with the POCI code and with the proposed LCI code. From the figure, we can conclude that the proposed code has gain about 3.6dB compared with POCI code and 7.5dB compared with QPSK OFDM at the same average BER of 10^{-4}. It can be concluded that the proposed LCI code provides a better performance in multipath fading channel than the POCI and QPSK OFDM without spreading code.

For the MC-CDMA system, with the same fading model, BER performance

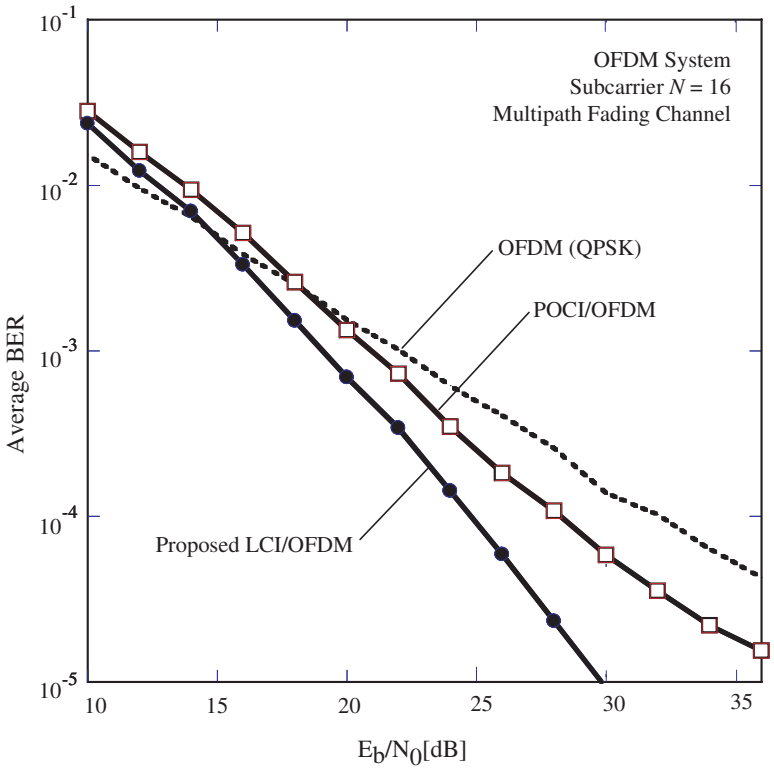

Figure 5.10. The BER performance of an OFDM system with the POCI and the proposed LCI code in a multipath fading channel

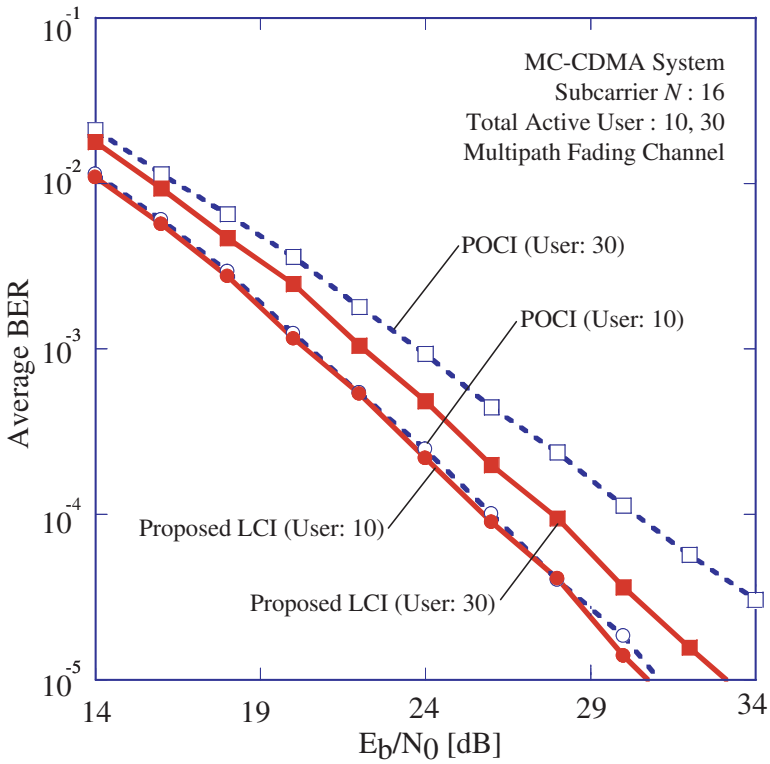

Figure 5.11. BER performance of MC-CDMA with POCI and the proposed LCI code in multipath fading channel

results are plotted in Fig. 5.11 for several numbers of users K_{user} of 10 and 30 or load factor of 62% and 188%, respectively. When the $K_{\text{user}} = 10$, it is observed that POCI and LCI code has a similar performance. It is interesting to note that the proposed LCI code with a uniform cross-correlation of $\varphi = |-\frac{1}{2N}|$ provides similar performance as that of the POCI code, though for $K_{\text{user}} \leq N$, the POCI may have cross-correlation $\varphi = 0$ (orthogonal). However, the BER performance of the POCI code degrades as the number of active user increases above 16 users ($K_{\text{user}} > N$). The ($K_{\text{user}} > N$) is the condition when the POCI code suffers from interference with higher cross-correlation of $\varphi = \frac{1}{N}$. For $K_{\text{user}} = 30$, the proposed LCI code improves BER performance about 2.8dB at average BER of 10^{-4}.

5.5.3 The BER Performance in the Presence of Error Correction Coding

This section evaluates the performance when the error correction coding is employed. A convolutional coding with coding rate $r = 1/2$ and $r = 2/3$ is employed. The convolutional encoder has a constraint length $K = 7$ with a generator polynomials in octal representation is [171,133]. Although the evaluation is performed for the OFDM system, the MC-CDMA system is expected to have a similar trend as the results in OFDM system.

Fig. 5.12 plotted the BER performance in the AWGN and multipath fading channel. As shown in Fig. 5.12(a), with a coding rate $r = 2/3$, the proposed LCI code provides the best performance even with the BER performance of QPSK in OFDM system. When the coding rate is set to $r = 1/2$, the proposed LCI code has a small degradation compared with OFDM and the POCI code.

Fig. 5.12(b) plotted the BER in multipath fading channel. For a code rate $r = 1/2$, the proposed LCI code has a similar performance with the POCI and QPSK OFDM systems. However, with $r = 2/3$, the proposed LCI code has the best performance about 2.5dB and 1dB better compared with the BER performance of OFDM and POCI/OFDM at BER of 10^{-4}, respectively.

The performance is similar to what was reported in [22] that a coded spread OFDM outperforms a coded OFDM for code rate $r > 1/2$, while no significant difference when code rate $r < 1/2$. An explanation of this phenomenon is that the high redundancy of low code rates (associated with interleaving) already performs a kind of spreading by linking a number of subcarriers through the memory introduced by the convolutional encoder. It exploits all the diversity of the channel.

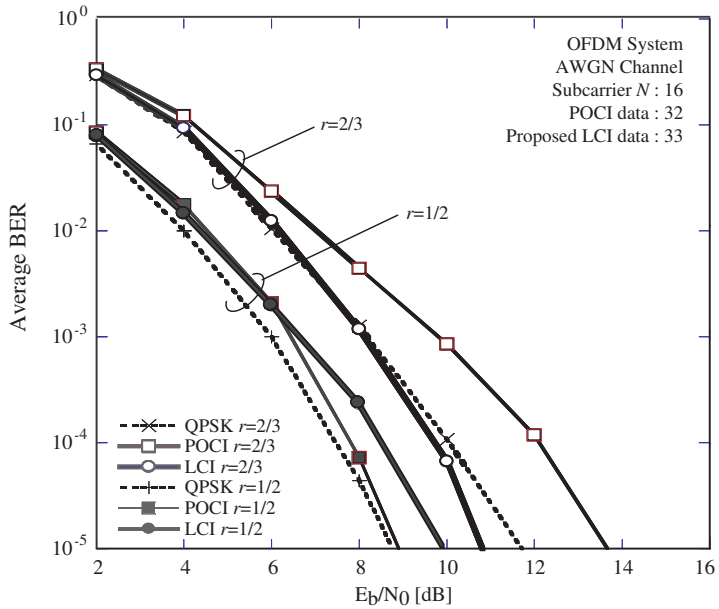

(a) The BER in AWGN

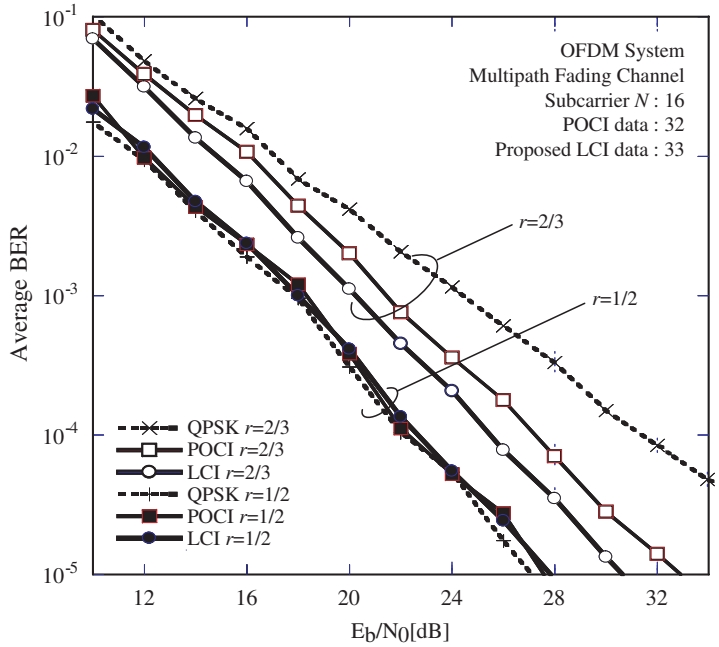

(b) BER in a multipath fading channel

Figure 5.12. The BER performances of coded system with coding rate $r = 1/2$ and $r = 2/3$

Chapter 6

Iterative Clipping for OFDM over Nonlinear Channels

THIS chapter proposes an iterative clipping (IC) for the CI-FFT/OFDM system in Chapter 4 for improving the performance of OFDM and guaranteing lower peak power level and lower OOB spectrum radiation. The proposed method is then called carrier interferometry with iterative clipping (CI-IC) method. The iterative clipping developed in this chapter ensures low PAPR level and lower OOB spectrum radiation. Therefore, additional filtering is not required to remove the OOB spectrum radiation that appears in the conventional clipping method.

It is interesting to investigate the instantaneous normalized power (INP) that measures the distribution of power levels in all samples rather than only one sample (of maximum value) as in the PAPR measurement. Thus, INP can be a powerful tool to show the power distribution of OFDM system in a practical hardware implementation. The proposed CI-IC method offers new advantages to produce OFDM signal with lower INP level and minimize BER degradation as well as OOB spectrum radiation.

With a similar computational complexity, the proposed CI-IC method outperforms the well known PTS, SLM and iterative processing (IP) techniques in terms of INP performance. Interesting results on the evaluations on OFDM through the nonlinear channel show that the proposed technique is efficient and has potential

for future applications.

The remainder of this chapter is as follows. Section 6.1 reviews OFDM System model over the non-linear channel. The proposed method is presented in Section 6.2, computational complexity and performance evaluation are in Section 6.3 and 6.4, respectively. Section 6.5 optimizes the proposed method.

6.1. Nonlinear Channel Model

As described in Chapter 1, an OFDM symbol is obtained by mapping of N parallel data symbols using M IFFT size (M is the IFFT size which usually is power of two for efficient implementation) as

$$s(t) = \frac{1}{\sqrt{M}} \sum_{m=1}^{M-1} d(m) \cdot e^{j\left(\frac{2\pi mp}{M}\right)},\ t = 0,\ 1,\ 2,\ \cdots,\ M-1\,, \tag{6.1}$$

where $d(m)$ is the m-th complex transmit quadrature amplitude modulation (QAM) symbol at m-th subcarrier ($M - N$ zeros for guard-band and oversampling are included). The random superposition of subcarriers with random phases can yield high peaks, and thus gives rise to a signal with large dynamic range. PAPR is one way to measure the amplitude variation of transmitted signal and mathematically has been defined in (2.9). Though the PAPR is widely used to measure the signal dynamic range, it is interesting to evaluate the INP performance due to its capability in measuring power level in all samples. INP has been mathematically expressed in (2.10).

The upper bound of PAPR and INP, theoretically, increases linearly with the increasing of the number of subcarriers. However, the probability of coherent superposition that results in high peak becomes small with increasing number of subcarriers. In [54] theoretical distribution based on heuristic assumptions was shown to well match computer simulation results. One of major system deterioration due to the dynamic range is given by the nonlinear distortion generated by HPA at the transmitter end [39]. The HPA model, especially SSPA is considered in this chapter. The evaluation is performed on PSD and BER performance after the nonlinear channel. OFDM through SSPA model is shown in Fig. 6.1.

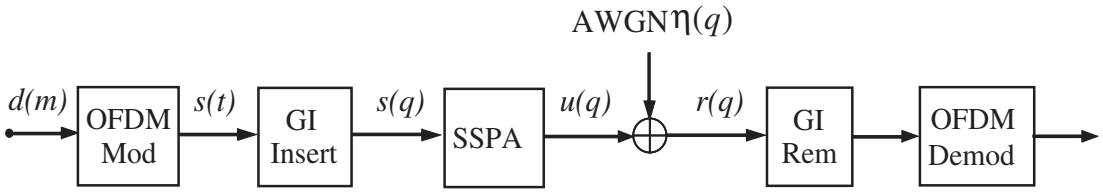

Figure 6.1. OFDM system model over the nonlinear channel

Throughout this chapter, we consider discrete time signal representation. $d(k)$ is input data, $s(n)$ and $s(q)$ are the OFDM symbols before and after guard interval (GI) insertion, $u(q)$ is output of SSPA, $\eta(q)$ is additive white Gaussian noise (AWGN) and $r(q)$ is the received OFDM signals. Signal $u(q)$, as the amplified OFDM signals, can be expressed as

$$u(q) \triangleq s(q)G\left(|s(q)|^2\right), \tag{6.2}$$

where $G(\cdot)$ is the amplifier gain as

$$G(|s(n)|) \triangleq \frac{A(|s(q)|)}{|s(q)|} \cdot e^{j\Phi(|s(q)|)}. \tag{6.3}$$

The function of $A(\cdot)$ represents AM/AM and $\Phi(\cdot)$ corresponds to AM/PM conversion. We refer to an SSPA model with a nonlinear memoryless transformation between complex envelopes of input and output signals as described in [39]. The considered $A(\cdot)$ and $\Phi(\cdot)$ of the SSPA model were expressed in (2.14). To obtain appropriate value of smoothness factor p, the actual SSPA for wireless LAN application is considered. This chapter considers the SSPA design as previously described in Chapter 2.

6.2. Proposed CI-IC Method

This section discusses the proposed CI-IC method for CI-FFT/OFDM system. Because the detail of CI-FFT/OFDM system has been described in Chapter 4, this section will focus on the design of CI-IC method.

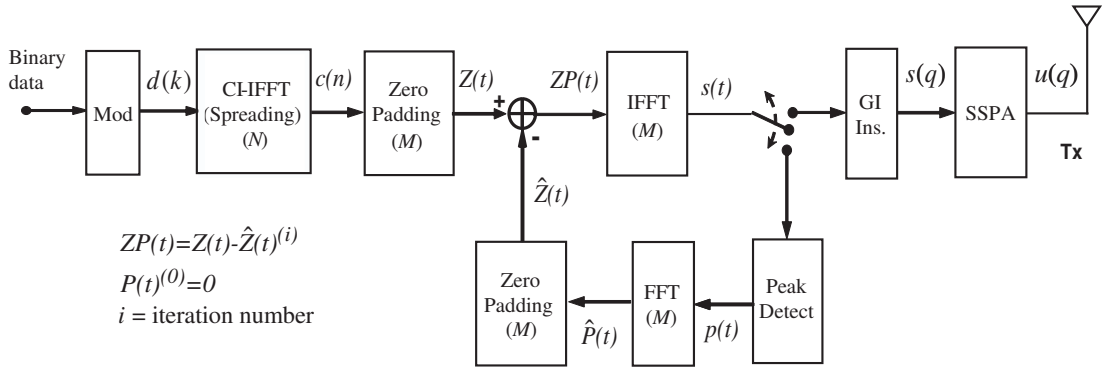

(a) Proposed CI-IC/OFDM transmitter

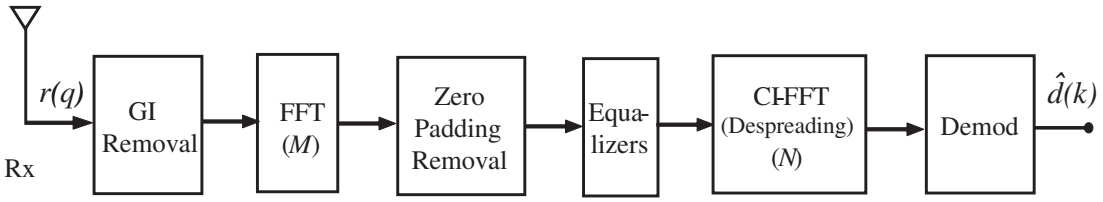

(b) Proposed CI-IC/OFDM receiver

Figure 6.2. Block diagram of the proposed CI-IC method

Iterative clipping (IC) is then combined with CI-(I)FFT spreading and called as CI-IC method. The proposed CI-IC uses iterative clipping instead of the repeated clipping method as in [35] with cascaded clipping to reduce the number of FFTs. Instead of normal clipping that passes the signal lower than the clipping level (threshold T_h level), we clip the signal and pass only the upper parts. The frequency domain of this upper part is zero padded to remove the OOB spectrum radiation caused by clipping. The zero padded signal is then subtracted from the spread data. The detail of the proposed CI-IC is presented below.

Figs. 6.2(a) and 6.2(b) illustrate the proposed block diagrams of CI-IC for OFDM transmitter and receiver, respectively. At the transmitter the information sequence to be transmitted is assumed QAM data modulated $d(k)$ then serial-to-parallel transformed before spreading with CI-IFFT.

The spread data, $c(n)$, as the result of CI-IFFT spreading (with number of

input data is N), can be expressed as

$$c(n) = \frac{1}{\sqrt{N}} \sum_{k=0}^{N-1} d(k) \cdot e^{j\left(\frac{2\pi}{N} \cdot k \cdot n\right)},\ s\ =\ 0,\ 1,\ \cdots,\ N-1, \tag{6.4}$$

where N is also the total number of subcarriers. After data are spread using CI-IFFT, zero padding with $M - N$ zeros is applied to $c(n)$ and to get Z with length of M as

$$Z = [\underbrace{c(0)\ c(1)\ \cdots\ c\left(\tfrac{s}{2}-1\right)}_{\frac{N}{2}}\ \underbrace{0\,0\,\cdots,\,0\,0}_{Z}\ \underbrace{c\left(\tfrac{s}{2}\right),\,\cdots,\,c(S-1)}_{\frac{N}{2}}]. \tag{6.5}$$

$Z(t)$ of (6.5) is then subtracted with $\hat{Z}(t)$ to get $ZP(t)$, where $\hat{Z}$ is the upper part of the clipped signal and ZP is the result of the subtraction. The $ZP(t)$ performed to obtain the discrete-time domain signal $s(t)$ as

$$s(t) = \frac{1}{\sqrt{M}} \sum_{m=0}^{M-1} ZP(m) \cdot e^{j\left(\frac{2\pi}{N} \cdot m \cdot t\right)},\ t\ =\ 0,\ 1,\ \cdots,\ M-1. \tag{6.6}$$

Next, the iterative clipping (IC) is performed on the OFDM signal $s(t)$. Being different from the conventional clipping, the clipping here is performed by detecting the signal portion, called as peak signal $p(t)$, that exceeds the given threshold (T_h). The peak signal $p(t)$ is described as

$$p(t) = \begin{cases} 0 & \text{for } |s(t)| \leqslant T_h \\ s(t) \cdot \left(1 - \frac{T_h}{|s(t)|}\right) & \text{for } |s(t)| > T_h \end{cases}, \tag{6.7}$$

where T_h is the desired PAPR threshold (dB) in the peak detection part of Fig. 6.2(a). Signal $p(t)$ is then transformed by FFT to obtain frequency domain signal $\hat{P}(t)$. Finally, zero padding is performed to $\hat{P}(t)$. Zero padding in this operation is another kind of filtering in frequency domain to avoid OOB spectrum radiation. The unused subcarriers in $\hat{P}(t)$ are zeroed as in (6.5) to obtain zero padded signal $\hat{Z}(t)$. $\hat{Z}(t)$ is then subtracted from $Z(t)$ so that the peak generation is avoided. Now, the new OFDM signal for the first iteration is generated from $Z(t) - -\hat{Z}(t)^{(1)}$

as

$$s(t)^{(1)} = \frac{1}{\sqrt{M}} \sum_{m=0}^{M-1} \left\{ Z(t) - \hat{Z}(t)^{(1)} \right\} e^{j\frac{2\pi}{M} \cdot m \cdot t}, \;\; t = 0,\, 1,\, \cdots,\, M-1, \qquad (6.8)$$

where $\hat{Z}^{(1)}$ is the $\hat{Z}$ of the 1-st iteration.

Generally, for the i-th iteration, the process of (6.6)–(6.8) is repeated so that new $s(t)^{(i)}$ is obtained as

$$s(t)^{(i)} = \frac{1}{\sqrt{M}} \sum_{m=0}^{M-1} \left\{ Z(t) - \hat{Z}(t)^{(i)} \right\} \cdot e^{j\frac{2\pi}{M} \cdot m \cdot t}, \;\; t = 0,\, 1,\, \cdots,\, N-1, \qquad (6.9)$$

where (i) is the number of iterations. If $i = 0$, it means the iteration (and clipping) is not performed so $\hat{Z}(t)^{(0)} = 0$.

Because the peak is still re-growing due to the zero padding in the previous iteration, the target PAPR bound can not be attained in single execution, therefore it requires further iterations. In addition, the lower PAPR obtained by iteration can give the advantage of lower OOB radiation after the nonlinear SSPA amplifier. CI-IFFT, however, guarantees a small number of iteration to obtain similar PAPR. At the last stage of iteration, GI is inserted to produce the transmit signal $s(q)$, where $q = 0,\, 1,\, \cdots,\, G$ and $G = N + GI_{length}$. Here, GI_{length} is the length of GI. The SSPA is then employed to obtain $u(q)$.

The corrupted signal by AWGN $r(q)$ is obtained at the receiver. GI is first removed before transformed to the frequency domain signal by FFT and equalized. Both de-spreading (generally with the complex conjugate complex of spreading code) in the frequency domain and combining are performed by CI-FFT (note that CI-FFT equals to CI-IFFT*) before parallel-to-serial conversion followed by QAM demapper to get the information sequence $\hat{d}(k)$.

6.3. Computational Complexity

This section discusses the additional computational complexity of the proposed technique compared with the well-known partial transmit sequence (PTS),

Table 6.1. The comparison of additional complexities

Methods	**Transmitter**	**Receiver**
PTS ($U = 2$)	1 IFFT, code mult., optimizations	Side info., scrambling [55] or ML Decoder [56]
PTS ($U = 8$)	7 IFFTs, code mult. optimizations	Side info., scrambling [55] or ML decoder [56]
SLM ($M = 2$)	1 IFFT, code mult., selection	Side info., scrambling [55] or ML decoder [56]
SLM ($M = 8$)	7 IFFTs, code mult., selection	Side info., scrambling [55] or ML decoder [56]
IP 1 iter.	1 FFT, 1 IFFT, 1 clipping	0
IP 3 iter.	3 FFTs, 3 IFFTs, 3 clippings	0
Prop. CI-IC 1 iter.	2 IFFTs, 1 FFT, 1 clipping	1 FFT
Prop. CI-IC 3 iter.	4 IFFTs, 3 FFTs, 3 clippings	1 FFT

selected mapping (SLM) and IP technique. The comparison is presented in Table 6.1.

It can be observed from Table 6.1 that the proposed CI-IC with 3 iteration has similar complexity with PTS with $U = 8$, SLM with $M = 8$ and IP with 3 iterations. IP iteration may be simpler since there is no additional complexity (such as side information detection and scrambling) at the receiver, while in CI-IC method, at least one additional FFT is required.

6.4. Peak Power Evaluations

We performed computer simulations to clarify the performance of the proposed CI-IC technique. Major simulation parameters have been shown in Table 6.2 to constitute the system of future Wireless LAN i.e. by doubling FFT point to 128 for higher data transmission. However, the proposed technique can be easily adapted to other parameters of Wireless LAN technologies.

The SSPA is assumed to have OBO of 4dB for QPSK and 8dB for 64QAM as the reasonable OBO for a different modulation [57]. The normalization after

Table 6.2. Simulation parameters for performance evaluation of the CI-IC method

	Parameter	**Value(s)**
Transmitter	Modulation	QPSK, 64QAM
	Subcarrier number (S)	96
	FFT size (N)	128
	Oversampling factor (L)	2
	Error correction coding	Convolutional, $R = 1/2$
	PAPR threshold (T_h)	0dB - 8dB
	Number of iteration (i)	1 - 4
	CI spreading ($C(k, n)$)	IFFT (size: $96 = 3 \times 2^5$)
Channel	Nonlinear	SSPA ($p = 4$), OBO=4dB, 8dB
	AWGN	–
Receiver	Equalizer	MMSE
	CI De-spreading ($C^{\star}(k, n)$)	FFT (size: $96{=}3{\times}2^5$)

clipping is performed to get the same power as the signal before clipping. For a fair computational complexity, the parameters for PTS and SLM are set to $U = 2, 8$ and $M = 2, 8$, respectively.

With the parameters presented above, we present four criteria in this section to evaluate the performance of the proposed CI-IC method. INP performance of the proposed CI-IC method is compared with PTS, SLM and IP and plotted in Figs. 6.3, 6.4 and 6.5, respectively.

Figs. 6.3, 6.4, and 6.5 show the complementary cumulative distribution function (CCDF) of the INP distribution with QPSK in PTS, SLM, IP and the proposed CI-IC. With peak threshold $T_h = 3dB$, we used 100,000 randomly distributed symbols to produce the graphs. However, the number of symbols beyond the value shall not drastically change the curves characteristics. The CCDF of OFDM's PAPR without clipping (for OFDM it is noted as IP0 and for CI is CI-IC0) are also shown for a baseline comparison. PTS with $U = 2$ and 8 are noted as PTS2 and PTS8, while SLM with $M = 2$ and 8 are noted as SLM2 and SLM8. The IP with 0, 1 and 3 iterations are noted as IP0, IP1 and IP3, while the

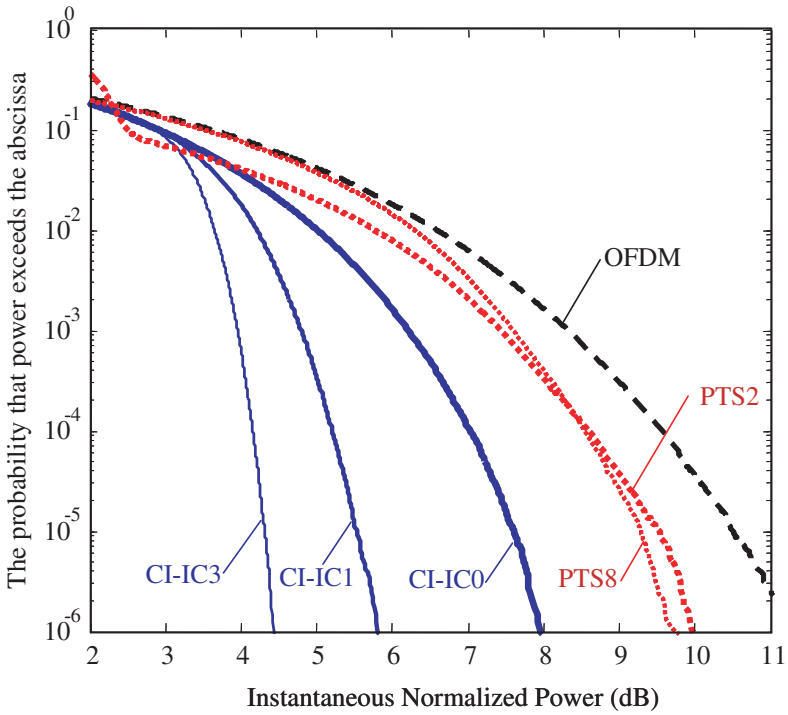

Figure 6.3. INP performance of PTS and the proposed CI-IC

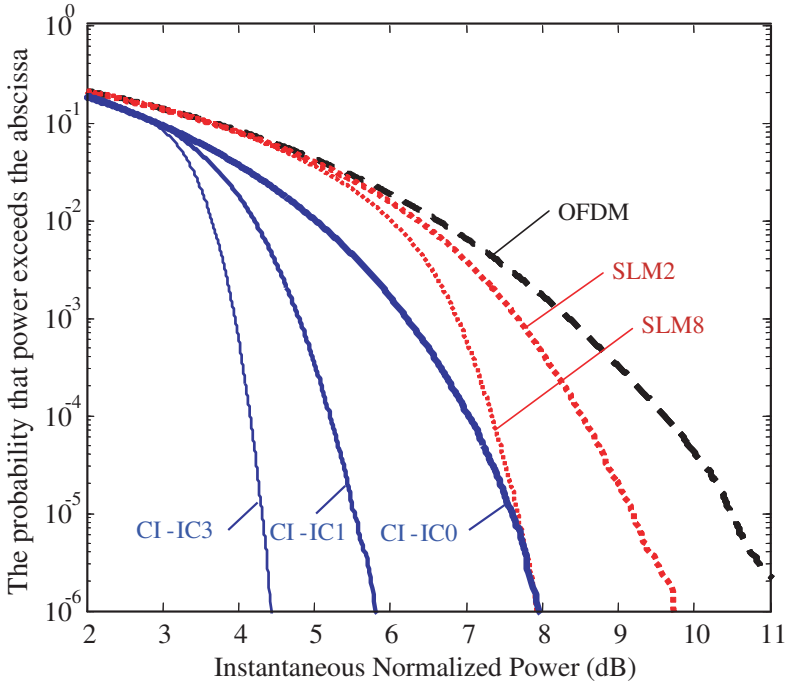

Figure 6.4. INP performance of SLM and the proposed CI-IC

CI-IC is noted as CI-IC0, CI-IC1 and CI-IC3 for 0, 1 and 3 iteration of clipping.

The performance of PTS and SLM are evaluated with a simple code i.e. $+1, -1, +j, -j$ to keep the complexity is comparable with the iterative clipping which do not require code multiplication for search the lowest PAPR. The performance of PTS and SLM may change if the code is carefully selected from other sequences accompanied by the complexity enhancement.

With a comparable complexity, it can be concluded from the figures that the proposed method greatly reduces the PAPR of conventional OFDM and outperforms the well-known PTS and SLM technique with the same computational complexity. Since the IP method has a performance which is close to the proposed CI-IC method, therefore, further comparison will be focused on the IP method. Comparing in detail the proposed method with IP, we get the improvement by the proposed Ci-IC is about 0.5dB at 99.9% point. We also observe that the gap of the proposed method and IP method diminishes by increasing the number of iterations in clipping. With 3 iterations at CCDF of 10^{-5}, the INP level of IP

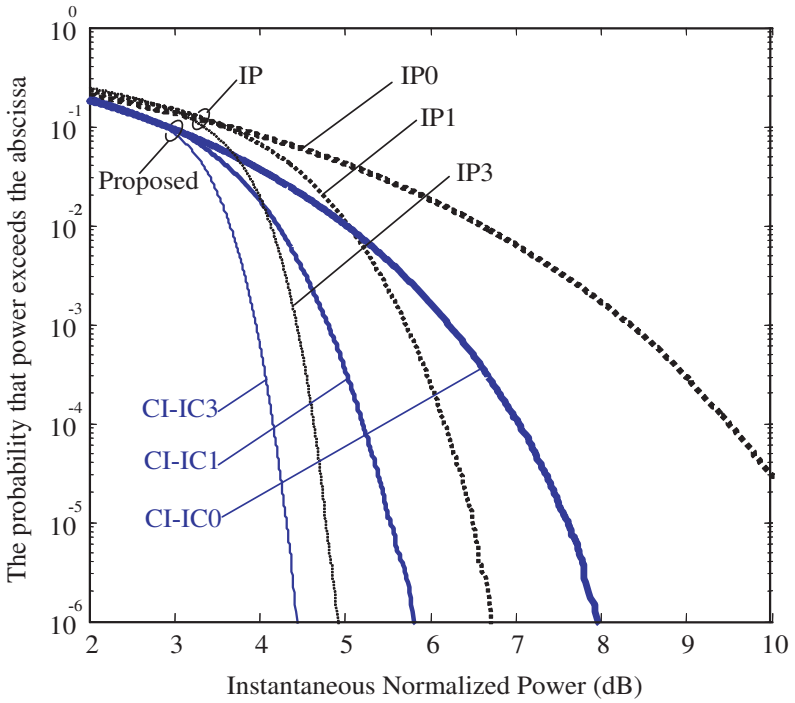

Figure 6.5. INP performance of IP and the proposed CI-IC

is 4.75dB, while the INP of the proposed CI-IC method is 4.25dB. It shows that the proposed method is superior to IP that can reduce the number of iterations required to attain a given clipping threshold.

6.5. Numerical Results and Analysis

This section presents a numerical results in terms of PSD and total degradation (TD) [39]. TD is in this chapter is defined as [39]

$$TD = \left(\frac{E_b}{N_0}\right)_{SSPA} - \left(\frac{E_b}{N_0}\right)_{linear} + OBO\,[dB] \tag{6.10}$$

where the $(\frac{E_b}{N_0})_{linear}$ is the required E_b/N_0 to ensure a fix BER $= 10^{-3}$ on the linear channel (without SSPA), $\frac{E_b}{N_0}{}_{SSPA}$ is the required E_b/N_0 in the presence of SSPA.

We observed the PSD of the proposed CI-IC method and IP method for

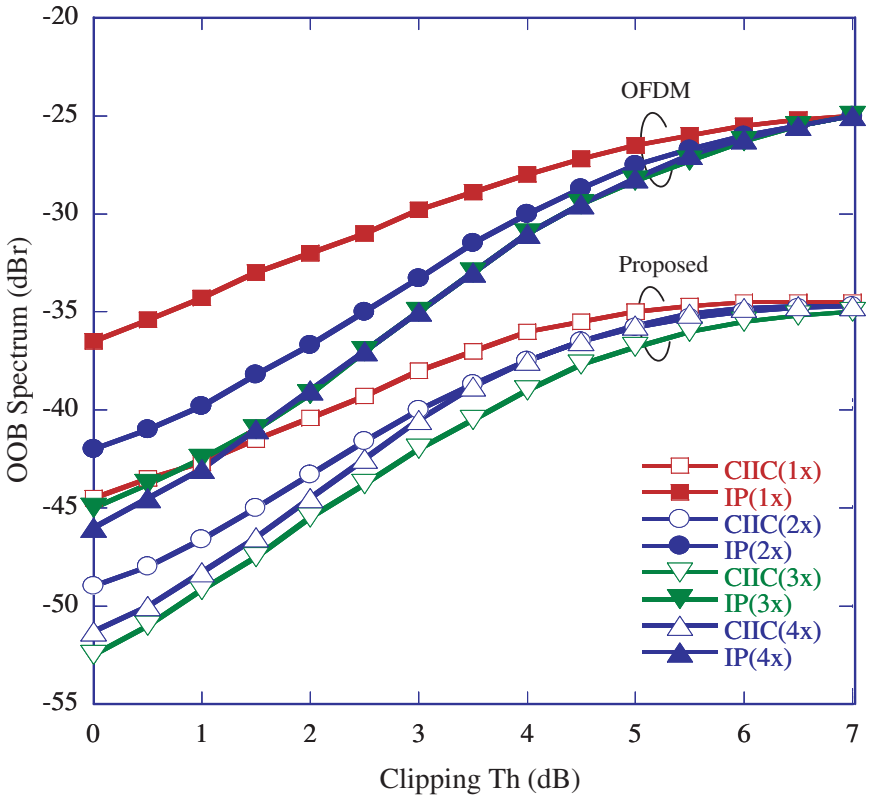

Figure 6.6. Performance of OOB spectrum for several clipping thresholds (T_h) in QPSK modulation

OFDM systems. The PSD is observed at the output of SSPA. The PSD is plotted from 50 OFDM symbols after the SSPA with $p = 4$. The OBO is set to OBO=4dB for QPSK and 8dB for 64QAM. By keeping the same OBO, the PSD for several clipping thresholds T_h are plotted in Figs. 6.6 and 6.7 for QPSK and 64QAM, respectively. The OOB spectrum radiation is measured in a fixed frequency at 46% outside the desired bandwith.

As shown in Fig. 6.6 for $T_h = 0dB - 7dB$, the OOB spectrums of OFDM with IP method vary from -45dBr to -26dBr. OOB decreases as T_h decreases. At the same T_h, the OOB can be reduced moreover by increasing the number of iterations. It is, however, shown that increasing the number of iteration more than 3 ($i > 3$) does not reduce the OOB level.

With the similar trend, OOB of the proposed method can be reduced to the

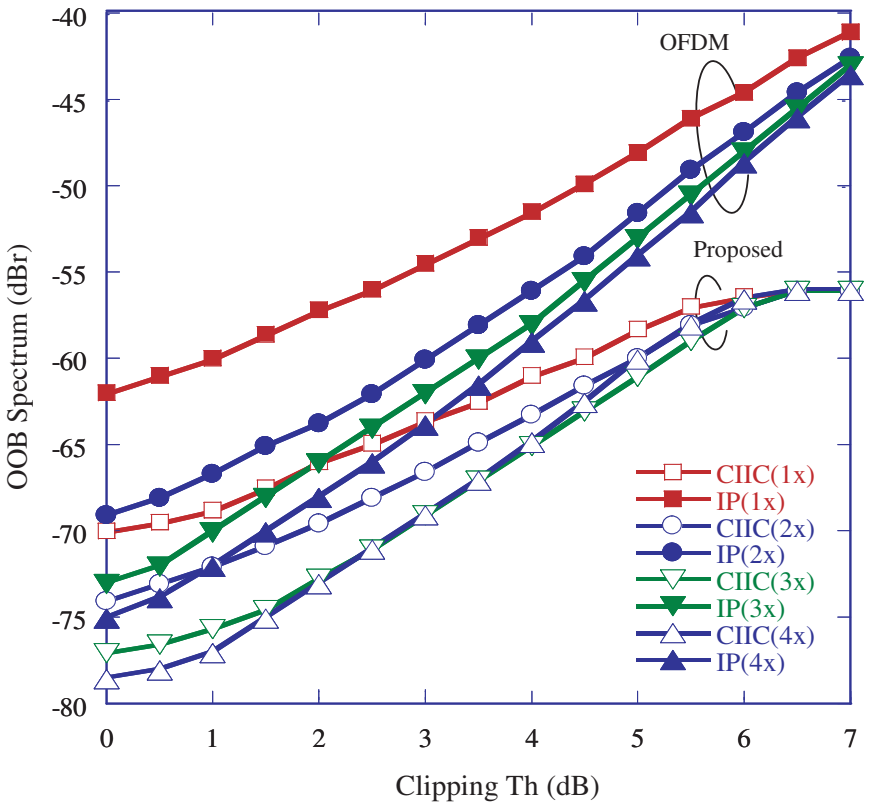

Figure 6.7. Performance of OOB spectrum for several clipping thresholds T_h in 64QAM modulation

level of -52.5dBr to -37dBr. From the figure, it is confirmed that almost for all T_h values, the OOB of the proposed CI-IC method is about 15dB better than the OOB of IP method. Increasing the number of iteration more than 3 does not reduce the OOB level. For example at $T_h = 3dB$, the OOB of IP with 3 iterations is similar with 4 iterations. In CI-IC method, 4 iterations does not give any improvements than 3 iterations. Therefore iteration more than 3 is ineffective in term of OOB reduction.

For OOB performances of 64QAM as shown in Fig. 6.7, the trend of OOB of OFDM and CI-FFT/OFDM is similar. The difference is only on the range of OOB level i.e. -75dBr to -40dBr and -78dBr to -57dBr for IP method and the proposed method, respectively. This lower OOB level is mainly caused by the higher OBO of 64QAM i.e. OBO=8dB (instead of OBO=4dB in QPSK).

For example with $T_h = 3dB$ in QPSK, CI-IC method presents OOB radiation at -42dBr (3 iterations, 4 iterations does not present a better OOB) and -37dBr (1 iteration), while the IP can only present -35dBr (4 iterations) and -29dBr(1 iteration). For 64QAM, the OOB radiations of the proposed CI-IC are about -72dBr (3 iteration) and -65dBr (1 iteration), while in IP method are -65dBr (3 iterations) and -60dBr (1 iteration).

From both Figs. 6.6 and 6.7, it is confirmed that the proposed CI-IC method improves the performance of IP. About 7dB improvement is presented by CI-IC for both QPSK and 64QAM at $T_h = 3dB$.

The BER degradation caused by inter-carrier interference due to clipping is evaluated in AWGN channel. The results BER degradation are plotted in Fig. 6.8 and 6.9, as a function of clipping threshold T_h [dB]. Fig. 6.8 plots the total degradation for OBO=4dB and several T_h values. For example at $T_h = 2dB$, the proposed CI-IC method degrades with TD=4dB - 4.25dB while IP with TD=4.4dB - 5.75dB.

The performances of coded system for 64QAM with OBO=8dB and serveral T_h values are plotted in Fig. 6.9. For example at $T_h = 5dB$, the proposed CI-IC method degrades about 8.2dB to 8.4dB while IP method about 8.6dB to 10.4dB.

Finally, from Figs. 6.8 and 6.9, we can conclude that the proposed method improves the degradation about 0.4dB - 1.5dB with QPSK modulation. In 64QAM modulation, the improvement is about 0.4dB– 2dB. It is, however, important to note that there is a trade-off between OOB and TD. Consequently, an analysis to find an efficient iteration is required to obtain lower OOB and lower TD.

Fig. 6.10 analyzes the total degradation (TD) of the coded cases with iteration number $i = 1, 2, 3$, and 4 at a specified OOB spectrum level. It is shown that the proposed CI-IC method has minimum TD=4.07dB with 3 iteration at OOB=-44dBr, while IP method has minimum TD=4.35dB with 2 iterations at OOB=-33dBr. For 64QAM, the minimum TD of OFDM is about 10.45dB while TD of CI/OFDM is about 8.55dB.

It is concluded that the efficient iteration number for IP method in coded OFDM is $i = 2$, while for CI-IC method in coded CI-FFT/OFDM is $i = 3$. The

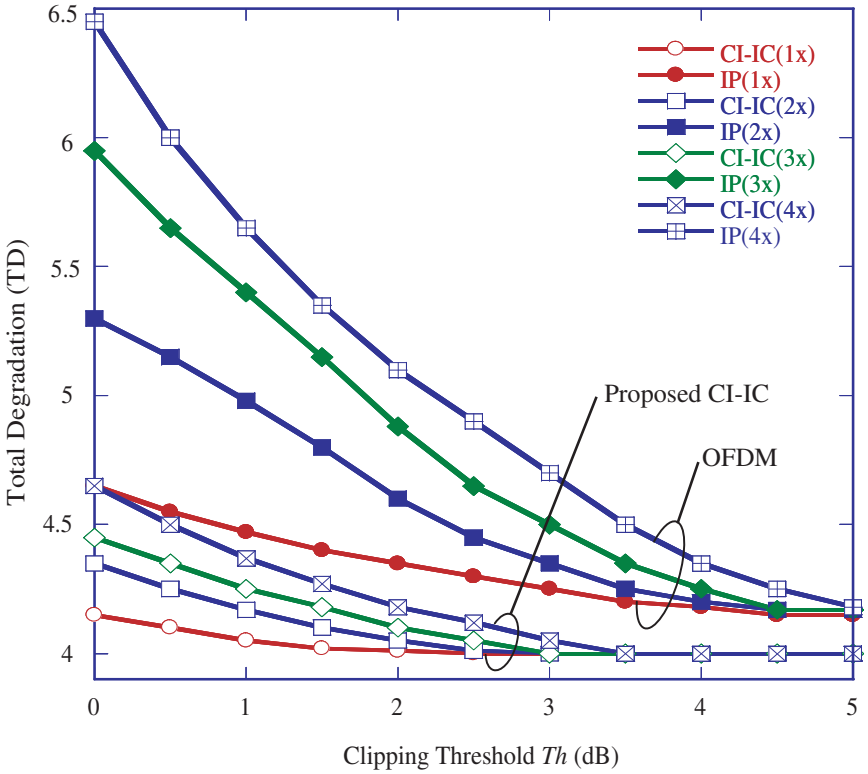

Figure 6.8. Total degradation of coded QPSK for several clipping thresholds T_h in the presence of SSPA with OBO=4dB

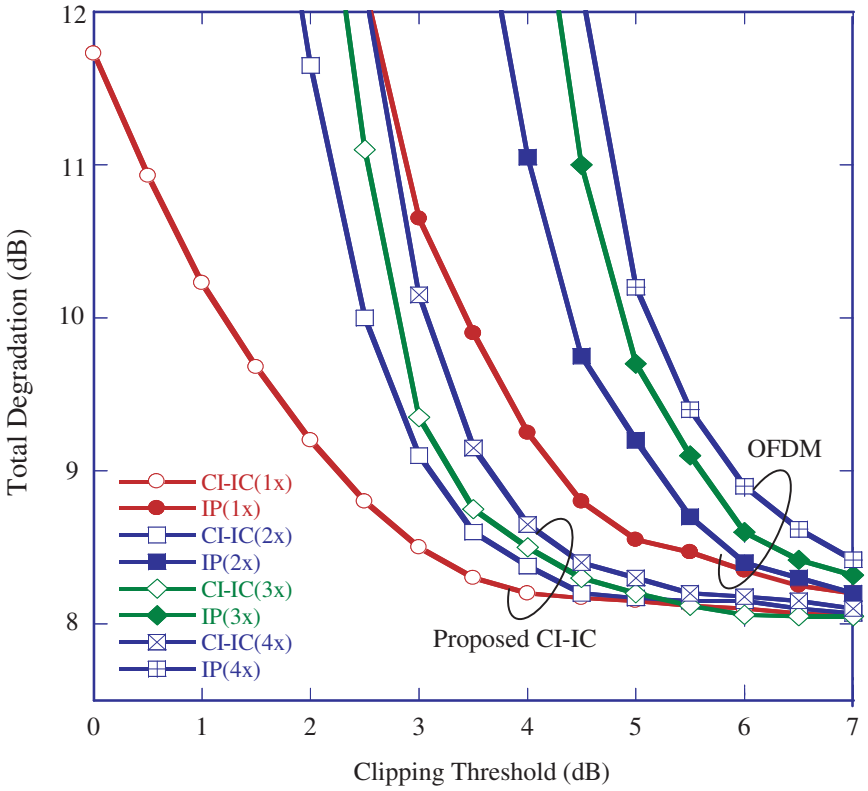

Figure 6.9. Total degradation of coded 64QAM for several clipping threshold T_h in the presence of SSPA with OBO=8dB

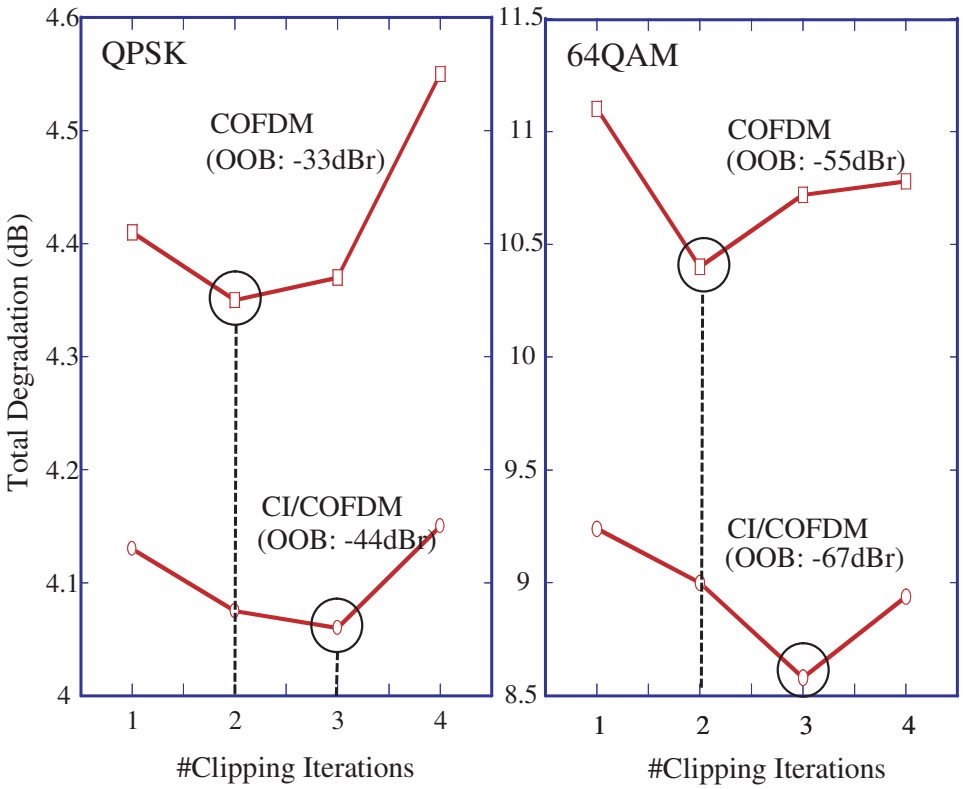

Figure 6.10. Efficient iterative clipping for minimizing the total degradation

reason is that the number of iterations more than 3 does not improve the PSD performance, while at the same time, the BER performance degrades significantly. It is important to note that a different iteration employs a different threshold T_h. This result is very important to confirm that iteration with $(i > 3)$ is an ineffective iteration both in computation and total degradation. At the stand point of efficient iteration number, the proposed CI-IC improved the TD about 0.32dB in QPSK and 2.1dB in 64QAM.

By observing the results as plotted in Figs. 6.6 - 6.9 and the analysis of iteration number in Fig. 6.10, the proposed CI-IC method provides both lower OOB radiation and lower BER degradation compared with the IP method in [36].

Chapter 7

Conclusions

This dissertation formulated the peak power problem of multicarrier modulations in satellite and radio communication systems and proposed four new methods for improving the performances.

Chapter 2 introduced the peak power problem and SSPA design in multicarrier systems for satellite and radio/terrestrial communications. The basic characteristic of PSD and theoretical BER, as the important baseline comparisons, were introduced in this chapter.

Chapter 3 proposed a technique to transmit digital television signal via satellite link to the uncovered area such as mountainous regions and far islands. This chapter designed an OFDM with clipping and filtering, then re-modulated into FM to obtain signal with a constant envelope. The clipped OFDM signal has advantage to increase the FM gain because the required bandwidth of FM is determined by the maximum amplitude of the OFDM signal. The resulted signal is called as OFDM-FM signals, that has a constant envelope which is strong to the nonlinearity effect of the satellite power amplifier. At the receiver, FM demodulation is performed to obtain the OFDM signal (digital television signal) and re-broadcasted. With the presence of FM gain, the results demonstrated that the proposed OFDM-FM is effective ith gain margin about 6.3dB compared with those of transmitting OFDM signals directly to the satellite without FM modulation.

Chapter 4 proposed a new design of CI/OFDM and POCI/OFDM called CI-FFT and POCI-FFT, respectively, by utilizing the butterfly of FFT instead of the conventional matrix multiplications. In addition, this chapter introduced an improvement to the incorrect design of the conventional CI/OFDM and provided significant computational cost reduction of the spreading process. The result confirms that a low PAPR and better BER performances are kept equal with the conventional CI/OFDM system.

Chapter 5 innovated a new large code set to improve the BER performance of OFDM and MC-CDMA systems while keeping a lower PAPR level for both systems. To improve lower BER degradation, the proposed code introduced low and uniform cross-correlations. Considering the user capacity, the proposed code is capable of assigning $2N+1$ users on the N subcarriers with better BER performances both in AWGN and multipath fading environment. The results confirm significant improvements about 5dB and 3.6dB in AWGN and multipath fading channel, respectively.

Chapter 6 proposed iterative clipping (with lower hardware complexity) while minimizing the OOB spectrum broadening for OFDM over the nonlinear channel i.e. SSPA. The results confirm that an iterative clipping is really advantageous to improve the total degradation while minimizing the OOB spectrum radiation. The discovered efficient iteration number for coded OFDM is 2 iterations and coded CI-FFT/OFDM is 3 iterations. This result is an important contribution to show the advantages of an effective iterative clipping for coded OFDM and coded CI-FFT/OFDM systems..

Acknowledgements

First of all and foremost, I thank to the God for His bless and merciful throughout all of my life. I also have many people to thank for helping to make my NAIST experience both enriching and rewarding.

First, I would like to express my profound gratitude to Professor Minoru Okada for the valuable ideas, discussion and research guidance. His encouragement has been the most valuable throughout my study at NAIST.

My acknowledgements are also to Professor Hiroyuki Seki for his time of guiding me in writing this dissertation.

I would like to express my gratitude to Associate Professor Takao Hara, for his outstanding guidance and limitless patient and fatherly support during my study and research. Prof. Hara is a fascinating teacher, thoughtful mentor and I benefited greatly working under his guidance.

I would like to thank Assistant Professor Masato Saito, for excellent technical discussion throughout all of my academic activities at NAIST.

I would like to thank the Sagawa Scholarship Foundation, International Communications Foundation (ICF) of KDDI, and Panasonic Scholarship Inc., for giving me a chance to pursue my master to doctoral degree in Japan and valuable help and support during my stay in Japan.

Finally, I'll give my acknowledgements to all my Japanese friends or abroad, my present and past members of Communications Laboratory, who helped creating a very enjoyable and productive environment in the laboratory.

Through it all, I owe my greatest debt to my family, my parents, my wife and children. Your love, patient and support are the most rewarding experience of my graduate years.

References

[1] R. V. Nee and R. Prasad, *OFDM for Wireless Multimedia Communications*. Artech House Publisher, 2001.

[2] K. Anwar, "Peak-to-average power ratio reduction of OFDM signals using carrier interferometry codes and iterative processing," Master's thesis, Nara Institute of Science and Technology, Japan, 2005.

[3] "Technical requirements for retransmission with IP satellite supplemental provisions - plan," December 2005. `http://www.soumu.go.jp`.

[4] ARIB Standard B31, *Transmission System for Digital Terrestrial Television Broadcasting*, January 2002.

[5] D. A. Wiegandt, C. R. Nassar, and Z. Wu, "Overcoming peak-to-average power ratio issues in OFDM via carrier interferometry codes," in *Vehicular Technology Conference (VTC2001)*, (Atlantic City, NJ), pp. 660–663, May 2001.

[6] K. Anwar, A. U. Priantoro, M. Saito, T. Hara, M. Okada, H. Yamamoto, and K. Ando, "PAPR reduction of OFDM signals using iterative processing and carrier interferometry codes," in *IEEE International Symposium on Intelligent Signal Processing and Communications System*, (Korea), pp. 48–51, November 2004.

[7] K. Anwar, M. Saito, T. Hara, M. Okada, and H. Yamamoto, "Simplified realization of carrier interferometry OFDM by FFT algorithm," in *IEEE VTS Asia Pacific Wireless Communications System*, (Hokkaido, Japan), pp. 199–203, August 2005.

[8] K. Anwar, M. Saito, H. T, M. Okada, and H. Yamamoto, "Simplified realization of pseudo-orthogonal carrier interferometry OFDM by FFT algorithm," in *Multicarrier Spread Spectrum from IEEE Multi-Carrier Spread Spectrum (MC-SS 2005) Khaled Fazel, Stefan Kaiser (Eds.) 2006, XVII, 502p, Hardcover, ISBN:1-4020-4435-6, Oberpfaffenhofen*, pp. 167–174, September 2005.

[9] K. Anwar, T. Hara, and K. Ando, "Simplified design of carrier interferometry OFDM and pseudo-orthogonal carrier interferometry OFDM," 2006. granted.

[10] E. F. Casas and C. Leung, "OFDM for data communication over mobile radio FM channels-part i: Analysis and experimental results," *IEEE Transaction on Communications*, vol. 39, pp. 783–793, May 1991.

[11] E. F. Casas and C. Leung, "OFDM for data communication over mobile radio FM channels-part ii: Performance improvement," *IEEE Transaction on Communications*, vol. 40, pp. 680–683, April 1992.

[12] P. Scalart, M. Leclerc, P. Fortier, and H. T. H., "Performance analysis of a COFDM/FM in-band digital audio broadcasting system," *IEEE Transaction on Broadcasting*, vol. 43, pp. 191–198, June 1997.

[13] M. J. R. G., R. Prasad, and J. H. Bons, "Analysis of new methods for broadcasting digital data to mobile terminals over an FM-channel," *IEEE Transaction on Broadcasting*, vol. 40, pp. 29–37, March 1994.

[14] C. R. Nassar, B. Natarajan, Z. Wu., D. Wiegandt, S. Zekavat, and S. Shatill, *Multi-carrier technologies for wireless communication.* Kluwer Academic Publishers, 2002.

[15] D. A. Wiegandt, Z. Wu, and C. R. Nassar, "High-performance carrier interferometry OFDM WLANs: RF testing," in *IEEE International Conference on Communications (ICC)*, pp. 203–207, May 2003.

[16] D. A. Wiegandt and C. R. N. Z. Wu, "High-throughput, high-performance OFDM via pseudo-orthogonal carrier interferometry spreading codes," *IEEE Transaction on Communications*, July 2003.

[17] D. A. Wiegandt and C. R. Nassar, "High-throughput, high-performance OFDM via pseudo-orthogonal carrier interferometry type 2," in *IEEE International Symposium Wireless Personal Multimedia Communications (WPMC)*, Oct. 2002.

[18] K. Anwar, M. Saito, T. Hara, M. Okada, and H. Yamamoto, "Impact of using partial number of subcarrier on the PAPR carrier interferometry ofdm," in *IEICE General Conferences*, vol. BS-9-1, (Osaka, Japan), March 2005.

[19] D. A. Wiegandt, C. R. Nassar, and Z. Wu, "Overcoming peak-to-average power ratio issues in OFDM via carrier interferometry codes," in *IEEE Vehicular Technology Conference (VTC2001)*, (Atlantic City, NJ), pp. 660–663, May 2001.

[20] B. Natarajan, C. R. Nassar, S. Shattil, M. Michelini, and Z. Wu, "High-performance MC-CDMA via carrier interferometry codes," *IEEE Transaction on Vehicular Technology*, vol. 50, pp. 1344–1353, November 2001.

[21] S. Hara and R. Prasad, "Overview of multicarrier CDMA," *IEEE Communications Magazine*, vol. 35, pp. 126–133, Dec. 1997.

[22] M. Debbah, P. Loubaton, and M. de Courville, "Spread OFDM performance with MMSE equalization," in *IEEE International Conference on Acoustics, Speech, and Signal Processing (ICASSP)*, vol. 4, pp. 2385–2388, May 2001.

[23] N. Yee, P. Linnartz, and G. Fettweis, "Multi-carrier CDMA in indoor wireless networks," *IEICE Tansaction on Communications, Japan*, vol. E77-B, pp. 900–904, July 1994.

[24] A. Bury, J. Eagle, and J. Lindner, "Diversity comparison of spreading transforms for multicarrier spread spectrum transmission," *IEEE Transaction on Communications*, vol. 51, pp. 774–781, May 2003.

[25] K. Anwar and H. Yamamoto, "A new design of carrier interferometry OFDM with FFT as spreading codes," in *IEEE Radio and Wireless Symposium (RWS)*, pp. 543–546, January 2006.

[26] K. Anwar, M. Saito, T. Hara, M. Okada, and H. Yamamoto, "On the PAPR reduction of wavelet-based multicarrier modulation systems," in *IASTED Communications and Computer Network*, (MIT, CA, USA), pp. 138–143, November 2004.

[27] F. Vanhaverbeke, M. Moeneclay, and H. Sari, "DS/CDMA with two sets of orthogonal spreading sequences and iterative detection," *IEEE Communications Letter*, vol. 4, pp. 289–291, September 2000.

[28] B. M. Popovic, N. Suehiro, and P. Z. Fan, "Orthogonal sets of quadriphase sequences with good cross correlation properties," *IEEE Transaction on Information Theory*, vol. 48, pp. 956–959, April 2002.

[29] B. Natarajan, Z. Wu, C. R. Nassar, and S. Shatill, "Large set of CI spreading codes for high capacity MC-CDMA," *IEEE Transaction on Communications*, vol. 52, pp. 1862–1866, November 2004.

[30] N. Taylor, M. A. Cooper, S. M. D. Armour, and G. P. McGeehan, "Performance evaluation of carrier interferometry implementations of MC-CDMA over a wideband channel suffering phase noise," in *IEEE Vehicular Technology Conference Spring*, vol. 5, pp. 3043–3047, June 2005.

[31] J. Max, "Signal set with uniform correlation properties," *Journal of Society for Industrial and Applied Mathematics*, vol. 10, pp. 113–118, Mar. 1962.

[32] G. Chandran and J. S. Jaffe, "Signal set design with constrained amplitude spectrum and specified time-bandwidth product," *IEEE Transaction on Communications*, vol. 44, June 1996.

[33] P. Xia, S. Zhou, and G. B. Giannakis, "Achieving the welch bound with difference sets," *IEEE Transaction on Information Theory*, vol. 51, pp. 1900–1907, May 2003.

[34] S. H. Han and J. H. Lee, "An overview of peak-to-average power ratio reduction techniques for multicarrier transmission," *IEEE Wireless Communications*, pp. 56–65, April 2005.

[35] J. Armstrong, "Peak-to-average power ratio reduction for OFDM by repeated clipping and frequency domain filtering," *Electronic Letter*, vol. 38, pp. 246–247, February 2002.

[36] S. Tomisato, H. Suda, and M. Hata, "PAPR reduction method using iterative processing for OFDM transmission systems," in *IEEE VTS Asia Pacific Wireless Communications APWCS2004*, pp. 7–10, January 2004.

[37] X. Li and L. J. C. Jr., "Effect of clipping and filtering on the performance of OFDM," *IEEE Comm. Letters*, vol. 2, pp. 131–133, May 1998.

[38] A. Kubo, S. Tomisato, and M. Hata, "Transmission performance of highly efficient OFDM signals with iterative peak reduction," in *IEEE Vehicular Technology Ssociety Asia Pacific Wireless Communications Symposium*, (Hokkaido, Japan), pp. 145–148, August 2005.

[39] E. Costa and S. Pupolin, "M-QAM-OFDM system performance in the presence of a nonlinear amplifier and phase noise," *IEEE Transaction on Communications*, vol. 50, pp. 462–472, March 2002.

[40] IEEE.802.11a-1999, *High Speed physical layer in the 5GHz band*, 1999.

[41] S. Miyamoto, S. Harada, and N. Morinaga, "Performance of 2.4 GHz-band wireless LAN system using orthogonal frequency division multiplexing scheme under microwave oven noise environment," in *IEEE International Symposium on Electromagnetic Compatibility (EMC)*, pp. 157–162, August 2005.

[42] K. Anwar, A. Priantoro, M. Saito, T. Hara, M. Okada, and H. Yamamoto, "Digital television transmission over OFDM/FM using satellite communications system," in *International Conference on Communications, Internet, and Information Technology (CIIT2004)*, (St. Thomas, Virgin Island, USA), pp. 358–363, Nov. 2004.

[43] K. Anwar, T. Hara, M. Okada, and H. Yamamoto, "Digital terrestial television transmissions over OFDM/FM via satellite communications system," *IEICE Transaction on Communications (Japanese)*, vol. J89-B, pp. 2117–2126, Nov. 2006.

[44] K. Anwar, T. Hara, M. Okada, and H. Yamamoto, "Digital terrestial television transmissions over OFDM/FM via satellite communications system," *IEICE Transaction on Communications (Japanese)*, vol. 90, no. 11, pp. 74–84, 2007.

[45] T. Namekawa and S. Okui, *Communications Systems (Japanese Edition)*. Morikita, 2001.

[46] H. Ochiai and H. Imai, "On clipping for peak power reduction of OFDM signals," in *IEEE Globecom*, vol. 2, pp. 731–735, 2000.

[47] T. Hara, M. Ichikawa, M. Okada, and H. Yamamoto, "Design of frequency reuse carrier superposition method and signal canceller for VSAT satellite communications," *IEICE Transaction on Communications J86-B (Japanese Edition)*, vol. 10, no. 7, pp. 1300–1309, 2005.

[48] H. Sari, G. Karam, and I. Jeanclaude, "Frequency-domain equalization of mobile radio and terrestrial broadcast channels," in *IEEE Globecom*, (San Fransisco, CA), 2004.

[49] Y. Kuang, K. Long, C. Wu, and Q. Chen, "Comments on high-througput high performance OFDM via pseudo-orthogonal carrier interferometry spreading codes," *IEEE Transaction on Communications*, vol. 55, pp. 232–234, January 2007.

[50] J. lei and L. Wu, "Comments on high-througput high performance OFDM via pseudo-orthogonal carrier interferometry spreading codes," *IEEE Transaction on Communications*, vol. 55, p. 1088, 5 2007.

[51] A. V. Oppenheim and R. W. Schafer, *Discrete-time signal processing*. Prentice Hall International Edition, 1999.

[52] B. D. Sameraro, "Parallel fast Fourier transform for non power of two data," in *Intel Supercomputing Users Group Meeting*, (San Diego, CA), pp. 25–29, June 1994.

[53] M. Patzold, *Mobile Fading Channel*. John Wiley & Sons, 2002.

[54] H. Ochiai and H. Imai, "On the distribution of peak-to-average power ratio in OFDM signals," *IEEE Transaction on Communications*, vol. 49, pp. 282–289, Feb 2001.

[55] M. Breiling, S. H. Muller, and J. H. Huber, "SLM peak-power reduction without explicit side information," *IEEE Communications Letter*, vol. 5, pp. 239–241, June 2001.

[56] A. D. S. Jayalath and C. Tellambura, "SLM and PTS peak-power reduction of OFDM signals without side information," *IEEE Transaction on Wireless Communications*, vol. 4, September 2005.

[57] Project Document, *WiMax and Mobile/Broadband Satellite*, February 2006.

Achievements and Publications

Journals

1. K. Anwar, T. Hara, M. Okada and H. Yamamoto, "Digital Terrestrial Television Transmission over OFDM/FM Using Satellite Communications System", *IEICE Transaction on Communications (Japanese Edition)*, Vol. J89-B, No. 11, pp. 2117-2126, November 2006.
   Selected to be translated and re-published in:
   (ECJA 1365), Electronic and Communications in Japan, Part II: Electronics, Wiley Interscience, Inc., Vol. 90, No.11, pp. 74-84, November 2007.

2. K. Anwar, M. Saito, T. Hara and M. Okada, "Large Code Set for Double User Capacity and Low PAPR Level in Multicarrier Systems", *IEICE Transaction on Fundamentals* (Conditional Accepted).

International Conferences (Peer Reviewed)

1. K. Anwar and M. Okada, "On the High Speed Satellite Communications System with Carrier Interferometry OFDM", *25th AIAA International Communications Satellite Systems Conference*, Korea, April 2007.

2. K. Anwar, T. Hara, M. Okada, M. Shigaki, K. Yamanaka and R. Suzuki, "Performance Improvement of Ka-band Small Earth Stations for WINDS Utilizing Superconductive Filter", *25th AIAA International Communications Satellite Systems Conference*, Korea, April 2007.

3. K. Anwar, T. Hara, M. Saito, M. Okada and H. Yamamoto, "Large Code Set for PAPR Reduction of OFDM Signals and Capacity Increasing in MC-CDMA System", *ACM International Wireless Communications and Mobile Computing (IWCMC)*, Vancouver, Canada, pp. 887-892, July, 2006.

4. K. Anwar, T. Hara, M. Saito, M. Okada and H. Yamamoto, "A New Spreading Code for MC-CDMA and OFDM Systems", *IEEE International Sympo-*

sium on Computer and Communications (ISCC), Italy, pp. 283-288, June 2006.

5. K. Anwar, T. Hara, M. Saito, M. Okada and H. Yamamoto, "A New Code for Increasing Capacity of OFDM and MC-CDMA Systems", *IEEE International Conference on Computer and Communications Engineering (ICCCE)*, Kuala Lumpur, Malaysia, pp. 721-726, May 2006.

6. K. Anwar, T. Hara, M. Saito, M. Okada and H. Yamamoto, "A Novel Fast Computation without Division for MMSE Equalizer and Combiner", *IEEE Industrial, Electrical and Electronic GCC*, Manama, Bahrain, March 2006.

7. K. Anwar, M. Saito, T. Hara, M. Okada and H. Yamamoto, "Simplified Realization of Pseudo-Orthogonal Carrier Interferometry OFDM by FFT Algorithm", *5th IEEE Multi-Carrier Spread Spectrum (MC-SS)*, Oberpfaffenhofen, Munich, Germany, pp. 167-174, September 2005 (Khaled; Kaiser, Stefan (Eds.) 2006, XVII, 502 p., Hardcover ISBN: 1-4020-4435-6).

8. K. Anwar and H. Yamamoto, "A New Design of Carrier Interferometry OFDM with FFT as Spreading Codes", *IEEE Radio and Wireless Symposium (RWS 2006)*, San Diego, California, pp. 543-546, January 2006. **(Selected as the BEST STUDENT PAPER)**.

9. K. Anwar, M. Saito, T. Hara, M. Okada and H. Yamamoto, "Simplified Realization of Carrier Interferometry OFDM by FFT Algorithm", *IEEE VTS Asia Pacific Wireless Communications System (APWCS)*, Hokkaido, Japan, pp. 199-203, August 2005.

10. K. Anwar, A.U. Priantoro, K. Ando, M. Saito, T. Hara, M. Okada and H. Yamamoto, "PAPR Reduction of OFDM Signals Using Iterative Processing and Carrier Interferometry Codes", *IEEE Int. Symposium on Intelligent Signal Processing and Communications System (ISPACS)*, pp. 48-51, Seoul, Korea, November 2004.

11. K. Anwar, A.U. Priantoro, M. Saito, T. Hara, M. Okada, H. Yamamoto and K. Ando, "Digital Television Transmission over OFDM/FM Using Satellite

Communications System", *International Conference on Communications, Internet and Information Technology (CIIT)*, pp. 358-363, St. Thomas, Virgin Island, USA, November 2004.

12. K. Anwar, A.U. Priantoro, M. Saito, T. Hara, M. Okada and H. Yamamoto, "On The PAPR Reduction of Wavelet Based Multicarrier Modulation System", *International Conference on Communications and Computer Networks (CCN)*, pp. 138-143, MIT, Cambridge, USA, November 2004.

13. K. Anwar, A.U. Priantoro, M. Saito, T. Hara, M. Okada and H. Yamamoto, "On The PAPR Reduction for Wavelet Based Transmultiplexer", *IEEE Int. Symposium on Communications and Information Technology (ISCIT)*, Sapporo, Japan, pp. 812-815, October 2004.

14. H. Takahashi, K. Anwar, M. Saito and M. Okada,"Low Complexity Fourier Transform using Double Square-waves", *IEEE 7th International Symposium on Communications and Information Technologies (ISCIT)*, Sydney, Australia, pp. 921-925, October 2007.

15. L. Sampebatu, K. Anwar, T. Hara and M. Okada,"Performances of Real and Complex Spreading Codes for OFDM in Fading Channel", *IEEE 12th International OFDM Workshop Hamburg*, Germany, pp. 231-235, August 2007.

16. H. Okamoto, K. Anwar, T. Hara, M. Saito, M. Okada and H. Yamamoto, "A New Concept of Clipping without Spectrum broadening for Carrier Interferometry OFDM system", *IEEE Industrial, Electrical and Electronic GCC*, Manama, Bahrain, March 2006.

17. H. Okamoto, K. Anwar, M. Saito, T. Hara, M. Okada and H. Yamamoto, "PAPR Reduction of OFDM Signals Using Clipping and Carrier Interferometry Codes", *IEEE VTS Asia Pacific Wireless Communications System (APWCS)*, Hokkaido, Japan, pp. 164-168, August 2005.

Local Conferences

1. K. Anwar, M. Saito, T. Hara, M. Okada and H. Yamamoto, "Impact of Using Partial Number of Subcarrier on the PAPR Carrier Interferometry OFDM", *IEICE General Conferences 2005*, BS-9-1, Osaka, Japan, March 2005.

2. M. Okada, K. Anwar, H. Miyoshi, K. Nose, T. Masaki and T. Izumi, "A study on Broadband Satellite Communication Systems with CI/OFDM", *IEICE Technical Report*: SAT2005-51 (In Japanese), February 2006.

3. M. Saito, K. Anwar, T. Hara, M. Okada and H. Yamamoto, "Effect of Imperfect Orthogonality PO-CI Codes on the Performances of M-QAM OFDM and MC-CDMA", *IEICE General Conferences 2005*, BS-9-2, Osaka, Japan, March 2005.

4. H. Okamoto, K. Anwar, M. Saito, T. Hara, M. Okada and H. Yamamoto, "PAPR Reduction of OFDM Signal Using Carrier Interferometry Codes and Clipping Technique (in Japanese)", *IEICE General Conferences 2005*, B-5-47, Osaka, Japan, March 2005

5. Khoirul Anwar, "Solar Power for Internet Rakyat in Rural Area", *The 16th 2007 Indonesian Scientific Conference (TI-2007)*, Kyoto, August 2007.

6. K. Anwar, M. Saito, T. Hara and M. Okada "On the Design of Digital Television Broadcasting for Indonesia", *The 15th 2006 Indonesian Scientific Conference (TI-2006)*, Hiroshima, August 2006 (An Abstract).

7. K. Anwar, M. Saito, T. Hara, M. Okada and H. Yamamoto, "Achieving OFDM with Very Low PAPR and High Performance using Carrier Interferometry Spreading Codes and Iterative Processing", *The 14th 2005 Indonesian Scientific Conference*, Nagoya, September 2005.

8. K. Anwar, A.U. Priantoro, M. Saito, T. Hara, M. Okada and H. Yamamoto, "On The PAPR Reduction for Wavelet Based Transmultiplexer", *The 13th Indonesian Scientific Conference (TI-2004)*, Tokyo, Japan, September 2004.

9. K. Anwar, K. Ragab and Kinji Mori, "Autonomous Decentralized Sensor Networks and Its Applications on ITS", *The 12th Indonensian Scientific Conference (TI-2003)*, Osaka, September 2003.

10. K. Anwar, Ian Y. and Hendrawan, "Interoperability of Digital Switching system (5ESS, EWSD, NEAX61E) on the implementation of Signalling System No.7", *The 11th Indonesian Scientific Conference (TI-2002)*, Nagoya, Japan, Sept. 2002.

Patent (Granted)

- K. Anwar, T. Hara and K. Ando, *"A New Design of Carrier Interferometry OFDM and Pseudo-Orthogonal Carrier Interferometry OFDM"*, Publication No. WO/2007/015490, Pub. Date PCT/JP2006/315230. International Filling Date: 01.08.2006.

Awards

- Best Student Paper Award, IEEE Radio and Wireless Symposium, San Diego, California, USA, 2006.
- Best Paper Award, Indonesian Scientific Conference, TI-2007, Kyoto, Japan, 2007.
- Excellent Educational Contribution Award, Indonesian Ministry of Foreign Affairs, Consulate General Republic Indonesia, Osaka, 2007.
- Best Student Award, PIP-PKS Japan, Tokyo, 2007.

Index